Blue-Light Hazard Risk Assessment of Incoherent High-Power Spotlights

The Planck Approximation

baua: Report

baua
Federal Institute for Occupational Safety and Health

Project F 2483

S. Bauer

Blue-Light Hazard Risk Assessment of Incoherent High-Power Spotlights

The Planck Approximation

1st edition 2022
Dortmund

This publication is the final report for project F 2483 “Simplified Risk Assessment of Incoherent High-Power Spotlights” on behalf of the Federal Institute for Occupational Safety and Health. The responsibility for the contents of this publication lies with the author.

Author: Dr. rer. nat. Stefan Bauer
Federal Institute for Occupational Safety and Health

Cover figure: Dr. rer. nat. Stefan Bauer
Federal Institute for Occupational Safety and Health

Cover design: Christiane Zay
wbv Media GmbH & Co. KG, Bielefeld

Publisher: Federal Institute for Occupational Safety and Health (BAuA)
Friedrich-Henkel-Weg 1–25, 44149 Dortmund, Germany
Postal address: Postbox 17 02 02, 44061 Dortmund, Germany
Telephone +49 0231 9071-2071
Fax +49 0231 9071-2070
Email *info-zentrum@baua.bund.de*
Web *www.baua.de*

10.21934/baua:bericht20220825 (online)

https://doi.org/10.21934/baua:bericht20220825

Contents

Blue-Light Hazard Risk Assessment of Incoherent High-Power Spotlights

Abstract

Photochemical retinal damages caused by light with a high proportion of blue (blue light hazard, BLH) can in principle be excluded for screens, ceiling lights, smartphones, etc. upon normal viewing behavior. In contrast, high-power spotlights, e. g. in building construction and civil engineering, for events or large storage areas, can be a BLH source. Due to different built-in technologies, lamp designs, setting parameters, and exposure situations, risk assessment is demanding, not least because of the determination of radiances being required in many cases. Therefore, the aim of this project was to develop a practical, simplified BLH risk assessment method.

In order to evaluate the suitability of such an approach, the accuracy of optical instruments commonly used for risk assessment is decisive. In this respect, several broadband and spectroradiometers were investigated. Although the measurement demands were increased in three steps (radiance standard, LED Fresnel stage light, inhomogeneously emitting spotlight), the determined radiances with an approx. 5 – 12 % standard deviation were more or less independent of the source complexity. A verification of the simplified risk assessment approach, the so-called Planck Approximation, yielded an acceptable result with less than 20 % deviation.

The idea of the Planck Approximation is based on a single illuminance measurement, which is converted into BLH weighted radiance by means of the diameter of the spotlight's front side aperture and the well-known BLH efficacy of luminous radiation for a blackbody radiator. Taking into account various influencing parameters (correlated color temperature, optical power, distance), two simple equations could be derived for maximum permissible exposure durations as a function of source size. Their usage in lab as well as at an exemplary test workplace resulted in an accuracy of approx. $\pm$30 %.

In principle, the applicability of the Planck Approximation for BLH risk assessment can be concluded. Especially the estimation of the actual exposure conditions, among others, the cumulative duration of a direct view into the source, is of crucial importance, but commonly quite difficult to record. In this context, a simplified determination of BLH weighted radiances via the Planck Approximation seems justifiable.

Keywords
photobiological lamp safety, blue-light hazard (BLH), risk assessment, influencing factors, instrument comparison, BLH efficacy of luminous radiation ($K_{\mathrm{B,v}}$), Planck Approximation

Beurteilung der Blaulichtgefährdung inkohärenter Hochleistungsscheinwerfer

Kurzreferat

Eine Netzhautschädigung durch Licht mit hohen Blauanteilen (Blaulichtgefährdung, BLH) kann im Prinzip bei natürlichem Blickverhalten für Bildschirme, Deckenbeleuchtungen, Smartphones etc. ausgeschlossen werden. Hochleistungsscheinwerfer, z. B. im Hoch- und Tiefbau, in der Veranstaltungstechnik oder für große Lagerflächen, können hingegen eine BLH-Gefahrenquelle sein. Je nach verbauter Technologie, Design, Einstellungsparameter und Expositionsbedingungen ist eine Gefährdungsbeurteilung anspruchsvoll, nicht zuletzt auch wegen der in vielen Fällen geforderten Strahldichtebestimmung. Ziel dieses Projektes war daher die Entwicklung einer praxistauglichen, vereinfachten BLH-Beurteilungsmethode.

Um die Tauglichkeit eines solchen Ansatzes bewerten zu können, ist die Genauigkeit optischer Messgeräte, die üblicherweise zur Gefährdungsbeurteilung verwendet werden, maßgeblich. Diesbezüglich wurde eine Reihe von Breitband- und Spektralradiometern untersucht. Obwohl die Messanforderungen in drei Schritten (Strahldichtenormal, LED Fresnel Bühnenlicht, inhomogen emittierender Scheinwerfer) erhöht wurden, liegt für die bestimmten Strahldichten mit einer ca. 5 – 12 %-igen Standardabweichung ein von der Komplexität der Quelle mehr oder weniger unabhängiger Wert vor. Die Überprüfung des vereinfachten Beurteilungsverfahrens, der sog. Planck Approximation, ergab mit weniger als 20 % Abweichung ein akzeptables Ergebnis.

Das Prinzip der Planck Approximation basiert auf einer einzelnen Beleuchtungsstärkemessung, die mit Hilfe des Durchmessers der Austrittsöffnung und der für einen Schwarzkörperstrahler bekannten Blaulicht gefährdenden Ausbeute sichtbarer Strahlung in BLH-gewichtete Strahldichte umgerechnet wird. Unter Berücksichtigung verschiedener Einflussparameter (korrelierte Farbtemperatur, optische Leistung, Entfernung) konnten darauf aufbauend zwei einfache Gleichungen für die maximal zulässigen Expositionsdauern als Funktion der Quellengröße abgeleitet werden. Ihre Verwendung, auch an einem exemplarischen Test-Arbeitsplatz, resultierte in einer Genauigkeit von ca. $\pm$30 %.

Damit ist die grundsätzliche Anwendbarkeit der Planck Approximation zur Beurteilung von BLH-Gefährdungen gezeigt. Insbesondere die Abschätzung der tatsächlichen Expositionsbedingungen, u. a. der kummulativen Zeitdauer des direkten Blickes in die Quelle, ist von entscheidender Bedeutung, für gewöhnlich jedoch schwer zu erfassen. In diesem Kontext ist eine vereinfachte Bestimmung der BLH-gewichteten Strahldichte mit Hilfe der Planck Approximation vertretbar.

Schlagwörter
photobiologische Lampensicherheit, Blaulichtgefährdung (BLH), Gefährdungsbeurteilung, Einflussfaktoren, Messgerätevergleich, Blaulicht gefährdende Ausbeute sichtbarer Strahlung ($K_{\mathrm{B,v}}$), Planck Approximation

1 Introduction

Each wavelength band of optical radiation can be associated with beneficial but also with detrimental health effects. For example, an acute overexposure to ultraviolet radiation (UVR) can lead to erythema, and high chronic UVR doses increase the risk for skin cancers (ICNIRP 2004). On the other hand, UVR is essential for vitamin D synthesis (Webb 2006). Longer wavelengths, i.e. visible radiation or light, are fundamental for vision and serve as a zeitgeber for the internal human clock with regard to the circadian rhythm. Adverse health effects in this spectral region are predominantly photochemically induced retinal hazards usually referred to as blue-light hazard (BLH) (ICNIRP 1997, ICNIRP 2013). Together with infrared (IR) radiation, light also contributes to retinal thermal hazards (RTH). Until today, no convincing correlation has been proven for age-related macular degeneration (AMD) induced by chronic light exposure (Modenese 2019).

For a long time, BLH of white-light emitting diodes (LEDs), in particular, of phosphor-conversion white LEDs (pc-LED) has been thought to be a major health problem not only for the public but also for the occupational sector. The built-in blue diode that stimulates the phosphor emission raised safety concerns because of the widespread application of this technology in general lighting service (GLS), displays, screens, etc. Indeed, the visible spectrum of cool-white LEDs with high correlated color temperatures (CCTs) have large relative BLH proportions (Bauer 2021). However, it was clearly demonstrated that no real-life BLH risk results from such pc-LEDs under normal viewing conditions (O'Hagan 2016), in agreement with statements of international commissions (SCHEER 2018, CIE 2019). In addition, LEDs with lower CCTs, thus smaller BLH proportions, are usually preferred because of their warm-white light emission.

In contrast, a severe BLH risk can emerge from special applications like stage lights (Weber 2016) or high-power spotlights at construction sites, especially from improper usage or lacking risk awareness. For example, actors in theaters, moderators, or news speakers are more or less "forced" to look towards the light sources despite maybe somehow being glared. Such viewing conditions increase the exposure duration, and these spotlights are usually quite powerful and/or several of them are applied simultaneously for the purpose of illumination. Therefore, the BLH dose can be very high leading to an exceedance of the legal exposure limit value (ELV).
It is important to note that although nowadays built-in LEDs are the most common technology, discharge lamps are still widely used. They are usually operated with several hundreds of watts emitting high-power radiation not only in the visible but also in the UV and IR spectral regions.

1.1 Workplace Risk Assessment

To account for adverse health effects originating from intense light, the European Directive 2006/25/EC prescribes the determination of radiance values for the assessment of workplaces being exposed to high-power spotlights where the compliance of the BLH ELV is uncertain. However, radiance measurements can be challenging, in particular, for extended light sources with an inhomogeneously emitting surface. The required measuring instruments often have built-in optics, and they must be handled with expe-

rience. Spotlights based on LED technology are usually tunable within a wide range of CCT. They are continuously dimmable and can be operated in spot as well as in flood mode. At many workplaces, several spotlights are used simultaneously; altogether, further enhancing the complex BLH risk assessment.

However, as already mentioned above, the experimental determination of radiances is only necessary when an exceedance of the BLH ELV is uncertain. If it is unambiguously clear that there are no photobiological risks or that the BLH ELV will be exceeded in any case, this finding then can be documented in the workplace risk assessment protocol and no radiance measurements are necessary.
Otherwise, the employer or more precisely the person commissioned with the workplace risk assessment, should compile a list of all radiation sources being present. By means of information from the manufacturer (e. g. manual, Internet) or operating instructions, details like spectral (ir-)radiances as function of diverse lamp parameters or photometric data sheets depending on distance and spot/flood operation can be applied for a first BLH risk estimation. If such information is not available, comparable workplaces already having been assessed can also be regarded; however, considering actual on-site conditions like distances to the lamps, exposure durations, viewing angles, employees' movements, etc.
Finally, if it is still unclear whether the BLH ELV is exceeded or not, (ir-)radiances have to be measured. Several influencing parameters exist that affect the determination.

1.2 Influencing Parameters

First of all, the **source and lamp technology** plays a major role. For example, LED spotlights can be associated with a significant BLH risk, but due to the LED's "narrow" band light emission, detrimental health effects from other spectral components, i. e. UV or IR, are rather unlikely. It can also be of importance whether the output lens, for example, has a smooth glass surface or is a Fresnel lens, and whether a diffusor has been integrated or not. This can lead to an inhomogeneous emission of optical radiation complicating radiance measurements with different field of views (FOV).
Directly connected to their technologies are the **lamps' adjustable parameters**. Probably the most prominent one is the CCT that can have an immense impact on the BLH risk. In general, higher CCTs (cool-white light) pose an increased BLH risk. Obviously, the dimmer intensity, i. e. the percentage of maximum light emission, and the zoom (spot or flood) are of equal importance. For the latter, Weber et al. give a so-called reduction factor accounting for different beam angles (Weber 2018).

A simple but effective protective measure reducing exposures to optical radiation is the increase of **distance** to the lamp, at least as long as the related ELVs are expressed as irradiances or radiant exposures. Then, for more or less point-like sources, the inverse square law can be applied, see Eq. 2.12, describing that, for example, a doubling of the distance decreases the irradiance to a quarter. However, most lamps have extended **source sizes** α that must be taken into account. Applying the common rule of thumb "The inverse square law can be applied beginning at a distance of 5 times the source dimension" leads to an error smaller than 1 % according to IEC TR 62471-2.

Physical radiances refer to the α-dependent solid angle, but they are no function of distance assuming an ideal, loss-free surrounding. For the risk assessment of workplaces, however, measurement devices are required that allow the determination of spatially averaged radiances based on certain fixed FOVs or **acceptance (averaging) angles** γ, see Section 2.1.2. In this way, typical eye movements blurring the retinal picture are considered (ICNIRP 2013). Such "biological" radiances can have a complex distance dependence, see Section 5.2.

Averaging angles can also take the real **exposure scenario** into account. This is probably the most important but also the most imprecise influencing factor of all. For example, it makes a huge difference whether the employee is forced to look towards the spotlights (e. g. the newscaster) or has them in the back (e. g. the cameraman). Additionally, the newscaster might talk to a guest during the broadcast and just looks occasionally in the light sources' directions. Depending on his head movements, the averaging angle either can be quite large or certain spotlights can be excluded completely from the risk assessment. The International Commission on Non-Ionizing Radiation Protection (ICNIRP) states that "If the visual task and the behavior can be characterized, a safety analysis can account for more realistic eye movements and a larger averaging angle [author's note: $\gamma > 110\,\mathrm{mrad}$] can be used" (ICNIRP 2013). It should also be mentioned that bright light sources are usually accompanied by a strong glare, and the natural aversion response leads to a reduced exposure duration.

Even if all influencing factors are well known, there always exists the instrument's **measurement uncertainty**, in particular, with regard to radiances. In addition, the operator's experience can have a significant impact on the measurement outcome. Altogether, the sum of potential error sources is high so that a simplified method might be accurate enough for workplace risk assessment.

1.3 Standards

It can also be supportive for a workplace risk assessment when lamps are classified according to certain standards. The most prominent one is certainly "The Lamp Safety Standard" EN 62471. Initially published in 2002, the CIE S009 was based on the ANSI/IESNA recommended practice document series RP 27. Four years later, the first edition of IEC 62471, being identical to CIE S009, was prepared, and in 2008 the European Standard was released (Sliney 2016, Schulmeister 2019). Therein, a risk group (RG) classification is presented that depends on the compliance of emission limits for wavelengths within 200 – 3000 nm. A brief RG overview is given in Tab. 1.1.

The RG classification must be performed at a distance of 200 mm to the radiation source or, for GLS lamps, at the location where an illuminance of 500 lx is measured. RG 0 and RG 1 are usually considered being safe for consumers and thus also for workers. The RGs provide valuable information supporting risk assessment; however, the standardized classification distances are not useful in practice. Additionally, a high-power spotlight with RG 3 does not necessarily mean that there is a severe health threat at the workplace. For example, the lamp parameters can be set in such a way that all ELVs are complied with. The real exposure situation can be even more vague for RG2.

Tab. 1.1 Risk groups (RG) according to EN 62471.

RG 0	no photobiological risk even for long intentional viewing (exempt group)
RG 1	low risk, limited photobiological risk considering restrictions due to normal human behavior
RG 2	medium risk, limited photobiological risk taking aversion response and thermal uneasiness into account
RG 3	high risk, photobiological risk even for unintended short exposure

During the preparation of this report, a new RG classification system for “Light Sources and Luminaires Primarily Emitting Visible Radiation” (IEC 62471-7) has been developed. The 7th part of the 62471 series, among others, not only introduces different application-related BLH emission levels but also an additional assessment distance. Unfortunately, due to the current status of the standard (Committee Draft for Voting, CDV) no further information can be provided here.

There also exists an “Application of IEC 62471 for the Assessment of Blue Light Hazards to Light Sources and Luminaires” (IEC TR 62778) that focuses, among others, on CCT. Therein, (il-)luminances are given depending on certain CCT ranges that enable assigning the lamp of interest to RG 1 or lower if, for example, E_v is smaller than 4000 lx at a CCT below 2350 K. Indeed, this can also be supportive for workplace risk assessment. However, as already mentioned above, RG 0 and RG 1 are usually considered as safe, and if the (il-)luminance values are higher than those listed in IEC 62778, the only message would be that the lamp is potentially unsafe. In any case, (il-)luminances must be determined that can also be used for a comparison with the BLH ELV via the BLH efficacy of luminous radiation, $K_{\mathrm{B,v}}$, see Eq. 2.20.

Several other standards exist, for example, limiting the radiation emission from work equipment or describing the measurement procedure for a workplace risk assessment: EN 12198-1 “... gives advice to manufacturers for the construction of safe machinery ...” whereas EN 14255-2 determines measurement and assessment methods.

1.4 BLH Assessment Methods

It has been recognized that radiance measurements may be challenging for workplace risk assessment, and some researchers provide simplified methods, especially for BLH. Schulmeister et al. (Schulmeister 2011, Schulmeister 2013) report about a “Simplified Method to Assess the UV and Blue Light Hazard of Lamps” by determining so-called U-factors. These transformation factors are the ratios of either actinic, UVA, or BLH weighted irradiances to illuminance, the latter being identical to $K_{\mathrm{B,v}}$.
The same group of authors describe two other simplified methods to find out an ELV exceedance. They argue that light is only hazardous to the eyes when there is a strong effect of glare and when the exposed person is forced to stare into the light source, for example, due to its work task (Weber 2011). In addition, a known surface temperature can be used to estimate an exceedance of exposure limit values accounting for thermal detrimental health effects. These methods provide rather estimates; however, the presented flow charts can be supportive for workplace risk assessment.

The lamp safety standard EN 62471 described in the previous section not only introduces a risk group classification but also gives two indirect radiance determination methods: an optical imaging and an alternative one, the latter being explained in Section 2.1.1. Regarding the alternative method, the aperture diameter would be 340 µm at a distance of 200 mm with $\gamma = 1.7$ mrad for RG 3 lamps. In practice, such a hot-spot search would take too much time and therefore is not applicable at workplaces.
Weber et al. adapted the alternative method to a workplace situation by using an open FOV instead of the required 80° and by replacing the measurement aperture by the output lens of the spotlight (Weber 2018). This procedure will be used as one of the main measurement methods for this work. Later on, it will also be extended to illuminances because BLH weighted radiances can be calculated in conjunction with $K_{B,v}$. Hereinafter, this approach will be denoted as “Planck Approximation”.

Liu et al. applied a spectroradiometer to determine the relative spectral power distribution of LEDs and compact fluorescent lamps and an imaging luminance meter to find the maximum luminance (Liu 2014). By means of $K_{B,v}$, they evaluated BLH risks. A comparable approach was pursued by Fiorentin and Scroccaro (Fiorentin 2014); however, without the use of $K_{B,v}$. In general, two-dimensional BLH risk assessment methods using digital imaging luminance measuring devices are more frequently applied in order to find BLH hot spots (Haferkemper 2019), especially for non-uniform lights sources (Shibuya 2021). However, such measuring devices are usually expensive, and the BLH analysis is rather complex with several potential sources of error (Słomiński 2016); thus, making them impractical for a simplified workplace risk assessment.

1.5 Project Objectives

At the beginning, several instruments will be tested with regard to their measurement accuracies/errors starting by means of a calibrated radiance standard (Bentham SRS8, Section 4.1), and increasing the measurement challenge from a Fresnel lens LED spotlight (ARRI L7-C, Section 4.2) to a washbeam luminaire with 19 LEDs (Robe Robin Spiider, Section 4.3). The outcome is very important to get an idea of how accurate BLH weighted quantities can be measured, especially in the context of a simplified risk assessment approach.
In a second step, the influence of selected lamp parameters on BLH will be evaluated. The role of white-light generation will be investigated exemplarily for the ARRI L7-C and the Robe Spiider. The effect of different CCTs as well as of various output powers (dimmer intensities) will be examined by means of $K_{B,v}$. BLH weighted radiances will be measured or calculated as a function of the detector to lamp distance in order to learn about their complex distance dependence.

The overarching goal of project F 2483 is the development of a simplified BLH measurement or assessment approach that is sufficiently accurate to be applied at workplaces. Therefore, all project findings up to now will be compiled. The proposed method is denoted “Planck Approximation”, and it will be evaluated, among others, at a test workplace with several spotlights.

The main topics are listed below together with some key questions.

(1) **Instrument Comparison**

→ What instruments are sufficiently accurate to allow for an E_{B} to L_{B} conversion via the solid angle?

→ Are there accuracy differences between integrating devices and spectroradiometers?

→ Can illuminances be supportive for BLH risk assessment via $K_{\mathrm{B,v}}$?

(2) **Influencing Factors**

→ How is white light generated and how does this affect BLH?

→ Do $K_{\mathrm{B,v}}$ values determined experimentally for some spotlights as a function of T_{cp} agree with those for a blackbody radiator?

→ What correlation exists between dimmer intensity and BLH?

→ Can distance dependent BLH weighted radiances be determined via calculation?

(3) **Workplace Risk Assessment**

→ Is a simplified approach, the Planck Approximation, sufficiently accurate to rely on maximum permissible exposure durations (MPEs) determined with it?

→ Can a single illuminance measurement suffice for a complete BLH risk assessment, even for various distances?

→ What parameters affect the Planck Approximation?

Note: Due to unrealizable, very large measurement distances and a lack of appropriate instruments, a 1.7 mrad FOV will not be analyzed within this project. In addition, glare is also no part of this report, but information can be found, for example, in publications by Reidenbach et al. (Reidenbach 2008, Reidenbach 2014).

2 Fundamentals

2.1 Basic Quantities

According to the European Directive 2006/25/EC, the term “optical radiation” refers to photons with wavelengths $\lambda = c\nu^{-1}$ ranging from 100 nm to 1 mm. $c = 300\,000\,\mathrm{km\,s^{-1}}$ is the vacuum speed of light and ν is its frequency. This electromagnetic spectral region is divided into ultraviolet (UV), visible (VIS, light), and infrared radiation (IR) with three UV and IR subgroups each, see Fig. 2.1.

A fundamental description of N monochromatic photons can be made by means of radiant energy

$$Q = Nh\nu \qquad [Q] = \mathrm{J} \tag{2.1}$$

with Planck’s constant $h = 6.626 \times 10^{-34}\,\mathrm{J\,s}$. The change of Q with time t is called radiant power or radiant flux Φ.

$$\Phi = h\nu\frac{\mathrm{d}N}{\mathrm{d}t} \qquad [\Phi, \Phi_\mathrm{v}] = \mathrm{W, lm} \tag{2.2}$$

The perceived power of visible radiation, indicated by a subsript v, is termed luminous power or luminous flux Φ_v see also Section 2.3.1. To account for polychromatic radiation, an integration must be performed for the frequency distribution of the N photons.

$$\Phi = h\int_0^\infty \frac{\mathrm{d}^2N}{\mathrm{d}t\,\mathrm{d}\nu}\,\nu\,\mathrm{d}\nu \tag{2.3}$$

Usually, the measurement of radiant power is conducted with respect to a surface of area A yielding the measurands irradiance E (or flux density) or illuminance E_v.

$$E = \frac{\mathrm{d}\Phi}{\mathrm{d}A} \qquad [E] = \mathrm{W\,m^{-2}} \quad [E_\mathrm{v}] = \mathrm{lx} = \mathrm{lm\,m^{-2}} \tag{2.4}$$

Detecting the radiant/luminous power received by a surface for a certain time $\Delta t = t_\mathrm{f} - t_\mathrm{i}$ results in a dose called radiant or luminous exposure.

$$H = \int_{t_\mathrm{i}}^{t_\mathrm{f}} \frac{\mathrm{d}\Phi\,(t')}{\mathrm{d}A}\mathrm{d}t' = E\Delta t \qquad [H, H_\mathrm{v}] = \mathrm{J\,m^{-2}, lx\,s} \tag{2.5}$$

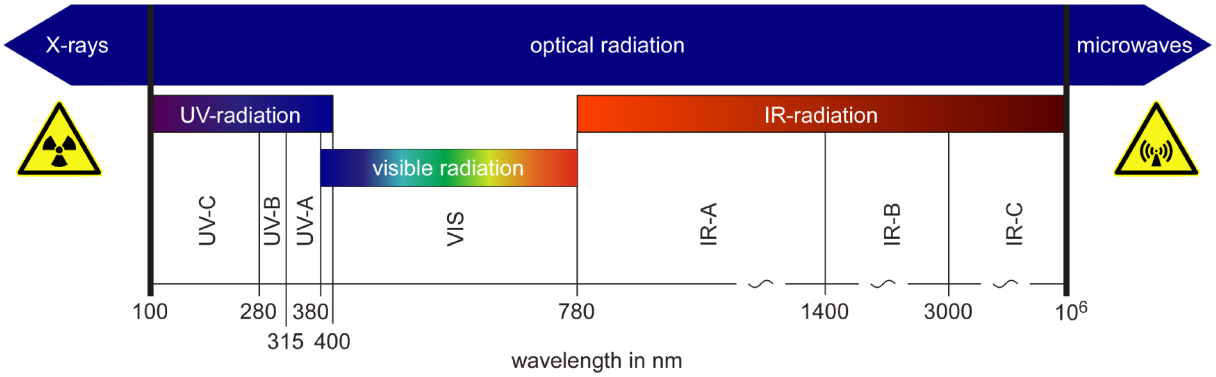

Fig. 2.1 Part of the electromagnetic spectrum visualizing the wavelength range of optical radiation and its division in several spectral bands.

2.1.1 Solid Angle Dependence

For most radiation sources, Φ or Φ_v are not emitted spatially equal, and the solid angle Ω must be considered. It can be calculated either with the area of a spherical calotte A_sc and the sphere's radius R or with the resulting cone's opening angle γ.

$$\Omega = \frac{A_\mathrm{sc}}{R^2} = 2\pi \left[1 - \cos\left(\frac{\gamma}{2}\right)\right] \qquad [\Omega] = \mathrm{m^2\,m^{-2}} = \mathrm{sr} \tag{2.6}$$

Being physically correct, the solid angle is a dimensionless quantity; however, Ω is usually given in units of steradian. The radiant or luminous power emitted per solid angle follows as

$$I = \frac{\mathrm{d}\Phi}{\mathrm{d}\Omega} \qquad [I] = \mathrm{W\,sr^{-1}} \quad [I_\mathrm{v}] = \mathrm{lm\,sr^{-1}} = \mathrm{cd} \tag{2.7}$$

and is termed radiant or luminous intensity. The quotient of I or I_v to an emitting surface of area A being tilted by ϵ is called radiance L or luminance L_v.

$$L = \frac{\mathrm{d}^2\Phi}{\mathrm{d}A\,\cos\epsilon\,\mathrm{d}\Omega} \overset{\epsilon = 90°}{=} \frac{\mathrm{d}E}{\mathrm{d}\Omega} \qquad [L, L_\mathrm{v}] = \mathrm{W\,m^{-2}\,sr^{-1}}, \mathrm{cd\,m^{-2}} \tag{2.8}$$

Similar to H, the radiance dose D (sometimes G) in $\mathrm{J\,m^{-2}\,sr^{-1}}$ is obtained by a time integration of Eq. 2.8. An overview of the main optical quantities is given in Tab. 2.1.

Tab. 2.1 Overview of selected radiometric and photometric quantities, their symbols and units. Cross-references to the related equations are listed, too.

Quantity	Symbol	Unit	Eq.
radiant energy	Q	J	2.1
luminous energy	Q_v		
radiant power/flux	Φ	W	2.2
luminous power/flux	Φ_v	lm	
irradiance	E	$\mathrm{W\,m^{-2}}$	2.4
illuminance	E_v	$\mathrm{lx} = \mathrm{lm\,m^{-2}}$	
radiant exposure	H	$\mathrm{J\,m^{-2}}$	2.5
luminous exposure	H_v	lx s	
radiant intensity	I	$\mathrm{W\,sr^{-1}}$	2.7
luminous intensity	I_v	$\mathrm{cd} = \mathrm{lm\,sr^{-1}}$	
radiance	L	$\mathrm{W\,m^{-2}\,sr^{-1}}$	2.8, 2.9
luminance	L_v	$\mathrm{cd\,m^{-2}}$	
radiance dose	D, G	$\mathrm{J\,m^{-2}\,sr^{-1}}$	

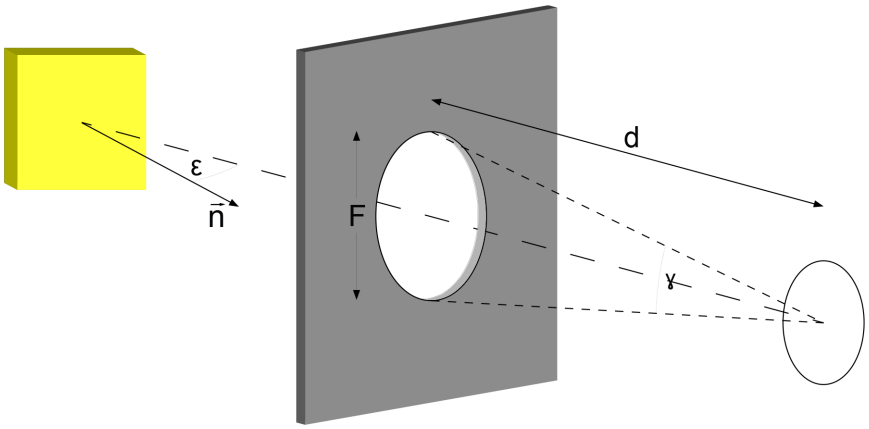

Fig. 2.2 Alternative method according to EN 62471 to determine L. The yellow colored square indicates a radiation source being tilted by ϵ with regard to the optical axis (long dashed line). The circle represents a detector being positioned at a distance d to an aperture with diameter F that must be placed close to the radiation source. γ denotes the limited FOV. Adapted from Bauer 2017.

In case of perpendicular incidence, $\epsilon = 90°$, radiances or luminances can be calculated from E or E_v measurements by using an aperture with diameter F that is placed at a distance of d to the detector, see Fig. 2.2. Applying a small angle approximation, $\tan\gamma \approx \gamma$, the detector's field-of-view (FOV) is given by $\gamma = Fd^{-1}$, and this angle can be used in Eq. 2.6. Alternatively, the area of the spherical calotte, A_sc, can be approximated by a plane surface with $A = \frac{1}{4}F^2\pi$, and in conjunction with Eq. 2.8 the radiance expression follows as

$$L = \frac{4}{\pi}\left(\frac{d}{F}\right)^2 E. \tag{2.9}$$

This approach is described, for example, in the lamp safety standard EN 62471.

2.1.2 Averaging Angles

Considering current occupational safety and health recommendations (ICNIRP 2013), radiances must account for eye movements. Biophysical limitations lead to a minimum angular subtense (often referred to as source size) of $\alpha_\mathrm{min} = 1.5\,\mathrm{mrad}$ for point-like radiation sources. Involuntary eye movements blur the retinal image, and for long exposure durations, $t \geq 1000\,\mathrm{s}$, task-determined eye movements dominate with an angular subtense of at least 100 mrad. These eye movements are considered by the (acceptance) averaging angle for photochemically induced retinal damages, γ_ph.

$$\gamma_\mathrm{ph} = \begin{cases} 11\,\mathrm{mrad} & t < 100\,\mathrm{s} \\ 1.1\,\mathrm{mrad}\,\sqrt{t} & 100\,\mathrm{s} \leq t \leq 10\,000\,\mathrm{s} \\ 110\,\mathrm{mrad} & t > 10\,000\,\mathrm{s} \end{cases} \tag{2.10}$$

Note that ICNIRP writes: "If the visual task and the behavior can be characterized, a safety analysis can account for more realistic eye movements and a larger averaging angle can be used."

There is some confusion about the application of γ_{ph} because the lamp safety standard EN 62471 defines different values and an additional time base. Therein, the source size that must be determined by the 50 % emission points is limited by $\alpha_{\text{min}} = 1.7\,\text{mrad}$ and $\alpha_{\text{max}} = 100\,\text{mrad}$. In addition, exposure durations shorter than 10 s are not related to a minimum averaging angle of 11 mrad, see Eq. 2.10, but γ_{ph} must be calculated according to line 1 of Eq. 2.11. The authors of EN 62471 have recognized the discrepancy between the third and fourth line of Eq. 2.11, but they adhere to $\alpha_{\text{max}} = 100\,\text{mrad}$. The European Standard EN 14255-2 prescribes identical measurement conditions.

$$\gamma_{\text{ph}} = \begin{cases} 1.7\,\text{mrad}\ \sqrt{4t} & 0.25\,\text{s} \leq t \leq 10\,\text{s} \\ 11\,\text{mrad} & 10\,\text{s} \leq t \leq 100\,\text{s} \\ 1.1\,\text{mrad}\ \sqrt{t} & 100\,\text{s} \leq t \leq 10\,000\,\text{s} \\ 100\,\text{mrad} & t \geq 10\,000\,\text{s} \end{cases} \tag{2.11}$$

The situation gets even more complicated because the European Directive 2006/25/EC does not contain any γ_{ph} requirements but only differentiates the BLH exposure limit values with respect to α, see Section 2.3.3. Hereinafter, the averaging angles 1.7, 11, and 100 mrad will be used because the radiance measurement devices XD-45-HB-SRT200 and the LDM-9811, see Section 3.1, are only designed to account for these γ_{ph}.

The averaging angles given in line 1 of Eq. 2.11 can also be applied for the assessment of thermal retinal hazards; however, the time limits must be expanded: $\gamma_{\text{th}} = 1.7\,\text{mrad}$ even for exposure durations shorter than 0.25 s, and for $t > 10\,\text{s}$, $\gamma_{\text{th}} = 11\,\text{mrad}$ is maximum. In contrast, ICNIRP recommends that $\gamma_{\text{th}} = 11\,\text{mrad}$ for exposure durations $t \geq 0.25\,\text{s}$, and add the criteria $\gamma_{\text{th}} = 5\,\text{mrad}$ for pulses shorter than 0.25 s (ICNIRP 2013).

2.2 Distance Dependence

2.2.1 Inverse Square Law

Irradiances decrease with growing distance d to the emitting source, and the related mathematical description is called inverse square law.

$$E = \frac{a}{d^2} + E_\infty \qquad \text{or} \qquad E_1 d_1^2 = E_2 d_2^2 \tag{2.12}$$

The parameter a describes the medium's (e.g. air) attenuation of radiation, and $E_\infty = \lim_{r\to\infty} E$ approaches zero. Consequently, doubling the distance leads to one fourth of the initial irradiance. If the photons do not pass different attenuating media, the product of irradiance and distance is constant (right side of Eq. 2.12). Note that the inverse square law is only valid for point sources or at a sufficiently long distance where the source size is point-like.

2.2.2 Physical and Spatially Averaged Radiances

In contrast to irradiances with an inverse square distance dependence, radiances (and luminances) can be constant. It is important to understand the differences between spatially averaged radiances, $L_{E,\gamma}$, and "physical" ones referring to the angular subtense of the radiation emitting source, $L_{E,\alpha}$, both based on irradiance measurements. For

example, a homogeneously emitting circular lens of diameter $D = 100\,\text{mm}$ is seen at a distance $d = 5\,\text{m}$ with a source size

$$\alpha = 2\arctan\left(\frac{D}{2d}\right) \approx \frac{D}{d} = 20\,\text{mrad} \tag{2.13}$$

under a solid angle $\Omega = 3.1 \times 10^{-4}\,\text{sr}$, see Eq. 2.6. Assuming a detected irradiance (open FOV) of $E = 1\,\text{W}\,\text{m}^{-2}$, the "physical" radiance can be determined via Eq. 2.9 yielding $L_{E,\alpha} = 3.2\,\text{kW}\,\text{m}^{-2}\,\text{sr}^{-1}$. If the exposure endures, e.g. for 100 s, then $\gamma_{\text{ph}} = 11\,\text{mrad}$ must be used, see Eq. 2.10. The associated solid angle is given by $\Omega = 9.5 \times 10^{-5}\,\text{sr}$, and the averaged radiance is more than three times higher with $L_{E,11} = 10.5\,\text{kW}\,\text{m}^{-2}\,\text{sr}^{-1}$.

According to the inverse square law, see Eq. 2.12, the initial irradiance is reduced to one quarter, $E = 0.25\,\text{W}\,\text{m}^{-2}$, at a distance of 10 m. However, Eq. 2.9 has a d^2 dependence yielding a factor of 4; thus, $L_{E,\alpha}$ still has a value of $3.2\,\text{kW}\,\text{m}^{-2}\,\text{sr}^{-1}$. This cancellation is not present for a fixed FOV, but $L_{E,\gamma}$ changes with distance: again using $\gamma_{\text{ph}} = 11\,\text{mrad}$ and $\Omega = 9.5 \times 10^{-5}\,\text{sr}$, $L_{E,11} = 2.6\,\text{kW}\,\text{m}^{-2}\,\text{sr}^{-1}$ is reduced to one fourth.

With respect to direct radiance measurements, L_γ, the relation of α to γ must be considered. At the beginning, the measurement spot size related to a certain γ (gray) is smaller than the circular lens of a homogeneously emitting lamp (red hatched yellow), $\gamma < \alpha$, see Fig. 2.3. In perspective, the source size decreases upon increasing the distance whereas the measurement spot gets larger. As long as $\gamma \leq \alpha$, the measured radiance, L_γ, will be constant and equal to $L_{E,\alpha}$. Upon further increasing the distance, the radiance detector's FOV becomes larger than the lamp's source size, $\gamma > \alpha$, so that L_γ no longer represents the physical radiance but declines with d^{-2}. For any distance, spatially averaged radiances, $L_{E,\gamma}$, will always show the prominent d^{-2} dependence.

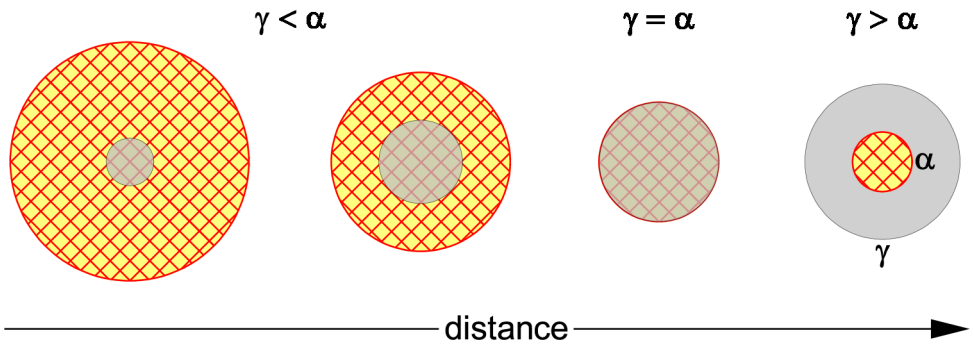

Fig. 2.3 Source size α (red hatched yellow circles) and averaging angle γ (gray circles) from the detector's perspective depending on distance.

2.3 Weighting and Risk Assessment

2.3.1 Relative Spectral Sensitivities

Optical radiation can affect human skin or eyes in many different ways depending on the wavelength region of interest. The relative spectral sensitivities of these radiation-induced biological effects are called action spectra or weighting functions. They are not spectrally separated from each other but they can overlap. For example, certain visible wavelengths can lead to photochemical as well as photothermal retinal injuries. The following section briefly explains some of these action spectra.

UVR Hazards
Excessive exposure to UVR is accompanied by adverse health effects. An overexposure of the anterior eye tissues (cornea and conjunctiva), particularly with $\lambda < 300\,\text{nm}$ (ICNIRP 2004), can lead to acute photokeratitis and conjunctivitis. UVR with wavelengths above ~295 nm can reach the lens and induce cataracts. The human skin reacts with reddening (erythema) to an intense UV irradiation, depending on the Fitzpatrick skin type (Fitzpatrick 1988), and a chronic UVR exposure increases the skin cancer risk. ICNIRP has taken these adverse health effects into account, and developed an envelope UVR action spectrum, $S(\lambda)$, see Fig. 2.4, occupying the wavelength region from 180 nm to 400 nm (ICNIRP 2004) with a maximum at 270 nm. Mathematical approximations to $S(\lambda)$ exit; however, only for $\lambda \geq 210\,\text{nm}$.

$$S(\lambda) = \begin{cases} 0.959^{(270-\lambda)} & 210\,\text{nm} \leq \lambda \leq 270\,\text{nm} \\ 1 - 0.36\left(\frac{\lambda-270}{20}\right)^{1.64} & 270\,\text{nm} < \lambda \leq 300\,\text{nm} \\ 0.3 \times 0.736^{(\lambda-300)} + 10^{(2-0.0163\lambda)} & 300\,\text{nm} < \lambda \leq 400\,\text{nm} \end{cases} \quad \textbf{(2.14)}$$

Photochemical Retinal Hazards
Two types of photochemically induced retinal damages are known. Comparably short exposures to bright light sources in the order of 10 s to 2 h are accompanied by radiation absorption in the retinal pigment epithelium and the choroid (ICNIRP 2013). The related damage is usually referred to as Blue-Light Hazard (BLH) or as Type II photochemically induced retinal damage. In contrast, for continued exposures over several days it is suggested that the photoreceptors themselves can be harmed due to the bleaching of rhodopsin (Type I). Taking characteristic exposure durations and the human aversion response to bright light sources into account caused ICNIRP to develop a BLH action spectrum, $B(\lambda)$ (ICNIRP 1997).

Starting at 300 nm, see Fig. 2.4, UVA radiation must be considered; thus, $B(\lambda)$ overlaps with ICNIRP's UVR hazards weighing function, $S(\lambda)$. The initial relative spectral sensitivity of 10^{-2} rapidly increases to the maximum located at 435 – 440 nm (for a healthy crystalline lens). There also exists an aphakic hazard function, $A(\lambda)$, that, however, will not be used within this report. $B(\lambda)$ decreases rather irregularly for longer wavelengths, and reaches its constant minimum of 10^{-3} at 590 – 700 nm. No mathematical expression is defined, but $B(\lambda)$ can be approximated by a sum of Gaussian functions (Chaopu 2018).

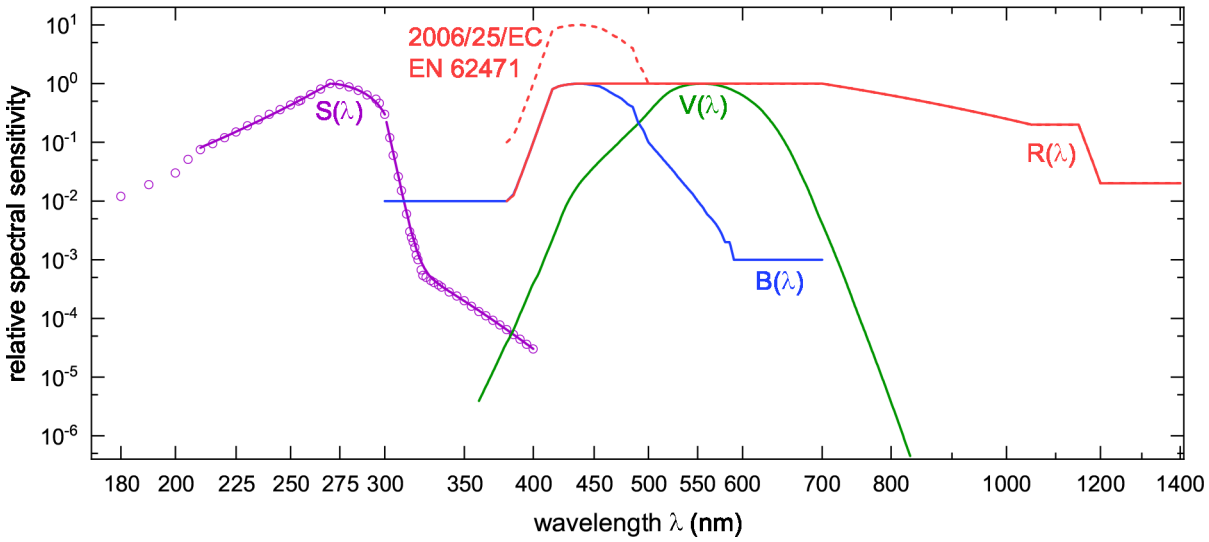

Fig. 2.4 Double-logarithmic presentation of relative spectral sensitivities for UVR hazards to human skin and eyes, $S(\lambda)$ (ICNIRP 2004), for photochemical, $B(\lambda)$, and for thermal retinal hazards, $R(\lambda)$ (ICNIRP 2013). The dashed line depicts $R(\lambda)$ given in the EU Directive 2006/25/EC and standardized in EN 62471, based on ICNIRP 1997. The spectral luminous efficiency for photopic vision, $V(\lambda)$, is equal to the CIE 1931 color-matching function $\bar{y}(\lambda)$ (ISO/CIE 11644-1). Discrete $S(\lambda)$ values (open circles) can be described by the interpolation formulas 2.14.

Retinal Thermal Hazards, RTH

Besides photochemically induced retinal damages, visible radiation also contributes to thermal hazards of the iris and the retina. IRA radiation can be focused on the retina and must also be considered. The relevant wavelengths cover 380 – 1400 nm. It is important to note that a retinal thermal injury varies with the exposed area. As a consequence, radiances must be assessed that take source sizes, α, into account, see Tab. 2.2.

The RTH function, $R(\lambda)$, starts at 380 nm and is equal to the BLH action spectrum up to its maximum. For longer wavelengths, it can be described mathematically.

$$R(\lambda) = \begin{cases} 1 & 435\,\text{nm} \le \lambda \le 700\,\text{nm} \\ 10^{(700-\lambda)/500} & 700\,\text{nm} \le \lambda \le 1050\,\text{nm} \\ 0.2 & 1050\,\text{nm} \le \lambda \le 1150\,\text{nm} \\ 0.2 \times 10^{0.02\,(1150-\lambda)} & 1150\,\text{nm} \le \lambda \le 1200\,\text{nm} \\ 0.02 & 1200\,\text{nm} \le \lambda \le 1400\,\text{nm} \end{cases} \qquad \textbf{(2.15)}$$

It is given in the European Directive 2006/25/EC and is standardized in (EN 62471); however, it dates back to the year 2008 when the revision of the 1997 ICNIRP guidelines has not been published yet. This “older” $R(\lambda)$ is by a factor of 10 higher than the BLH weighting function within 380 – 500 nm.

Photopic Vision

The aforementioned weighting functions consider detrimental health effects caused by optical radiation. With this report’s main focus on BLH, it is also important to take the

brightness perception of the human eye into account. The associated “action spectrum” is called the photopic luminous efficiency function or briefly the luminosity function, $V(\lambda)$, see Fig. 2.4, ranging from 380 to 830 nm. Its maximum relative spectral sensitivity at $\lambda = 555\,\text{nm}$ reflects the human eye’s perception of green light as the brightest one. Hereinafter, $V(\lambda)$ for a CIE 1931 standard colorimetric 2° observer will be used (ISO/CIE 11644-1) although it is questioned not to rebuild the real human visual perception of brightness (Judd 1951, Vos 1978, Sharpe 2005). There exists a similar function for scotopic vision, $V'(\lambda)$, that, however, will not be applied within this project.

2.3.2 Weighting/Convolution

Weighting is a main concept of optical radiation risk assessment because many biological effects are wavelength dependent as described in the previous Section 2.3.1. Radiometric (unweighted) quantities thus play a minor role. In general, the mathematical process of weighting, i. e. the convolution, is given by

$$X_{\text{biol}} = \int_{\lambda_{\text{min}}}^{\lambda_{\text{max}}} X(\lambda)\, A_{\text{biol}}(\lambda)\, \mathrm{d}\lambda \tag{2.16}$$

with $X(\lambda)$ representing a spectral optical quantity like irradiance or radiance and $A_{\text{biol}}(\lambda)$ as the relative spectral effectiveness for a certain biological effect. λ_{min} and λ_{max} are the wavelength boundaries within $A_{\text{biol}}(\lambda)$ is defined and for that $X(\lambda)$ is nonnegative. The convolution’s result, X_{biol}, is the biologically effective (weighted) quantity.

Regarding photochemically induced retinal damages, the BLH weighted irradiance, E_{B}, is determined by the convolution of the spectral irradiance, $E(\lambda)$, and the BLH weighting function, $B(\lambda)$, within 300 – 700 nm. BLH weighted radiances, L_{B}, are calculated similarly.

$$E_{\text{B}} = \int_{300\,\text{nm}}^{700\,\text{nm}} E(\lambda)\, B(\lambda)\, \mathrm{d}\lambda \tag{2.17}$$

Illuminance, E_{v}, is the convolution result of $E(\lambda)$ with the photopic luminous efficiency function, $V(\lambda)$, for wavelengths ranging from 360 – 830 nm.

$$E_{\text{v}} = K_{\text{m}} \int_{360\,\text{nm}}^{830\,\text{nm}} E(\lambda)\, V(\lambda)\, \mathrm{d}\lambda \tag{2.18}$$

The constant $K_{\text{m}} = 683\,\text{lm}\,\text{W}^{-1}$ represents the maximum spectral luminous efficacy. Replacing $E(\lambda)$ in Eq. 2.18 by spectral radiance, $L(\lambda)$, yields luminance, L_{v}.

These (ir-)radiances and (il-)luminances can be used to determine two additional quantities that may be helpful for risk assessment: The dimensionless BLH efficiency, η_{B}, that reflects the ratio of biologically weighted to radiometric (unweighted) irradiance, and the BLH efficacy of luminous radiation usually expressed in $\text{W}\,\text{klm}^{-1}$.

$$\eta_{\mathrm{B}} = E_{\mathrm{B}} \left[\int_{300\,\mathrm{nm}}^{700\,\mathrm{nm}} E(\lambda)\,\mathrm{d}\lambda \right]^{-1} \tag{2.19}$$

$$K_{\mathrm{B,v}} = \frac{E_{\mathrm{B}}}{E_{\mathrm{v}}} = \frac{L_{\mathrm{B}}}{L_{\mathrm{v}}} \tag{2.20}$$

$K_{\mathrm{B,v}}$ is often presented as a function of T_{cp} because many white-light sources are close to the Planckian Radiator's $K_{\mathrm{B,v}}(T_{\mathrm{cp}})$, see Section 2.4.2. η_{B} and $K_{\mathrm{B,v}}$ can be calculated with radiances and luminances, too. Both quantities are standardized by the International Electrotechnical Commission (IEC) (IEC TR 62778).

2.3.3 Exposure Limit Values

ICNIRP 2013 recommends a maximum effective radiance dose, $D_{\mathrm{B}} = 10^6\,\mathrm{J\,m^{-2}\,sr^{-1}}$ that shall be applied for $0.25\,\mathrm{s} \leq t \leq 10\,000\,\mathrm{s}$, whereas the European Directive 2006/25/EC dictates an effective radiance, L_{B}, that depends reciprocally on t without a lower exposure duration limit. Concerning the BLH ELV for small sources, $\alpha < 11\,\mathrm{mrad}$, exposure durations $t > 10\,000\,\mathrm{s}$ are limited by $E_{\mathrm{B}} = 10\,\mathrm{mW\,m^{-2}}$ that is two orders of magnitude lower than ICNIRP's $E_{\mathrm{B}} = 1\,\mathrm{W\,m^{-2}}$ for $100\,\mathrm{s} \leq t \leq 30\,000\,\mathrm{s}$. These are just two examples of differences between the ICNIRP guidelines and the European Directive and other ones exist; however, they will not be discussed hereinafter.

Furthermore, the German Technical Rules Optical Radiation - Incoherent Optical Radiation (TROS IOS 2013) add an ELV regarding thermal hazards to the skin for $10\,\mathrm{s} \leq t \leq 1000\,\mathrm{s}$, see Tab. 2.2, that is not listed in the European Directive. An argumentation supporting the application of $E_{\mathrm{skin}} = 7.7 \times 10^3\,\mathrm{W\,m^{-2}}\ t^{-0.34}$ is presented in Berlien 2016. Therein, it is also recommended to apply the radiant dose, $H_{\mathrm{IR}} = 3 \times 10^6\,\mathrm{J\,m^{-2}}$ instead of the irradiance $E_{\mathrm{IR}} = 10^2\,\mathrm{W\,m^{-2}}$ as ELV for the protection of the lens against long term IR damage. As for the ICNIRP guidelines, additional differences are present regarding a comparison of the TROS IOS 2013 and the 2006/25/EC that will not be reported hereinafter.

An overview of ELVs for incoherent optical radiation that are compulsory in Germany is presented in Tab. 2.2. Not all of these ELVs will be used within this project report.

2.4 Colorimetry

The following two sections, "Chromaticity Coordinates" and "Correlated Color Temperature", are mostly taken from the appendix of Bauer 2021.

2.4.1 Chromaticity Coordinates

Chromaticity coordinates, (x, y, z), are very useful regarding the color definition of light sources or reflecting surfaces (Hunt 2011). Calculating (x, y, z) is a well-known procedure and is standardized, for example, by ISO/CIE 11644-3. Briefly summarizing the basic concept, the light emission or reflection is convoluted with each of the three color-matching functions of the CIE 1931 2° standard colorimetric observer, $(\overline{x}, \overline{y}, \overline{z})$. These functions were derived by a linear transformation of the experimentally determined

Tab. 2.2 Exposure limit values according to 2006/25/EC for UVR induced hazards to the eye and skin, for retinal photochemical (BLH) and thermal hazards (RTH), including weak visual stimulus (RTH, wvs), as well as for thermal hazards (TH) to the skin and cornea/lens. Radiances L_R and L_IR are given in $\mathrm{W\,m^{-2}\,sr^{-1}}$, source sizes α in mrad.

	ELV	duration	note
UV	180 – 400 nm		
	$H_\mathrm{eff} = 30\,\mathrm{J\,m^{-2}}$	8 h	
	$H_\mathrm{UVA} = 10^4\,\mathrm{J\,m^{-2}}$	8 h	315 – 400 nm
BLH	380 – 780 nm		
	$L_\mathrm{B} = 10^6\,\mathrm{J\,m^{-2}\,sr^{-1}}\ t^{-1}$	$t \le 10\,000\,\mathrm{s}$	$\alpha \ge 11$
	$L_\mathrm{B} = 10^2\,\mathrm{W\,m^{-2}\,sr^{-1}}$	$t > 10\,000\,\mathrm{s}$	
	$E_\mathrm{B} = 10^2\,\mathrm{J\,m^{-2}}\ t^{-1}$	$t \le 10\,000\,\mathrm{s}$	$\alpha < 11$
	$E_\mathrm{B} = 10^{-2}\,\mathrm{W\,m^{-2}}$	$t > 10\,000\,\mathrm{s}$	
RTH	380 – 1400 nm		
	$L_\mathrm{R} = \begin{cases} 8.89 \times 10^8\ C_\alpha^{-1} \\ 5 \times 10^7\ C_\alpha^{-1}\ t^{-0.25} \\ 2.8 \times 10^7\ C_\alpha^{-1} \end{cases}$	$\begin{matrix} t < 10\,\mu\mathrm{s} \\ 10\,\mu\mathrm{s} \le t \le 10\,\mathrm{s} \\ t > 10\,\mathrm{s} \end{matrix}$	$C_\alpha = \begin{cases} 1.7 & \alpha < 1.7 \\ \alpha & 1.7 \le \alpha \le 100 \\ 100 & \alpha > 100 \end{cases}$
RTH, wvs	780 – 1400 nm		
	$L_\mathrm{IR} = \begin{cases} 8.89 \times 10^8\ C_\alpha^{-1} \\ 5 \times 10^7\ C_\alpha^{-1}\ t^{-0.25} \\ 6 \times 10^6\ C_\alpha^{-1} \end{cases}$	$\begin{matrix} t < 10\,\mu\mathrm{s} \\ 10\,\mu\mathrm{s} \le t \le 10\,\mathrm{s} \\ t > 10\,\mathrm{s} \end{matrix}$	$C_\alpha = \begin{cases} 11 & \alpha < 11 \\ \alpha & 11 \le \alpha \le 100 \\ 100 & \alpha > 100 \end{cases}$
TH	380 – 3000 nm		
	$H_\mathrm{skin} = 2 \times 10^4\,\mathrm{J\,m^{-2}}\ t^{0.25}$	$t < 10\,\mathrm{s}$	
	$E_\mathrm{skin} = 7.7 \times 10^3\,\mathrm{W\,m^{-2}}\ t^{-0.34}$	$10\,\mathrm{s} \le t \le 1000\,\mathrm{s}$	see (Berlien 2016)
	$E_\mathrm{IR} = \begin{cases} 1.8 \times 10^4\,\mathrm{W\,m^{-2}}\ t^{-0.75} \\ 10^2\,\mathrm{W\,m^{-2}} \end{cases}$	$\begin{matrix} t \le 1000\,\mathrm{s} \\ t > 1000\,\mathrm{s} \end{matrix}$	780 – 3000 nm

color-matching stimuli for green, blue, and red because the latter contains undesired negative values. Due to the dependence on the observer's view, there also exist $(\overline{x}, \overline{y}, \overline{z})$ for a CIE 1964 10° standard observer (not used in this work). Multiplying the convolution by K_m yields the tristimulus values.

$$\begin{pmatrix} X \\ Y \\ Z \end{pmatrix} = K_\mathrm{m} \int_{360\,\mathrm{nm}}^{830\,\mathrm{nm}} E(\lambda) \begin{pmatrix} \overline{x} \\ \overline{y} \\ \overline{z} \end{pmatrix} (\lambda)\,\mathrm{d}\lambda \qquad \textbf{(2.21)}$$

Note the integration limits running from 360 – 830 nm in contrast to the BLH spectral region, 300 – 700 nm, or the visible wavelength range, 380 – 780 nm. Normalizing (X, Y, Z) results in relative magnitudes called the chromaticity (or color) coordinates.

$$\begin{pmatrix} x \\ y \\ z \end{pmatrix} = \frac{1}{X+Y+Z} \begin{pmatrix} X \\ Y \\ Z \end{pmatrix} \qquad x+y+z=1 \tag{2.22}$$

With their sum being equal to one, it is sufficient to specify color by only two variables, typically (x, y), providing the basis for two-dimensional chromaticity diagrams. The "color" of white-light sources is also expressed by chromaticity coordinates, usually referred to as white points. For example, the theoretical equal energy illuminant *E* with its constant, wavelength independent emission has the white point $x = y = 1/3$, and the chromaticity coordinates for the daylight illuminant *D65*, part of CIE's standard illuminant series *D*, are given by $x = 0.312\,73$ and $y = 0.329\,02$. In addition to the color definition, chromaticity coordinates can also be applied to calculate the correlated color temperature (CCT) of light sources.

2.4.2 Correlated Color Temperature

The spectral radiation emission of a blackbody radiator is determined by its absolute temperature, T, via

$$M(\lambda, T) = 2\pi hc^2 \lambda^{-5} \left[\exp\left(\frac{hc}{\lambda k_\mathrm{B} T} \right) - 1 \right]^{-1} \tag{2.23}$$

with $h = 6.626 \times 10^{-34}\,\mathrm{J\,s}$ (Planck's constant), $c = 3 \times 10^9\,\mathrm{m\,s^{-1}}$ (speed of light), and $k_\mathrm{B} = 1.38 \times 10^{-23}\,\mathrm{J\,K^{-1}}$ (Boltzmann's constant). M is called radiant exitance. For any light source with its chromaticity coordinates being close to the Planckian (blackbody) locus, absolute and correlated color temperature (CCT), T_cp, match each other. If (x, y, z) are not equal, T_cp refers to the absolute temperature of that blackbody radiator whose chromaticity coordinates are nearest to those of the light source in a uniform chromaticity scale diagram. Apart from several algorithms to find this smallest off locus colorimetric distance, McCamy derived a T_cp formula using a cubic polynomial,

$$T_\mathrm{cp} = an^3 + bn^2 + cn + d \tag{2.24}$$

with parameters $a = -473\,\mathrm{K}$, $b = 3601\,\mathrm{K}$, $c = -6861\,\mathrm{K}$, and $d = 5514.31\,\mathrm{K}$ (McCamy 1992). The inverse isotemperature line slope n is given by

$$n = \frac{x - x_\mathrm{e}}{y - y_\mathrm{e}} \tag{2.25}$$

and the T_cp epicenter is located at $x_\mathrm{e} = 0.3320$ and $y_\mathrm{e} = 0.1858$. While McCamy's equation is restricted to $2000\,\mathrm{K} \leq T_\mathrm{cp} \leq 12\,500\,\mathrm{K}$, Hernández-Andrés et al. could increase the T_cp range up to $8 \times 10^5\,\mathrm{K}$ by using a sum of exponential functions

$$T_\mathrm{cp} = A_0 + A_1 \exp\left(-\frac{n}{t_1}\right) + A_2 \exp\left(-\frac{n}{t_2}\right) + A_3 \exp\left(-\frac{n}{t_3}\right) \tag{2.26}$$

with two sets of parameters A_i and t_i, one for 3000 K $\leq T_{cp} \leq$ 50 000 K and another one for 50 000 K $\leq T_{cp} \leq 8 \times 10^5$ K (Hernández-Andrés 1999). The inverse slope n is defined in accordance to Eq. 2.25 but with different CCT epicenters, x_e and y_e.

It is worth mentioning that "there have been reports that CCT is not appropriate for a source like LEDs due to their spectral characteristics" (ICNIRP 2020). A comparison not only of Eq. 2.24 with Eq. 2.26 but also with additional CCT computation methods can be found in Li 2016. Finally, CCTs of radiation sources can be divided into three main groups regarding their color perception (prEN 12464-1):

warm	$T_{cp} < 3300$ K
intermediate	3300 K $\leq T_{cp} \leq$ 5300 K
cool	$T_{cp} > 5300$ K

2.5 BLH of Blackbody Radiators – the Planck Approximation

The absolute temperature, T, is the only variable that is necessary to describe the wavelength dependent radiation emission of a blackbody radiator. All parameters are physical constants, see Eq. 2.23. By means of a convolution with the action spectrum for BLH and with the photopic luminous efficiency function, $B(\lambda)$ and $V(\lambda)$, respectively, the BLH weighted irradiance and illuminance can be calculated as a function of T, see Eq. 2.17 and Eq. 2.18. However, it is more common to visualize the ratio of E_B to its unweighted radiometric pendant, η_B, or to the illuminance, $K_{B,v}$. A semi-logarithmic presentation of their T dependences is given in Fig. 2.5.

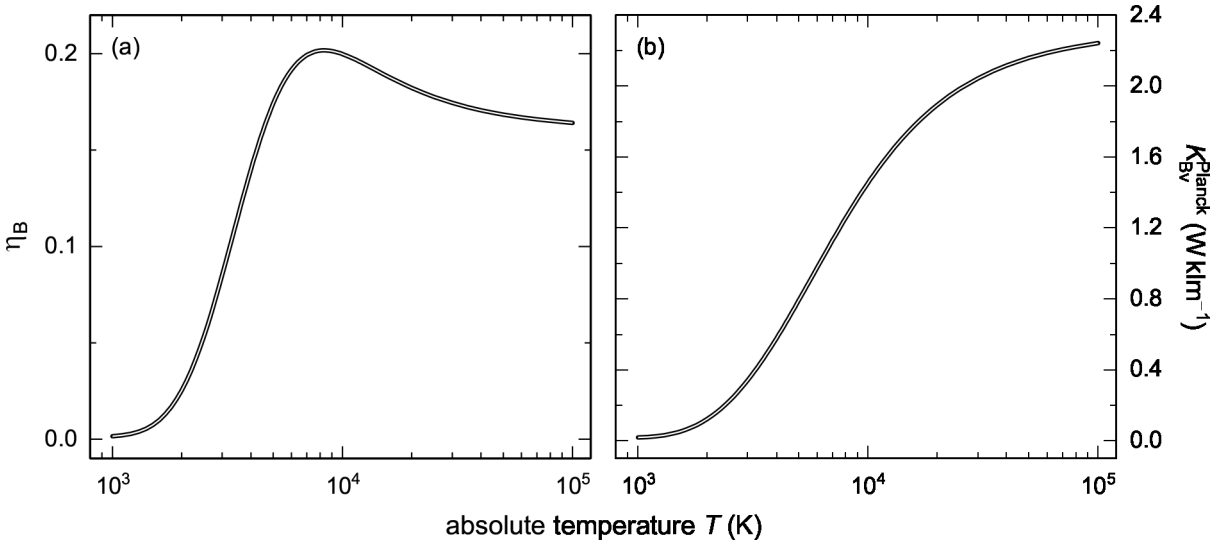

Fig. 2.5 (a) BLH efficiency, η_B and (b) BLH efficacy of luminous radiation, $K_{B,v}^{Planck}$, as a function of absolute temperature T for a blackbody radiator. Note the logarithmic T scale.

The $K_{\mathrm{B,v}}^{\mathrm{Planck}}$ data can be described empirically via an s-shaped five-parameter logistic function

$$K_{\mathrm{B,v}}^{\mathrm{Planck}} = K_{\infty}\left[1+\left(\frac{T_0}{T}\right)^{h}\right]^{-s} \tag{2.27}$$

with saturation value $K_{\infty} = (2.289 \pm 0.001)\,\mathrm{W\,klm^{-1}}$, $T_0 = (1573 \pm 32)\,\mathrm{K}$ as the temperature at which the curvature changes direction or sign, $h = 1.307 \pm 0.003$ as hill slope (steepness of curve), and with $s = 5.3 \pm 0.1$ reflecting the asymmetry regarding T_0 ($s = 1$ means symmetry). A selection of $K_{\mathrm{B,v}}^{\mathrm{Planck}}$ values for certain absolute temperatures is listed in Tab. 2.3.

Tab. 2.3 BLH efficacy of luminous radiation, $K_{\mathrm{B,v}}^{\mathrm{Planck}}$, given in $\mathrm{W\,klm^{-1}}$ according to Eq. 2.27 for a Planckian radiator that is described by Eq. 2.23 with absolute temperature T in K.

T	$K_{\mathrm{B,v}}^{\mathrm{Planck}}$	T	$K_{\mathrm{B,v}}^{\mathrm{Planck}}$	T	$K_{\mathrm{B,v}}^{\mathrm{Planck}}$	T	$K_{\mathrm{B,v}}^{\mathrm{Planck}}$
2000	0.123	3600	0.485	5400	0.869	8600	1.324
2100	0.142	3700	0.508	5600	0.906	8800	1.344
2200	0.161	3800	0.532	5800	0.941	9000	1.364
2300	0.182	3900	0.555	6000	0.975	9200	1.384
2400	0.203	4000	0.578	6200	1.008	9400	1.402
2500	0.226	4100	0.601	6400	1.040	9600	1.420
2600	0.248	4200	0.623	6600	1.071	9800	1.438
2700	0.271	4300	0.645	6800	1.100	10 000	1.455
2800	0.294	4400	0.667	7000	1.129	10 250	1.475
2900	0.318	4500	0.689	7200	1.157	10 500	1.494
3000	0.342	4600	0.710	7400	1.183	10 750	1.513
3100	0.366	4700	0.731	7600	1.209	11 000	1.531
3200	0.390	4800	0.752	7800	1.233	11 250	1.548
3300	0.413	4900	0.772	8000	1.257	11 500	1.565
3400	0.437	5000	0.792	8200	1.280	11 750	1.581
3500	0.461	5200	0.831	8400	1.302	12 000	1.596

Such a look-up-table can be helpful with regard to a simplified BLH workplace risk assessment method, that hereinafter will be denoted as “Planck Approximation”. According to Eq. 2.20, one illuminance measurement is enough to calculate E_{B} for known $K_{\mathrm{B,v}}$ and L_{B} via the solid angle. If $K_{\mathrm{B,v}}$ cannot be determined experimentally, the use of $K_{\mathrm{B,v}}^{\mathrm{Planck}}$ might serve as an approximation. It is one aim of this project to find out the applicability and accuracy of this Planck Approximation.

3 Metrology and Radiation Sources

3.1 Measurement Equipment

Several devices and detectors have been verified for this project regarding the comparability of their luminance and illuminance measurements or their BLH weighted radiances and irradiances. A brief description of each tested instrument is presented in the following focusing solely on project relevant details. Tab. 3.1 summarizes their measurands. Unless otherwise specified, the devices or sensors were calibrated by their manufacturers prior to the project measurements.

3.1.1 Radiometers

HD2402. The HD2402 multi-channel radiometer from Delta OHM is designed to detect radiation from several spectral bands. 7 of the instrument's 9 channels are assigned to sensors or to a laser module. Channels 4 and 8 are without usage.

①	alignment laser	
②	$S(\lambda)$ weighted UV radiometer	$220\,\text{nm} \leq \lambda \leq 400\,\text{nm}$
③	$R(\lambda)$ weighted IR radiometer	$660\,\text{nm} \leq \lambda \leq 1300\,\text{nm}$
⑤	UV-A radiometer	$315\,\text{nm} \leq \lambda \leq 400\,\text{nm}$
⑥	$V(\lambda)$ weighted Luxmeter	$380\,\text{nm} \leq \lambda \leq 780\,\text{nm}$
⑦	$B(\lambda)$ weighted radiometer	$400\,\text{nm} \leq \lambda \leq 600\,\text{nm}$
⑨	pyranometer	$400\,\text{nm} \leq \lambda \leq 3000\,\text{nm}$

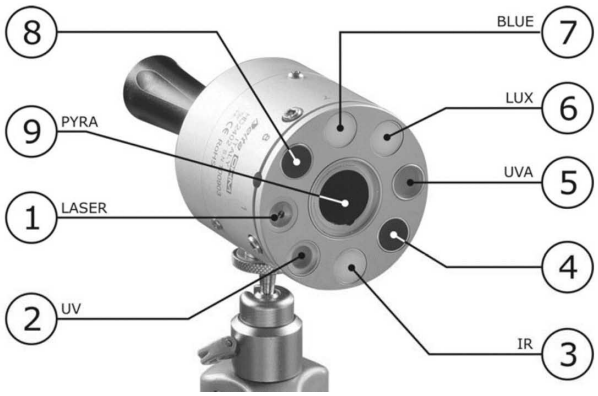

Fig. 3.1 Channel assignment of the HD2402 radiometer (DeltaOHM).

The laser allows for an alignment of the detecting head towards the radiation source of interest. However, it must be noted that the laser is not positioned centrally which leads to an alignment error, especially at short measurement distances. The HD2402 radiometer was not calibrated after purchase because it has hardly been used prior to this project.

X1$_1$, X1$_3$. The hand-held radiometers X1$_1$ and X1$_3$ from Gigahertz-Optik can be connected to several integral detectors. For this work, the X1$_1$ was used in conjunction with four different measurement heads and the X1$_3$ with an XD-45-HB BLH detector. Their

Tab. 3.1 Overview of measurement devices and detectors grouped by their ability to measure integral or spectral (ir-) radiance or (il-) luminance. The LMK 98-4 is a color camera system. The accessible wavelength ranges are given in nm in the third column. Measurands of each device are highlighted by checkmarks.

				E_v	E_B	E_{IR}	E_H	L_v	L_B	L_R	L_{IR}	T_{cp}
integral	HD2402		α	✓	✓		✓				✓$^{\beta}$	
	X1$_3$, XD-45-HB		300 – 700	✓	✓			✓$^{\gamma}$	✓$^{\gamma}$			
	X1$_1$	VL-3701	380 – 780	✓								
		RW-3704	800 – 1000			✓						
		RW-3708	1000 – 1700									
		RW-3703	400 – 800				✓$^{\delta}$					
	LDM-9811	PD-16BLH	400 – 520						✓			
		PD-16RTH	500 – 1150							✓		
		PD-16RTHA	800 – 1150								✓	
spectral	BTS256-E		380 – 750	✓								✓
	CAS 140CT-152		250 – 800	✓	✓							✓
	BTS2048-VL-TEC		350 – 1050	✓	✓							✓
	CAS 140CT-171		780 – 1650			✓	✓$^{\epsilon}$					
	BTS256-BLH		380 – 750					✓	✓			✓
	TOP 200		380 – 800					✓$^{\epsilon}$	✓$^{\epsilon}$			✓
pic	LMK 98-4 Color							✓	✓			

$^{\alpha}$ E_v (380 – 780 nm), E_B (400 – 600 nm), E_H (400 – 3000 nm)

$^{\beta}$ $R(\lambda)$ weighted irradiance detector, 660 – 1300 nm

$^{\gamma}$ in conjunction with XD-45-HB-SRT200

$^{\delta}$ in conjunction with RW-3704 and RW-3708

$^{\epsilon}$ in conjunction with CAS 140CT-152

spectral ranges and measurands are listed in Tab. 3.1. The VL-3701 is a $V(\lambda)$ filtered illuminance detector, whereas the RW-3703, RW-3704, and RW-3708 measurement heads detect radiometric irradiances. Combining two or three of them allows to estimate either E_{IR} or E_H, however, only within limited wavelength ranges.
Gigahertz-Optik also offers a tube, XD-45-HB-SRT, of 200 mm length with two exchangeable apertures (diameters 2.2 and 20 mm) that can be mounted on the XD-45-HB detector allowing the subsequent calculation of luminances, L_v, and BLH weighted radiances, L_B, for 11 and 100 mrad.

LDM-9811. Integral radiance measurements can be performed with sensors from the PD-16 series connected to an LDM-9811 (both from Gigahertz-Optik) that serves as a viewer module providing the optics for three FOVs, $\gamma = 100$, 11, and 1.7 mrad. It

can be operated from a minimum distance of 30 cm to infinity. By means of an ocular viewfinder, that can be equipped with several neutral density filters, the LDM-9811 can be aligned and focused to the radiation source of interest. The three PD-16 sensors detect BLH (PD-16BLH), retinal thermal hazards (PD-16RTH) or RTH with low visual stimulus limited to the IR-A spectral range (PD-16RTHA).

3.1.2 Spectroradiometers

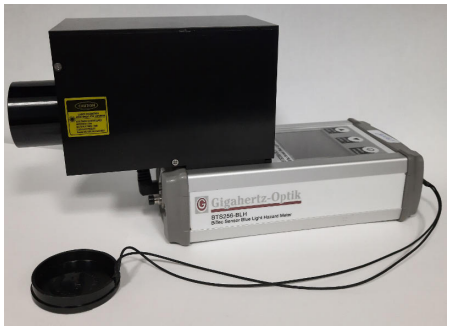

Fig. 3.2 BTS256-BLH

BTS256-E, BTS256-BLH. The BTS256-E is a luxmeter from Gigahertz-Optik equipped with a so-called BiTec-Sensor that combines a $V(\lambda)$ filtered diode with a CMOS diode array of 10 nm spectral bandwidth. Due to this spectroradiometer, the BTS256-E also gives information on chromaticity coordinates, CCT, and other light parameters. Basically, the BTS256-BLH is a BTS256-E but with an additional component mounted on the entrance optic providing an 11 mrad FOV, see Fig. 3.2. A laser with a divergence of 11 mrad can be used to align the device with the radiation source of interest.

CAS 140CT. Optical core component of both CAS 140CT spectroradiometers from Instrument Systems is an optimized crossed Czerny-Turner spectrograph that efficiently suppresses stray light. The back-thinned CCD chip of the 152 model with its 1024 $\times$ 128 pixels allows spectral irradiance measurements from 200 to 800 nm with an optical bandwidth of $\Delta\lambda = 2.7$ nm, whereas the InGaAs diode array of the IR spectroradiometer (140CT-171, 512 elements) is sensitive for 780 nm $\leq \lambda \leq$ 1650 nm with $\Delta\lambda = 9$ nm. Optical radiation was coupled into the spectroradiometers by means of a Y-shaped fiber optical cable OFG-561 and an EOP-146 entrance optic with adequate cosine correction of 90 %, both from Instrument Systems, too. Note that the spectral range below 250 nm cannot be accessed because of the manufacturer's calibration with a halogen lamp. All integration times were adjusted automatically by the software to achieve a 70 – 90 % detector saturation.

BTS2048-VL-TEC. The compact diode array spectroradiometer BTS2048-VL-TEC from Gigahertz-Optik has a thermoelectrically coolded back-thinned CCD chip with 2048 pixels and a $V(\lambda)$ filtered Si-photodiode. This BiTec-sensor allows, among other things, spectral irradiance measurements from 350 – 1050 nm with an optical bandwidth of $\Delta\lambda = 2$ nm. The diffusor of the integrated entrance optic has a cosine corrected FOV with $f_2 \leq 3$ %. Integration times were adjusted automatically by the software.

TOP200. The Telescope Optical Probe TOP200-100-2 from Instrument Systems is designed to measure spectral radiances in conjunction with, for example, a CAS 140CT-152 spectroradiometer and a fiber optical cable TOP200-204 with integrated mode mixing. The optimized Pritchard-style optical system guarantees a round measuring spot that can be positioned at the radiation source of interest due to the build-in viewfinder camera with a resolution of 1600 $\times$ 1200 pixels. The combination of 6 different apertures (diameters ranging from 125 µm to 3.0 mm) and the UV lens TOP100-322 used for this project allows $L(\lambda)$ measurements from 200 – 800 nm with variable FOVs.

The complete system must be calibrated for each measurement distance (at least 101 cm) that was chosen to be 1.5 m with regard to an SRS8 radiance standard from Bentham, see Section 3.2.1. The in-house calibration was executed for the largest aperture diameter of 3.0 mm resulting in $\gamma = 21.6$ mrad and a measuring-spot diameter of 32.5 mm. Note that the accessible wavelengths only range from 380 – 800 nm due to the limited calibrated spectral radiance of the SRS8.

3.1.3 LMK 98-4 Color

The imaging light and color measuring photometer LMK 98-4 Color from TechnoTeam provides, among other things, spatially resolved luminance distribution pictures based upon a CCD camera. It can be equipped with full glass filters that account for $B(\lambda)$ or that attenuate the incoming light (neutral density filters).

3.2 Radiation Sources

The subsequent sections only deal with those radiation sources that have been studied extensively for this report.

3.2.1 SRS8 Spectral Radiance Standard

Bentham's SRS8 spectral radiance standard is an integrating sphere of 200 mm diameter coated with barium sulphate. A 50 W grit-blasted quartz halogen lamp is situated inside. The $D = 50.4$ mm large exist port is fitted with a ground glass window, see Fig. 3.3. Several years of use have stressed the diffusor, and diverse scratches are discernible. The spatial luminance distribution measured by an LMK 98-4 Color, Fig. 3.3

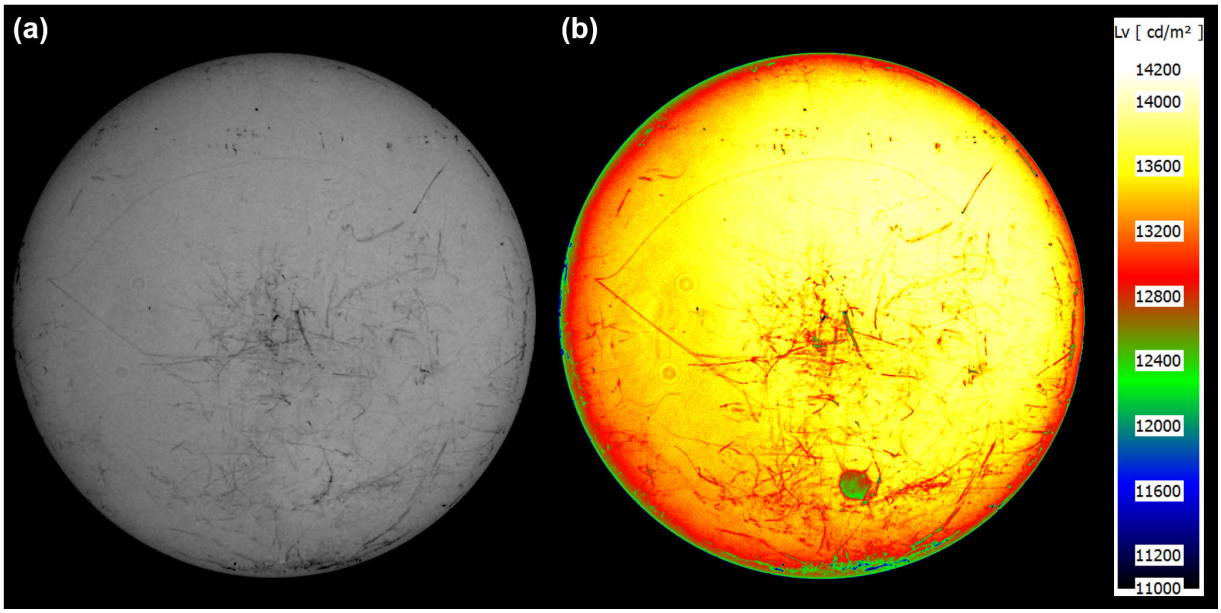

Fig. 3.3 (a) True color and (b) luminance distribution picture of the SRS8 spectral radiance standard exit port that were taken by an LMK 98-4 Color positioned at a distance of 50 cm. A calibrated ND3 neutral density filter was used with 0.1063 % transmission. Note that the range of the L_v scale starts at 11 kcd m^{-2} to better visualize irregularities on the diffusor surface.

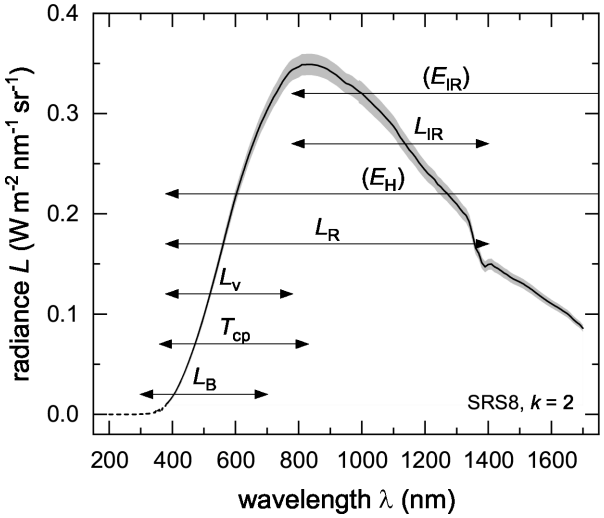

Quantity	Value + U
L_B	$(3.44 \pm 0.07)\,W\,m^{-2}\,sr^{-1}$
L_v	$(12.3 \pm 0.2)\,kcd\,m^{-2}$
L_R	$(139 \pm 2)\,W\,m^{-2}\,sr^{-1}$
L_{IR}	$(43.8 \pm 0.7)\,W\,m^{-2}\,sr^{-1}$
E_H	$(13.9 \pm 0.2)\,W\,m^{-2}$
E_{IR}	$(10.3 \pm 0.2)\,W\,m^{-2}$
T_{cp}	$(2858 \pm 1)\,K$
$K_{B,v}$	$(279 \pm 1)\,mW\,klm^{-1}$

Fig. 3.4 Calibrated spectral radiance, $L(\lambda)$, of Bentham's SRS8. The expanded uncertainty, $U = ku_c$, with standard uncertainty u_c and coverage factor $k = 2$, is visualized by the grey area. Double arrows represent specific wavelength regions related to basic optical radiation and risk assessment quantities. E_{IR} and E_H, calculated for a distance of 20 cm, are given in parentheses to indicate their non radiance nature. Spectral data ranging from 200 – 380 nm (dashed line) were measured with a BTS2048-UV-S (Gigahertz-Optik); thus, they are not calibrated.

(b), also visualizes the diffusor's irregularities. It is important to emphasize that neither the gray nor the color scale starts at zero but they are restricted to depict these inhomogeneities.

The SRS8 has been calibrated prior to F 2483 by Gigahertz-Optik with a single monochromator, and the spectral radiance, $L(\lambda)$, ranging from 380 – 1700 nm is presented in Fig. 3.4 together with the expanded uncertainty U ($k = 2$). In order to access all relevant BLH wavelengths, several high-precision measurements had to be performed with a BTS2048-UV-S (Gigahertz-Optik). The resulting mean spectral UV irradiance was transformed to radiance via Eq. 2.6 and adapted to the calibration curve. Finally, several quantities were derived from this $L(\lambda)$, see Fig. 3.4.

3.2.2 Discharge Short Arc Moving Head, Robe Robin MegaPointe

Robe's MegaPointe is equipped with an Osram Sirius HRI 470 W RO discharge lamp placed in front of an integrated reflector. The cutting edge optical system provides an adjustable zoom of 1.8 – 42°. The diameter D of the output lens is given by 150 mm; however, operating the spotlight at certain parameters leads to much smaller beam diameters. The CCT is listed in the manual with 7500 K for the lamp and 6300 K for the light output. T_{cp} calculated from a measured spectrum at 18 m, see Fig. 3.5, lies in between these two values with 6818 K. More than 99 % of the radiation emission stems from light with wavelengths ranging from 400 to 780 nm; thus, detrimental health effects from UV or IR radiation are rather unlikely. No RG classification is given in the manual (version 1.6) of the purchased spotlight, but a safety distance of 18 m is mentioned. In the manual's current version 2.7, the MegaPointe is classified as RG 2, see Tab. 1.1.

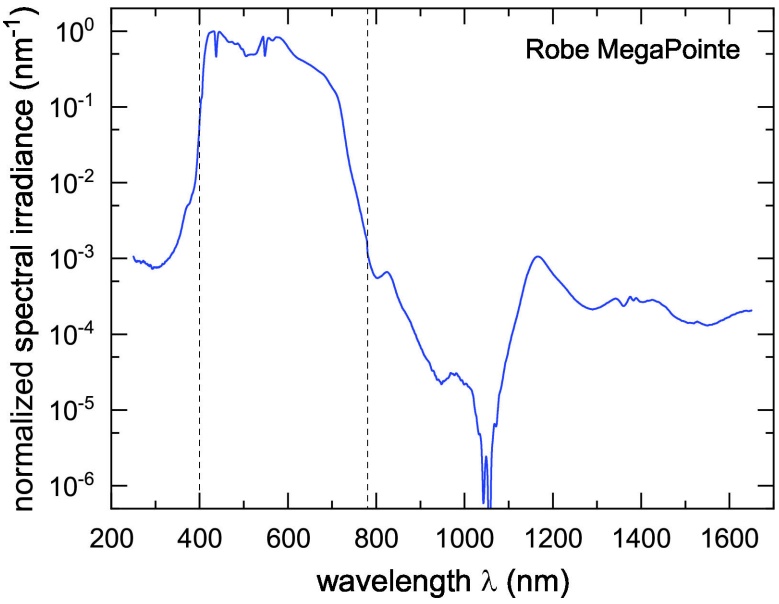

Fig. 3.5 Peak normalized spectral irradiance for a Robe MegaPointe. The spotlight was operated at full intensity in spot mode, and the measurement was conducted at a distance of 18 m. The dashed vertical lines mark 400 nm and 780 nm.

3.2.3 LED Fresnel Stage Light, ARRI L7-C

The L7-C spotlight from ARRI has a Fresnel lens with a diameter of 175 mm. Its RGBW LED light engine enables CCTs ranging from 2800 – 10 000 K. A continuous focusability of the lens is possible with half peak angles of 15° (spot) to 50° (flood). Additionally, the L7-C fully can be dimmed electronically, i. e. within 0 – 100 %. A typical power consumption at 230 V and 50 H is 220 W. According to the manual, the L7-C is classified to Risk Group 1 with, for example, 7511 lx at 3 m ($T_{\mathrm{cp}} = 5600$ K, spot).

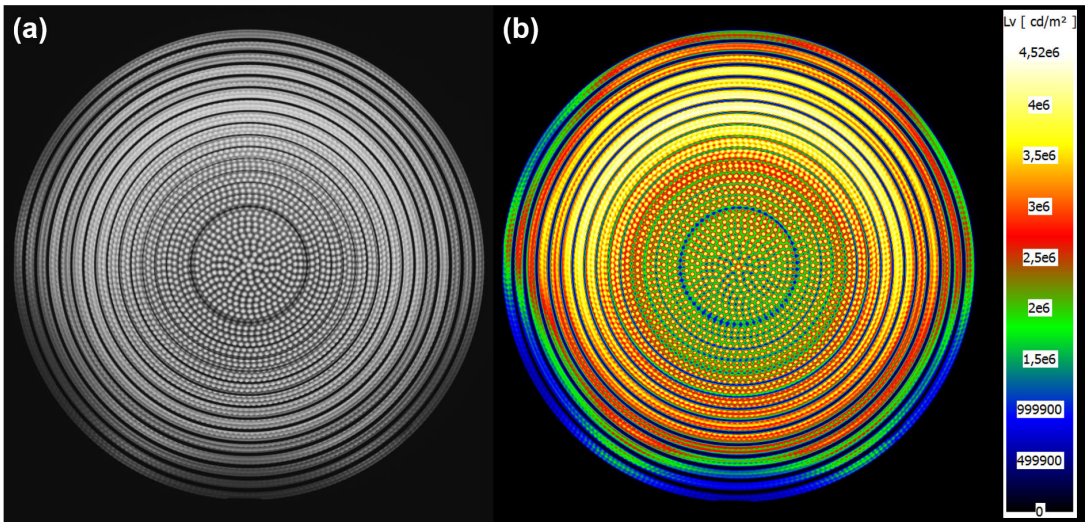

Fig. 3.6 ARRI L7-C pictures (100 % intensity, $T_{\mathrm{cp}} = 6550$ K) taken by an LMK 98-4 Color with a calibrated ND5 neutral density filter (0.0011 % transmission) at a distance of 1.75 m. (a) True color photo and (b) luminance distribution.

The gray scale picture and even more the luminance distribution of the Fresnel lens demonstrate the irregular light output, see Fig. 3.6. Although the diffusing lens with a diameter of 64 mm is placed in the center, no homogeneous L_v decrease form the mid to the edges of the Fresnel lens is discernible; thus, complicating the BLH risk assessment. The lower L_v at the bottom of the picture could also result partly from an off-axis alignment of the LMK 98-4 Color with regard to the L7-C.

3.2.4 LED Multichip Washbeam, Robe Robin Spiider

Fig. 3.7 Spiider's front side with violet light emission.

The washbeam luminaire Spiider from Robe uses 18×40 W RGBW LEDs circularly arranged around a centered 60 W LED, see Fig. 3.7. The zoom can be varied between tight 4° (beam) and wide 50° (wash). The spotlight is fully dimmable. The settable CCTs range from 2700 – 8000 K. Version 2.0 of the manual classifies the Spiider as RG 2, but this classification has been removed in the current version 3.1 without replacement.

It is expectable that a BLH risk assessment will be demanding for the Spiider because of the above mentioned arrangement of differently powered LEDs. An LMK 98-4 Color picture visualizes the complex distribution of light emission. Fig. 3.8 is a false color presentation of BLH weighted radiances with its scale ranging from 8 – 18 kW m^{-2} sr^{-1}. The L_B inhomogeneity can be seen for each of the 19 LEDs. The dark spaces between the rectangular shaped center LED and the other circular ones demonstrate that Spiider's front side inner diameter of 25.8 cm can only be used as a rough estimate for BLH risk assessment via the Planck Approximation.

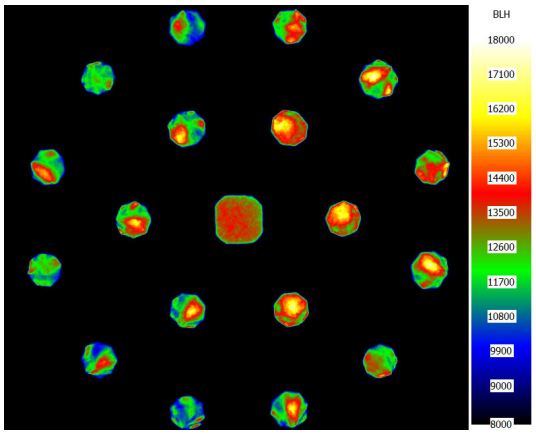

Fig. 3.8 False color L_B distribution.

Due to its complexity, the Spiider was selected for the last step of the instrument comparison ("challenging measurement conditions"), see Section 4.3, and it is also part of the test workplace, see Section 6.2. CCT dependent spectra will be discussed in Section 5.1.1.

3.3 Measurement Sites

The radiation sources explained in the previous sections were investigated at different places depending on their light emission power. The spectral radiance standard SRS8 from Bentham was mounted on an optical profile system with suitable carriers. Both walls, the floor, and the ceiling in the optics laboratory, air-conditioned to 20 °C, were covered with a black radiation absorbing textile.

The high-power spotlights, i. e. the ARRI L7-C as well as Robe's Spiider and MegaPointe were measured in two large cellar rooms connected by a door that served as a "natural" aperture. The EOPs were placed on a small wagon with fixed optical rail. Stray light from the surrounding could not be reduced, for example, by means of the above mentioned black textile, because of the large measurement distances up to 23 m and a limited amount of material.
For the test workplace described in Section 6.2, all spotlights should be positioned above eye level to approximate a real-life situation. Therefore, a low-emission noise measurement room was used; however, with a limited length of ca. 13 m. No stray light was suppressed.
At all measurement sites, the experimental investigations were performed with a laser-aligned probe that was checked for tilt by a mirror. Distances were also set by a laser device.

4 Comparison of Measurement Systems

Several integrating detectors as well as spectroradiometers, see Tab. 3.1, were applied in this project to assess the photobiological safety of spotlights. The following sections will focus on the comparability of their (spectral) measurements providing E_B, E_v, L_B, $E(\lambda)$, or $L(\lambda)$. The measured (spectral) irradiances were converted to radiance values by means of Eq. 2.9 with F being equal to the diameter D of the radiation source's emitting surface. The comparison of the instruments regarding their measurands is conducted in three steps with growing complexity of the radiation sources. Note that all measurements were performed only once if not stated otherwise.

4.1 Measurement Error

The Joint Committee for Guides in Metrology (JCGM) defines the measurement error (error of measurement or just error) as "measured quantity value minus a reference quantity value" (JCGM 200). Hereinafter, L_v and L_B have been determined from the calibrated spectral radiance, $L(\lambda)$, of a Bentham SRS8 radiance standard, see Fig. 3.4, and serve as reference quantity values. In order to improve intuitive handling, the resulting measurement errors are presented in terms of percentage deviations, δL_v and δL_B. It is important to note that all measurements have been performed in order to determine physical radiances or luminances, $L_{\mathrm{B},\alpha}$ and $L_{\mathrm{v},\alpha}$, respectively, and not spatially averaged ones, see Section 2.2.2.

Fig. 4.1 (a) presents δL_v for several measurement instruments with regard to the reference value $(12.3 \pm 0.2)\,\mathrm{kcd\,m^{-2}}$ of Bentham's SRS8 radiance standard, see Fig. 3.4. Originally designed to measure L_B with $\gamma = 11\,\mathrm{mrad}$, the BTS-BLH can also detect illuminance. The latter was measured at a distance of 2 m and converted to luminance. Its percentage deviation $\delta L_\mathrm{v} = 1.2\,\%$ is within the expanded uncertainty ($\pm 1.5\,\%$) of the reference value. The TOP200 was calibrated at a measurement distance of 1.5 m for that its FOV is 22 mrad, see Section 3.1.2. The related $\delta L_\mathrm{v} = -1.5\,\%$ is also within U.

In general, the $\delta L_{\mathrm{v},\alpha}$ values calculated from illuminances and spectral irradiance measurements show a comparable trend with respect to the four different distances: δL_v is most positive (or least negative for the HD2402) at 2 m where the SRS8's source size is 25 mrad. Despite all efforts to reduce stray light, e.g. using black, low reflecting clothes for the lamp's surrounding, those devices measuring with an open FOV presumably detect to much light resulting in positive δL_v. In case of the HD2402, its E_v sensor is not aligned to the optical axis; thus, it measures to less illuminance, and therefore has a small negative δL_v.
At a distance of 1 m corresponding to $\alpha = 50\,\mathrm{mrad}$ the percentage deviations are much less positive, or more negative for HD2402. Now, the VL-TEC also has negative δL_v. For the two closest distances that are 50.4 cm ($\alpha = 100\,\mathrm{mrad}$) and 20 cm ($\alpha = 250\,\mathrm{mrad}$), the percentage deviations are within or close to the expanded uncertainty except for the HD2402 due to the above mentioned off-center E_v sensor alignment. In addition, the analysis of a luminance picture taken by the LMK 98-4 resulted in the highest positive δL_v, but the reference luminance, $L_\mathrm{v} = (12.3 \pm 0.2)\,\mathrm{kcd\,m^{-2}}$, and the determined one, $L_\mathrm{v} = (13.4 \pm 0.8)\,\mathrm{kcd\,m^{-2}}$, are close to each other considering their standard deviations.

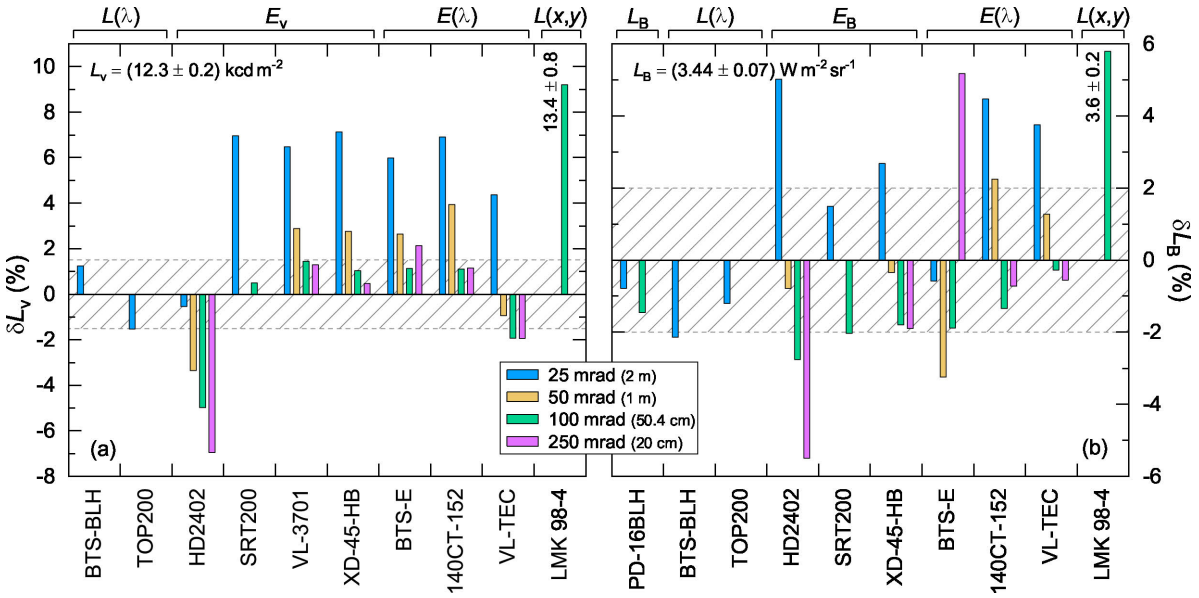

Fig. 4.1 Comparison of several devices listed in Tab. 3.1 regarding percentage deviations of (a) luminance, δL_v, and (b) BLH weighted radiance, δL_B, with respect to the SRS8 calibration values, the latter given as numbers in both panels. Four measurement distances, each represented by colored bars, were examined. Measurands are written on top of the figure grouping some devices. Hatched areas visualize the expanded uncertainties $U\ (k = 2)$ of the calibration values. Numbers shown for the LMK 98-4 reflect absolute radiances, L_v and L_B, with standard deviations.

The BLH weighted radiances, L_B, of the LDM-9811 (with sensor PD-16BLH), the BTS-BLH, and the TOP200, those devices that directly measure radiance, virtually agree with the SRS8 reference value, $L_\mathrm{B} = (3.44 \pm 0.07)\,\mathrm{W\,m^{-2}\,sr^{-1}}$, see Fig. 4.1 (b). The dependence on distance that has been observed for L_v largely reappears for the (spectral) irradiance measurements: δL_B becomes less positive or more negative upon approaching the SRS8 radiance standard. An exception thereof is found for the percentage deviations of the BTS-E. Even with additional measurements, it remains unclear why the 20 cm value is the only positive one. The δL_B range is relatively large for the HD2402 due to the off-center alignment of its BLH sensor. Again, δL_B is highest for the LMK 98-4, but the absolute value agrees with the reference L_B within the standard deviation.

4.2 Real-Life Approach

Measurement conditions are different for (high-power) spotlights compared to the SRS8 radiance standard: calibrated L_v and L_B values usually do not exist, source sizes are typically larger related to longer measurement distances in order to achieve $\alpha = 11$ mrad or 100 mrad, and the emitted optical radiation is much more powerful by several orders of magnitude addressing another part of the detectors' dynamic ranges. Conducting such a "real-life" test, an ARRI L7-C spotlight, equipped with an RGBW LED light engine, was chosen on the one hand because of its virtually single apparent source and on the other hand because of its Fresnel lens that does *not* lead to a homogeneous emitting surface. It was operated at full power (no dimming) and with $T_\mathrm{cp} = 6550\,\mathrm{K}$. Note that

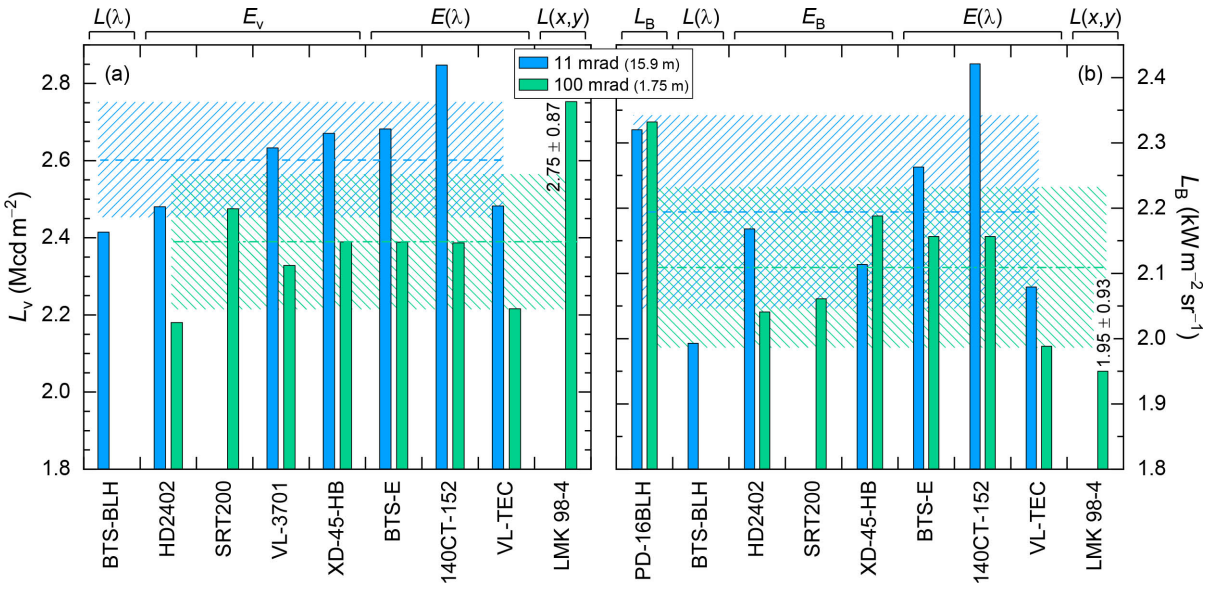

Fig. 4.2 Results for (a) the luminance, L_v, and (b) the BLH weighted radiance, L_B, of an ARRI L7-C spotlight measured by several of the devices listed in Tab. 3.1. Colored bars refer to two distances where $\alpha = 11\,\mathrm{mrad}$ or $100\,\mathrm{mrad}$. The upper abscissa groups some of the devices. The LMK 98-4 mean values with standard deviations are also given in both panels as numbers. Horizontally dashed (11 mrad) and dash-dotted lines (100 mrad) represent the overall mean L_v and L_B values, hatched areas reflect their standard deviations.

the TOP200 was excluded from the following evaluation as it must be calibrated for each measurement distance; thus, its applicability is rather minor out of laboratory.

No reference values exist for the ARRI L7-C spotlight; therefore, Fig. 4.2 depicts absolute L_v and L_B values. As it was found for the SRS8 radiance standard, longer measurement distances (here 15.9 m, equal to $\alpha = 11\,\mathrm{mrad}$) are related to higher L_v and L_B compared to 1.75 m ($\alpha = 100\,\mathrm{mrad}$) probably due to detected stray light from the surrounding. Exceptions thereof are given by the L_B values of the PD-16BLH that virtually agree with each other and the integrating E_B sensor XD-45-HB. Note that it was practically impossible to align the SRT200 to the ARRI L7-C at 15.9 m, and that no useful LMK 98-4 picture could be taken at that distance; thus, these data are missing. The large standard deviations of the L_v and L_B values determined from the LMK 98-4 pictures reflect the inhomogeneity of the Fresnel lens's (x, y) radiation emission distribution, see Fig. 3.6. The off-center alignments of the HD2402 sensors no longer play a significant role at both distances.

The mean values considering all devices are given by $\overline{L}_{\mathrm{v},100} = (2.39 \pm 0.18)\,\mathrm{Mcd\,m^{-2}}$ and $\overline{L}_{\mathrm{v},11} = (2.60 \pm 0.15)\,\mathrm{Mcd\,m^{-2}}$ as well as $\overline{L}_{\mathrm{B},100} = (2.11 \pm 0.12)\,\mathrm{kW\,m^{-2}\,sr^{-1}}$ and $\overline{L}_{\mathrm{B},11} = (2.19 \pm 0.15)\,\mathrm{kW\,m^{-2}\,sr^{-1}}$. Both $\overline{L}_\mathrm{v}$ and $\overline{L}_\mathrm{B}$ agree among each other within their percentage standard deviations ranging from $\pm 5.7\,\%$ to $\pm 7.5\,\%$. Consequently, these measurement results from different devices can be regarded as comparable.

However, it is important to emphasize that all of the data were determined from single measurements that can vary significantly even under laboratory conditions. For

example, the 140CT-152 spectroradiometer detects $L_{B,11} = 2.4\,\mathrm{kW\,m^{-2}\,sr^{-1}}$ whereas $L_{B,11} = 2.0\,\mathrm{kW\,m^{-2}\,sr^{-1}}$ for the BTS-BLH. Precise distance measurements and accurate detector alignments were only possible with laser radiation sources. A real-life workplace risk assessment will certainly not have the possibilities for laboratory-like measurement conditions so that deviations between different detectors will probably be much higher.

4.3 Challenging Measurement Conditions

More and more spotlights are equipped with one or several LED arrays because of diverse advantages for light modification. The built-in LEDs can vary, e.g. in size, spectral emission, or output power. In combination with a different spacing between single LEDs or groups of them, the complexity of metrological risk assessment can increase significantly. Consequently, for the third step of (ir-)radiance and (il-)luminance measurement device comparison, a Robe Robin Spiider was chosen as it has some of the characteristics mentioned above, see Section 3.2.4. It was operated with 100 % dimmer intensity and 150/255 zoom. The CCT was adjusted by channel 12 (64/255) in combination with channel 6 (82/255) equivalent to $T_{cp} \approx 5600\,\mathrm{K}$.

As in the previous both sections, measured illuminances and BLH weighted irradiances were converted to L_v and L_B values, respectively, via Eq. 2.9. The inner diameter of the Spiider's front, $D = 25.8\,\mathrm{cm}$, was used to calculate α by means of Eq. 2.13. However, it must be noted that this diameter is only an approximation of the emitting surface because of the non-emitting spaces between the 19 individual LEDs, see Section 3.2.4. The measured and calculated L_v and L_B are presented in Fig. 4.3.

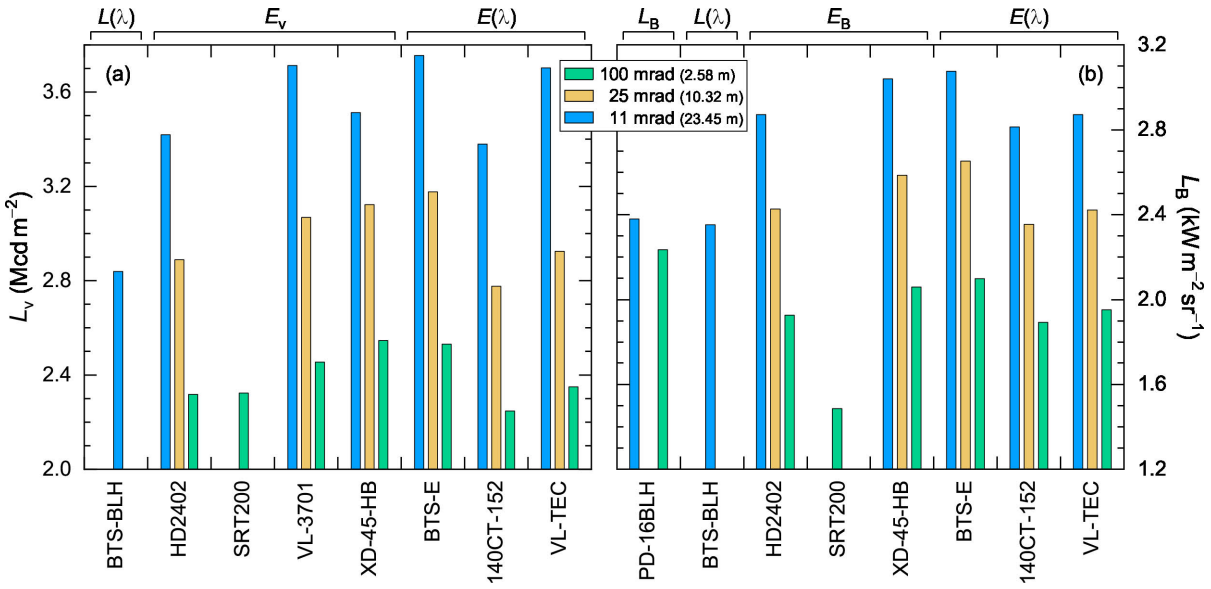

Fig. 4.3 Results from (a) (il-)luminance and (b) BLH weighted (ir-)radiance measurements from several instruments, see Tab. 3.1, of a Robe Spiider. Colored bars represent three different measurement distances equivalent to $\alpha = 100\,\mathrm{mrad}$, 25 mrad, and 11 mrad. The tested devices are grouped with respect to their measurands on the upper abscissa. Mean values are given in Tab. 4.1.

Tab. 4.1 Mean luminances and BLH weighted radiances with standard deviations (percentages in parentheses) calculated from the data presented in Fig. 4.3.

d (m)	α (mrad)	$\overline{L}_\mathrm{v}$ (Mcd m^{-2})	$\overline{L}_\mathrm{B}$ (kW m^{-2} sr^{-1})
2.58	100	2.40 ± 0.12 ($\pm$4.8 %)	1.95 ± 0.24 ($\pm$12.1 %)
10.32	25	2.99 ± 0.15 ($\pm$5.2 %)	2.49 ± 0.12 ($\pm$5.0 %)
23.45	11	3.47 ± 0.32 ($\pm$9.1 %)	2.77 ± 0.29 ($\pm$10.6 %)

The increase of L_v and L_B values with growing distance that was found for the SRS8 and the ARRI L7-C is also apparent in the measurement results for the Spiider; however, with much bigger impact. The related mean values $\overline{L}_\mathrm{v}$ and $\overline{L}_\mathrm{B}$ are more than 40 % higher at 23.45 m compared to 2.58 m, see Tab. 4.1. This finding is in contrast to the SRS8 and the ARRI L7-C for that the mean values agreed among each other. Having a closer look at panel (b) reveals that L_B from the two radiance instruments, PD-16BLH and BTS-BLH, are close to each other indicating that they might approximate the "true" BLH weighted radiance. In comparison to varying L_B from irradiance measurements, this finding again points out the importance of stray light from the surrounding although three single radiance measurements are certainly not sufficient for general conclusions. Remembering that at $d = 23.45$ m, equivalent to a source size $\alpha = 11$ mrad, E_B can be used for comparison with the BLH ELV, see Tab. 2.2, the question of how to assess the spotlight arises. This will be discussed in Chapter 6.

Despite the challenging measurement conditions, the percentage deviations determined from (il-)luminance and (ir-)radiance measurements of the Spiider are comparable to those for the SRS8 and ARRI L7-C, although with in parts higher values up to $\pm$12 %. This percentage deviation was found for $\overline{L}_\mathrm{B}$ at 2.58 m and mainly comes from the SRT200 with its demanding handling. Leaving out the corresponding radiance yields $\overline{L}_\mathrm{B} = (2.03 \pm 0.13)$ kW m^{-2} sr^{-1} with $\pm$6.4 % standard deviation.

4.4 Illuminance to BLH Weighted Radiance Conversion

Illuminance data collected in the previous sections for the SRS8, the ARRI L7-C, and the Robe Spiider will be converted to BLH weighted radiances by means of the Planck Approximation described in Section 2.5 in order to verify its applicability. Three instruments can measure E_v directly (HD2402, VL-3701, and XD-45-HB), whereas the BTS-E, the 140CT-152, and the VL-TEC are spectroradiometer. $K_\mathrm{B,v}^\mathrm{Planck}$ was taken from the look-up Tab. 2.3. Combining Eq. 2.6 and Eq. 2.20 yields L_B, see Tab. 4.2.

The mean BLH weighted radiance determined from illuminance measurements of the SRS8 at 50.4 cm is 5 % higher than its analog based on E_B and L_B data. Within their standard deviations ($k = 1$), both means match each other demonstrating the applicability of the Planck Approximation. Similar results were obtained at 1 m equivalent to $\alpha = 50$ mrad albeit with a slightly higher percentage deviation of 7 %. About 9 % was found for the ARRI L7-C at 1.75 m including comparable means within their standard deviations. The mean calculated from E_B and L_B measurements at a distance of 15.9 m, $\overline{L}_\mathrm{B} = (2.19 \pm 0.15)$ kW m^{-2} sr^{-1}, is equal to the one at 1.75 m, whereas $\overline{L}_\mathrm{B} = (2.61 \pm 0.12)$ kW m^{-2} sr^{-1} determined from E_v data is about 19 % higher. The

Tab. 4.2 Means calculated from E_v and E_B, L_B data based on Fig. 4.1 for the SRS8 (in $W\,m^{-2}\,sr^{-1}$), Fig. 4.2 for the ARRI L7-C, and Fig. 4.3 for the Robe Spiider (both in $kW\,m^{-2}\,sr^{-1}$). The conversion of E_v was made by means of the Planck Approximation. Percentage deviations δ are listed in %, α is given in mrad.

	α	SRS8	L7-C	Spiider
mean (E_v)	100	3.60 ± 0.09	2.29 ± 0.07	2.18 ± 0.11
mean (E_B, L_B)		3.44 ± 0.07	2.11 ± 0.12	1.95 ± 0.24
δ		5	9	12
mean (E_v)	11/50	3.66 ± 0.10	2.61 ± 0.12	3.24 ± 0.15
mean (E_B, L_B)		3.44 ± 0.07	2.19 ± 0.15	2.77 ± 0.29
δ		7	19	17

deviations for the Planck Approximation are more or less the same for the Robe Spiider.

Concluding the analysis of mean BLH weighted radiances determined from E_v measurements, the conversion process, i. e. the Planck Approximation yields less than 20 % higher $\overline{L}_B$. Taking the $\sim$10 % measurement uncertainty found for the Robe Spiider into account, see Tab. 4.1, this demonstrates the applicability of the Planck Approximation as a simplified workplace risk assessment method. In addition, higher radiances result in shorter maximum permissible exposure durations (MPE); thus, being on the restrictive side.

Conclusion “Comparison of Measurement Systems”

Measurement Error

→ results from radiance measurement instruments agree with the reference values within their expanded uncertainties
→ in general, L_v and L_B values determined from illuminances and irradiances (open FOV) measured close to the radiance standard ($\alpha \geq 100$ mrad) match the reference values
→ percentage deviations, δL_v and δL_B, are much higher at longer distances, probably due to low illuminances including stray light
→ the photometer LMK 98-4 shows the largest measurement errors

Real-Life Situation

→ in general, higher L_v and L_B values were determined at longer distances as in the case of the radiance standard SRS8
→ both mean L_v and L_B values agree with each other for 100 and 11 mrad
→ with standard deviations below $\pm$8 %, all devices show comparable results regardless of (ir-)radiance or (il-)luminance measurements
→ a real-life workplace risk assessment will not be conducted under laboratory-like conditions so that measurement results of different devices will probably be much higher

Challenging Measurement Conditions

→ mean L_v and L_B were found to be up to 40 % higher at longer distances
→ despite the challenging measurement conditions, each mean L_v and L_B is within ca. $\pm$10 % standard deviation
→ concluding the three-step instrument comparison, individual measurement results should be regarded with an at least $\pm$10 % uncertainty

Illuminance to BLH Weighted Radiance Conversion

→ $\overline{L}_B$ from E_v measurements converted via the Planck Approximation deviate $\lesssim$ 12 % close to the lamp and $\lesssim$ 20 % far away from it compared to their analogs based on E_B and L_B
→ higher radiances yield shorter MPEs; thus, being more restrictive
→ considering an approximate measurement uncertainty of $\pm$10 %, the Planck Approximation is a promising approach for a simplified BLH risk assessment

5 Influencing Factors

5.1 Adjustable Lamp Parameters

5.1.1 White-Light Generation

Many modern LED spotlights are tunable within product specific ranges regarding the CCT of their emitted light. T_{cp} is a highly computationally processed quantity calculated with chromaticity coordinates, for example, according to Eq. 2.24. As it is a directly perceivable light characteristic, most manufacturers provide the CCT (ranges) in their manuals. It is supportive to understand the underlying mechanisms of white-light generation. The subsequent ARRI L7-C and Robe Spiider data are only intended to demonstrate the very lamp specific mixtures of RGBW-LED emissions in order to achieve a certain CCT and not to draw general conclusions.

The spectra depicted in Fig. 5.1 (a) were measured with a BTS2048-VL-TEC within 350 – 1050 nm, but only a restricted spectral range is presented because the long wavelength tail above 700 nm is of no importance with $E(\lambda \geq 760\,\mathrm{nm}) \leq 0.01\,\mathrm{W\,m^{-2}}$. Several bands are apparent that can be assigned to the blue (444 nm), the green (521 nm), and the red LED (631 nm) as well as to the blue exciting diode (470 nm) and the phosphor emission (604 nm) of the pc-LED. It must be emphasized that the selection of these wavelengths is only based on the peak spectral irradiances and that their assignment to certain LED emissions does not necessarily mean that these are the peak wavelengths of the built-in RGBW LEDs. In addition, some bands strongly overlap with each other complicating to distinguish each contribution.

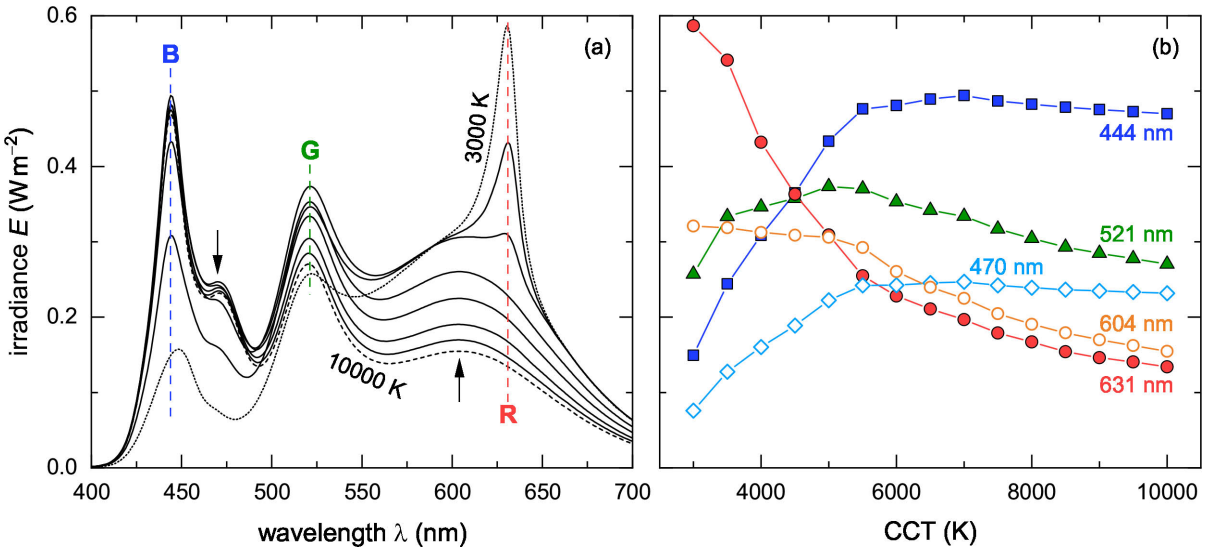

Fig. 5.1 (a) ARRI L7-C spectra (100 % output power) recorded at a distance of 1.75 m for several CCTs in steps of 1000 K. Spectral irradiances for 3000 K (dotted) and 10 000 K (short-dashed) are highlighted. (b) Peak irradiances as a function of T_{cp} for 444 nm (B), 521 nm (G), and 631 nm (R) as well as for the blue diode, 470 nm, and the presumable phosphor emission, 604 nm, of the pc-LED, both indicated by arrows in panel (a). Additional data for intermediate 500 K steps are included in panel (b).

To better visualize the spectral changes associated with varying CCTs, Fig. 5.1 (b) shows the peak irradiances for the above mentioned wavelengths. The warmest CCT of 3000 K is generated with a high red proportion and comparably small blue contributions. Increasing the CCT is accompanied by a reduced red signal and higher blue proportions. The peak values of the three RGB LEDs are equal at $T_{cp} = 4500$ K. Close to 5500 K and above, both blue signals are virtually constant, and higher CCTs are achieved by reduced intensities of the other three bands. It is worth mentioning that the combination of all LED signals must ensure that the emitted light is still perceived as "white", i.e. the chromaticity coordinates, see Section 2.4.1, have to lie within a certain (x, y) range. For the L7-C spotlight, (x, y) varies non-linearly from (0.43, 0.41) at 3000 K to (0.28, 0.29) at 10 000 K (not shown).

Unlike the ARRI L7-C, there is no CCT control knob on the Robe Spiider but T_{cp} must be set indirectly, for example, by varying DMX channel 12 in between 0 and 255. As can be seen in Fig. 5.2 (a), the emission of the pc-LED is heavily superimposed by those of the RGB LEDs, and no pc-LED band peak can be assigned although the long-wavelength shoulder on the green LED emission unambiguously results from the phosphor's excitation. Additionally, a CCT decrease leads to a spectral shift of the peak irradiances for the blue and the green LED emissions from 446 nm to 442 nm and from 522 nm to 520 nm, respectively, indicating the existence of the pc-LED. In contrast, the peak wavelength of the red LED band at 638 nm is CCT independent. It is worth mentioning that each of the Spiider's RGBW channels can be set separately thus changing the CCT, but such a variation together with its analysis is beyond the scope of this research project.

Analyzing the peak irradiances of Robe Spiider's CCT dependent emission spectra reveals two distinct T_{cp} regimes, see Fig. 5.2 (b): The emission of red LEDs is virtually

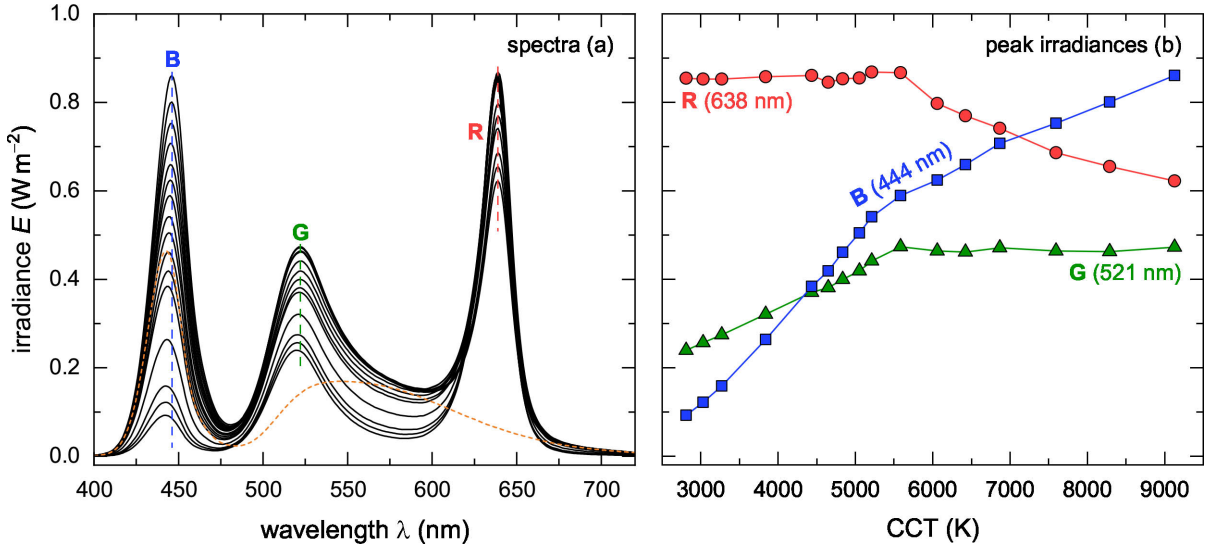

Fig. 5.2 CCT variation and associated spectral changes for a Robe Spiider operating at full dimmer intensity and with 150/255 zoom. (a) RGBW emission spectra measured at a distance of 2.58 m ($\widehat{=}\ \alpha = 100$ mrad) ranging from ca. 2800 – 9100 K. $E(\lambda)$ only of pc-LEDs is depicted as dashed line. (b) Peak irradiances as a function of T_{cp} taken from the spectra presented in panel (a).

constant up to ca. 5500 K, whereas the peak irradiances of blue and green LEDs increase linearly. For higher CCT, the red LEDs emissions now decrease non-linearly, the peak irradiance of blue LEDs still grows but less steeply, and that for green LEDs is more or less independent of CCT. Calling Fig. 5.1 (b) to mind, the combination of RGBW LED peak emissions for the ARRI L7-C also changed significantly around T_{cp}= 5500 K indicating that this CCT might be of technical importance for white-light generation. The chromaticity coordinates range from (0.45, 0.40) at 2840 K to (0.29, 0.29) at 9100 K (not shown), similar to those found for the L7-C spotlight.

5.1.2 BLH Weighted Irradiance and Illuminance Correlation

The T_{cp} dependent RGBW LED emission spectra can be further analyzed regarding the BLH weighted irradiance as a function of illuminance, i.e. $E_B\,(E_v)$. Beginning with the ARRI L7-C spotlight operating at 100 % dimmer intensity, blue squares in Fig. 5.3 (a), E_B triples from ca. 2800 – 5500 K while E_v only varies within 18 – 21 klx. For $T_{cp} > 5500$ K, E_B decreases rather weakly whereas E_v reduces from 20 klx to 12 klx. The special CCT of 5500 K that has already been observed in the peak analyses reappears, and it separates the E_B increase from the E_v decrease region. Reducing the dimmer intensity to 75 % (green diamonds) and 50 % (red circles) does not alter the general shapes of the E_B-E_v curves. Note, that all BLH weighted irradiance maxima are found at 8500 K and not at the highest CCT.

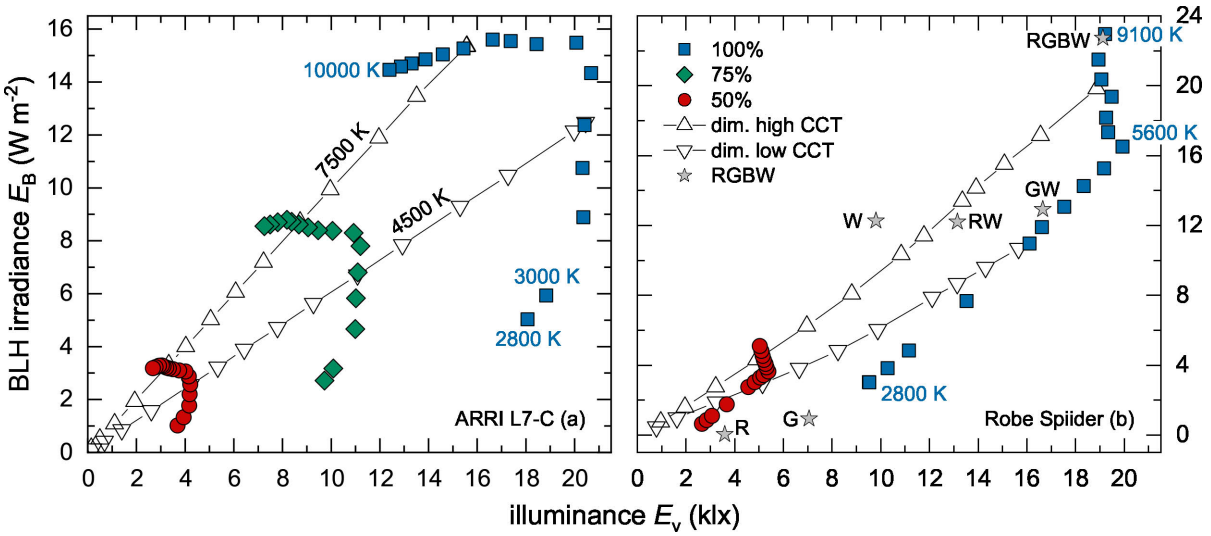

Fig. 5.3 E_B-E_v comparison of (a) an ARRI L7-C spotlight measured at 1.75 m and (b) a Robe Spiider investigated at 2.58 m. (a) Full symbols represent T_{cp} variations from 3000 – 10 000 K in steps of 500 K plus 2800 K for constant values of 100 % (squares), 75 % (diamonds), and 50 % (circles) dimmer intensity. Open triangles reflect E_B-E_v pairs for a discrete dimming of the lamp in steps of 10 % below half of the maximum dimmer intensity and 5 % else for two fixed CCTs, 4500 K and 7500 K. (b) The T_{cp} variation for 100 % as well as for 50 % dimmer intensity was performed by a gradual change of channel 12 from 255/255 (2700 K) to 0/255 (8000 K). The spotlight was dimmed for two starting CCTs, 7600 and 4400 K; however, T_{cp} strongly varied with dimming, see Fig. 5.4. E_B-E_v pairs are also depicted for some special RGBW combinations.

The Robe Spiider has a different $E_B\,(E_v)$ dependence, see Fig. 5.3 (b). For both investigated dimmer intensities, 100 % and 50 %, E_B increases linearly with E_v up to again 5500 K and then further grows, however, now at more or less constant illuminances. In contrast to the ARRI L7-C, E_B reaches its maximum for the highest T_{cp}. It is worth having a look at special RGBW combinations that are depicted as gray stars. As might be expected, the single red (255 0 0 0), green (0 255 0 0), and white LEDs (0 0 0 255) have much lower BLH weighted irradiances than the blue ones (0 0 255 0) with $E_B = 36\,W\,m^{-2}$ at $E_v = 1.2$ klx (not shown). The same is true for binary combinations of RGB with pc-LEDs for that BW (0 0 255 255) has the global E_B maximum with $58\,W\,m^{-2}$ at $E_v = 11$ klx (not shown). For RGB (255 255 255 0), $E_B = 49\,W\,m^{-2}$ at $E_v = 12$ klx (not shown); thus, it is much higher than RGBW (255 255 255 255) with $E_B = 23\,W\,m^{-2}$ at $E_v = 19$ klx.

5.1.3 Dimmer Intensity

The radiation output of a spotlight is one of the most important parameter affecting BLH, together with the CCT and the zoom/focus. Many or even most modern LED arrays are fully tunable with dimmer intensities ranging from 0 – 100 %. Such a variation is shown in Fig. 5.3 (a) for the ARRI L7-C and in panel (b) for the Robe Spiider.

Two CCT have been chosen for the ARRI L7-C spotlight: $T_{cp} = 7500$ K because E_B is maximum close to this CCT and $T_{cp} = 4500$ K as the measured illuminance is highest. In addition, these two CCTs are recognized as intermediate and cool white, see Section 2.4.2. The mean CCTs derived from a spectral analysis are given by $T_{cp} = (7419 \pm 63)$ K and $T_{cp} = (4563 \pm 44)$ K demonstrating an only weak CCT shift. For both CCT, the dimmer intensity variation leads to perfectly linearly correlated $E_B\,(E_v)$ with coefficients of determination $R^2 = 0.999\,97$ (7500 K) and $R^2 = 0.999\,99$ (4500 K). It should be recognized that setting the dimmer intensity from 100 % to 50 % (blue squares to red circles) reduces E_B by 80 %.

For the Robe Spiider, see Fig. 5.3 (b), the initial CCTs at 100 % dimmer intensity were chosen to be 4400 K and 7600 K with the aim to test both CCT regimes, above and below 5500 K, see Section 5.1.2, but also to be comparable to the ARRI L7-C dimmer intensity variation. Again, linear $E_B\,(E_v)$ relations were found; however, the linearities are slightly less ideal with $R^2 = 0.998$ (7600 K) and $R^2 = 0.997$ (4400 K). As already indicated in the figure caption, the decrease of the dimmer intensity from 100 % to 20 % is accompanied by T_{cp} reductions of 2700 K for the high CCT and 1800 K for the low CCT. Similar to the ARRI L7-C, E_B is only ⅕ at 50 % output power.

5.1.4 BLH Efficacy of Luminous Radiation

A common presentation of the $E_B\,(E_v)$ correlation is a $K_{B,v}(T_{cp})$ diagram that is shown in Fig. 5.4 with data of the previous sections. Open squares (100 %), diamonds (75 %), and circles (50 %) reflect T_{cp} variations for constant dimmer intensities. The $K_{B,v}$ in panel (a) for an ARRI L7-C have a similar T_{cp} dependence as those for the blackbody radiator (solid line), but all of them are smaller than $K_{B,v}^{Planck}$. The other way round, varying the dimmer intensity for two fixed CCTs (open triangles) yields constant values, $K_{B,v} = (0.606 \pm 0.003)\,W\,klm^{-1}$ and $K_{B,v} = (0.995 \pm 0.005)\,W\,klm^{-1}$. Exceptions thereof exist for the two lowest dimmer intensities (20 % and 10 %) highlighted by red color for

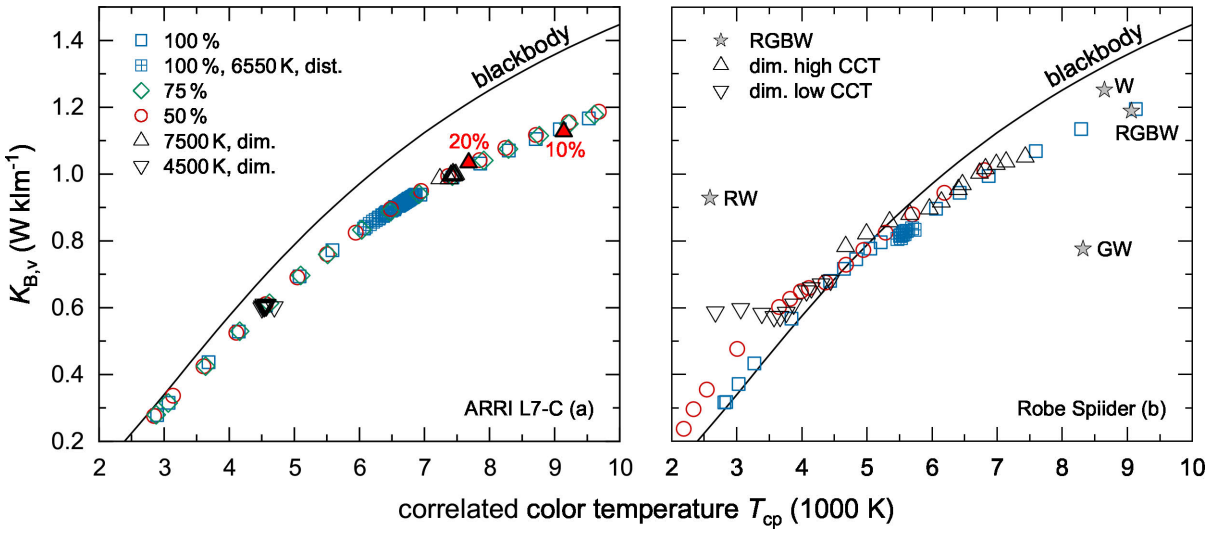

Fig. 5.4 $K_{B,v}$ presentation as a function of CCT for all data shown in Fig. 5.3 including results from distance dependent measurements presented later in Sections 5.2.2 and 5.2.3. In panel (a), two "outliers" are marked with red color. Some special RGBW combinations for the Robe Spiider are shown as stars in panel (b). Solid lines visualize the blackbody $K_{B,v}^{Planck}$ based on Eq. 2.27.

that increased $K_{B,v}$ are found at higher CCTs. In addition, distance dependent $K_{B,v}$ determined from measurements presented later in Section 5.2.2 are included as crossed squares, and they coincide well with the $K_{B,v}(T_{cp})$ curve. Their CCT dependence is linear with a 770 K decrease from 1 m to 14 m. This is an important finding because it demonstrates that the CCT can vary despite constant lamp parameters.

Two T_{cp} variations (squares and circles) for the Robe Spiider resulted in $K_{B,v}$ values close to or slightly higher than those for the blackbody radiator. In contrast to the ARRI L7-C, a reduction of dimmer intensity (triangles) is accompanied by strong T_{cp} decreases, but these $K_{B,v}$ more or less coincide with those from the T_{cp} variations. This is not true for the lower CCT (triangles down), initially set to $T_{cp} = 4400$ K, for that $K_{B,v}$ is virtually constant below 70 % dimmer intensity. This means that the ratio of E_B to E_v stays constant although E_B linearly decreases with E_v, see Fig. 5.3 (b). Distance dependent data from Fig. 5.7, recorded at 1.3 – 23.45 m, are centered around 5500 K and are smaller than $K_{B,v}^{Planck}$. In addition, some special RGBW combinations are included in panel (b) with the RW emission located far above the blackbody $K_{B,v}^{Planck}$.

Recalling the Planck Approximation, the fact that most experimentally determined $K_{B,v}$, especially those for CCTs above 4000 K with a potentially higher BLH, were found close to oder below $K_{B,v}^{Planck}(T_{cp})$ speaks in favor of this simplified BLH risk assessment approach. For any given illuminance measurement, increased E_B thus shorter MPEs will result from a higher $K_{B,v}^{Planck}$.

Note: For the Robe MegaPointe, no CCT variation is possible, but an average $K_{B,v} = (1.134 \pm 0.007)$ W klm^{-1} is found at $T_{cp} = (7024 \pm 54)$ K from distance dependent measurements, see Fig. 5.5. $K_{B,v}^{Planck}$ from Tab. 2.3 is given by 1.129 W klm^{-1}, and perfectly matches the experimentally determined value within its standard deviation.

Conclusion “Adjustable Lamp Parameters”

White-Light Generation

→ warm-white light from RGBW LEDs has high red with small blue and green proportions (and vice versa for high CCT)
→ $T_{cp} = 5500\,\mathrm{K}$ seems to be of technical importance for white-light generation from RGBW LEDs

BLH Weighted Irradiance and Illuminance Correlation

→ the shape of the $E_B\,(E_v)$ correlation is very different for the ARRI L7-C and the Robe Spiider
→ E_B is not necessarily highest at the maximum T_{cp}, and E_B can increase for constant or even smaller E_v

Dimmer Intensity

→ ideal linearity with $R^2 \geq 0.997$ was found for the ARRI L7-C and the Robe Spiider
→ reducing the dimmer intensity to 50 % only yields 20 % of the initial E_B
→ dimming can be accompanied by altered CCTs (Robe Spiider)

BLH Efficacy of Luminous Radiation

→ even for constant lamp parameters, $K_{B,v}$ can change, for example, with varying distance
→ CCT, dimmer intensity, and distance variations yield $K_{B,v}$ values mostly smaller than $K_{B,v}^{\mathrm{Planck}}(T_{cp})$
→ higher blackbody $K_{B,v}$ yield shorter MPEs (for constant E_v); thus, being more restrictive, and in favor of the Planck Approximation

5.2 Spotlight-to-Detector Distance

5.2.1 Robe MegaPointe

BLH weighted irradiances, E_B, for a Robe MegaPointe spotlight operated at 89 % dimmer intensity in flood mode are presented in Fig. 5.5 (a) as a function of inverse square distance, d^{-2}. The data consist of three independent measurement series conducted either with a CAS 140CT-152 or a BTS VL-TEC, both with open FOV. A least-squares fit analysis revealed a high linearity of $E_B(d^{-2})$ with the coefficient of determination $R^2 = 0.9992$; thus, the inverse square law, see Eq. 2.12, is applicable within the investigated distance range of $1.12\,\text{m} \leq d \leq 18\,\text{m}$.
For guidance, $d_{11} = 13.64\,\text{m}$, where the lamp can be regarded as a small source ($\alpha \leq 11\,\text{mrad}$), and $d_{100} = 1.50\,\text{m}$ ($\widehat{=} 100\,\text{mrad}$) are marked by vertical dashed lines. The rule of thumb “The inverse square law can be applied beginning at a distance of 5 times the source dimension” ($5 \times 150\,\text{mm} = 75\,\text{cm}$) was not tested due to the very high irradiances close to the spotlight. Anyway, the MegaPointe must be treated as a point-like source because of the built-in discharge lamp.

Fig. 5.5 (b) shows BLH weighted radiances with respect to a linear d axis. To avoid the panel to be cluttered with data points, only a few E_B from panel (a) were converted to physical radiances, $L_{EB,\alpha}$, by means of Eq. 2.9. $L_{EB,\alpha}$ increases from 6.0 kW m^{-2} sr^{-1} nearest to the lamp to 8.5 kW m^{-2} sr^{-1} at the largest distance. This mainly stems from the growing importance of ambient reflections, but experimental errors such as incorrect measured distances or off-optical axis detector alignments may also contribute.

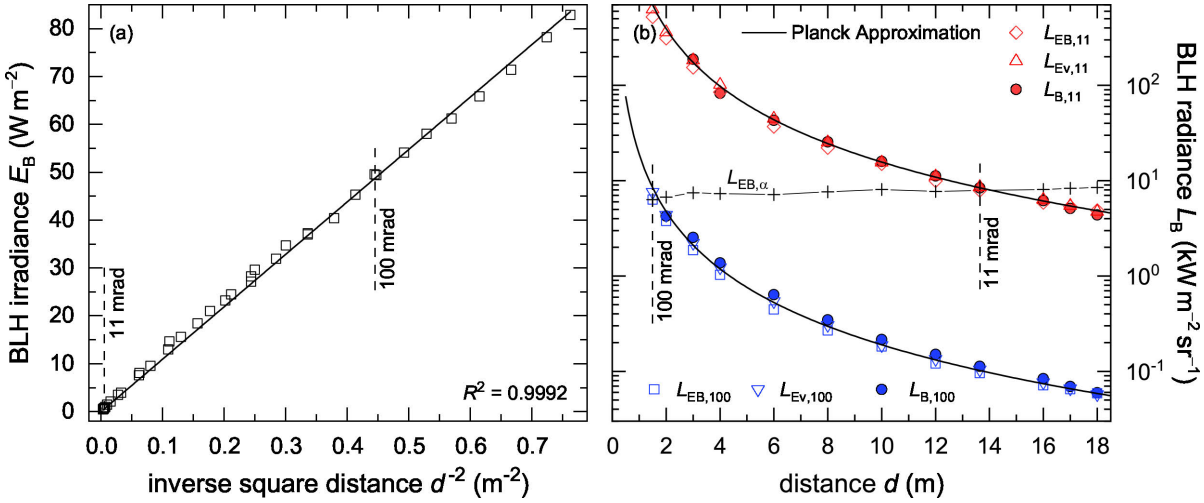

Fig. 5.5 Distance dependence of (a) E_B and (b) L_B for a Robe MegaPointe. A reduced number of E_B values from (a) was converted either by Eq. 2.8 ($L_{EB,11}$, $L_{EB,100}$) or by Eq. 2.9 with a beam diameter of 150 mm ($L_{EB,\alpha}$). Luminances were calculated from illuminances by Eq. 2.8 and then transformed to $L_{Ev,11}$ or $L_{Ev,100}$ via Eq. 2.20 with the experimentally determined $K_{B,v} = (1.134 \pm 0.007)\,\text{W klm}^{-1}$. Direct radiance measurements with $\gamma =$ 11 mrad and 100 mrad ($L_{B,11}$, $L_{B,100}$) are also depicted. L_B calculated with $K_{B,v}^{Planck} = 1.129\,\text{W klm}^{-1}$ for 7000 K, see Tab. 2.3, in conjunction with the inverse square law, see Eq. 2.12, and one illuminance $E_v\,(18\,\text{m}) = 406\,\text{lx}$ are depicted as solid curves in (b). Vertical dashed lines mark $\alpha = 100\,\text{mrad}$ and 11 mrad.

Spatially averaged radiances, $L_{\mathrm{EB},11}$ and $L_{\mathrm{EB},100}$, were calculated from some of the E_{B} data of Fig. 5.5 (a) in conjunction with $\gamma = 11$ mrad and 100 mrad. They decrease with increasing distance to the lamp (note the logarithmic y-axis). Both datasets intersect with $L_{\mathrm{EB},\alpha}$ at those distances, were $\alpha = \gamma$. In order to verify this irradiance to radiance conversion, direct L_{B} measurements were performed with an LDM-9811 (PD16-BLH). The related $L_{\mathrm{B},100}$ and $L_{\mathrm{B},11}$ are slightly higher than their analogues derived from irradiances, but in general they agree with each other.

Illuminances from an X1$_1$ luxmeter (VL-3701) were converted to luminances via Eq. 2.8. With the mean $K_{\mathrm{B,v}} = (1.134 \pm 0.007)\,\mathrm{W\,klm^{-1}}$ determined from the spectral data underlying Fig. 5.5 (a), $L_{\mathrm{Ev},11}$ and $L_{\mathrm{Ev},100}$ were calculated with Eq. 2.20. They virtually agree with the direct radiance measurements as well as with those L_{B} determined from BLH weighted irradiances.

The simplified BLH risk assessment approach introduced in Section 2.5 and denoted as "Planck Approximation" is based on a single illuminance measurement at an arbitrary distance, here for example at $d_0 = 18$ m. By means of the pre-calculated $K_{\mathrm{B,v}}^{\mathrm{Planck}} = 1.129\,\mathrm{W\,klm^{-1}}$ from Tab. 2.3 for a Planckian Radiator with $T_{\mathrm{cp}} = 7000$ K, L_{B} is determined via Eq. 2.8 and Eq. 2.20. In conjunction with the inverse square law, see Eq. 2.12, the Planck Approximation is accurate enough to describe the measured/calculated L_{B} values as can be seen from the solid lines in Fig. 5.5 (b). In addition, approximating $\Omega \approx \pi/4\ D^2 d_0^{-2}$ yields $L_{\mathrm{B},\alpha}^{\mathrm{Planck}} = 8.4\,\mathrm{kW\,m^{-2}\,sr^{-1}}$ being close to $L_{\mathrm{EB},\alpha} = 8.5\,\mathrm{kW\,m^{-2}\,sr^{-1}}$. Summarizing all underlying equations:

$$L_{\mathrm{B},\gamma}^{\mathrm{Planck}} \approx K_{\mathrm{B,v}}^{\mathrm{Planck}}\ E_{\mathrm{v}}\ d_0^2 \begin{cases} 10^4\ d^{-2} & \alpha < \gamma = 11\,\mathrm{mrad} \\ 127\ d^{-2} & \alpha < \gamma = 100\,\mathrm{mrad} \\ 1.27\ D^{-2} & \alpha \geq \gamma \end{cases} \qquad \textbf{(5.1)}$$

5.2.2 ARRI L7-C

ARRI's stage light L7-C was operated at full dimmer intensity, i.e. at 100 %, in spot mode, equal to a minimum beam angle of 15°. The maximum spot mode is realized by a displacement of the Fresnel lens with respect to the LED source by 12.5 cm. It is important to take this displacement into account when verifying the inverse square law. Spectra from two independent measurement series performed with a CAS140-CT spectroradiometer were weighted with the BLH action spectrum, and the related results are depicted in Fig. 5.6 (a) either with or without the source-lens distance. Considering the displacement yields a linearity with $R^2 = 0.999\,93$ whereas neglecting it leads to a lower $R^2 = 0.9987$ (line not shown).

The E_{B} data from panel (a) were converted to BLH weighted radiances with constant solid angles based on 100 and 11 mrad, open squares and diamonds in Fig. 5.6 (b), respectively, and they exhibit the prominent d^{-2} distance dependence. The $L_{\mathrm{EB},100}$ values are lower than $L_{\mathrm{B},100}$ from direct radiance measurements carried out with an LDM-9811 (full blue circles).
In contrast to MegaPointe's built-in point-like discharge lamp, the Fresnel lens with its diameter of 175 mm has an apparent source size $\alpha \geq 11$ mrad at $d \leq 15.91$ m; thus,

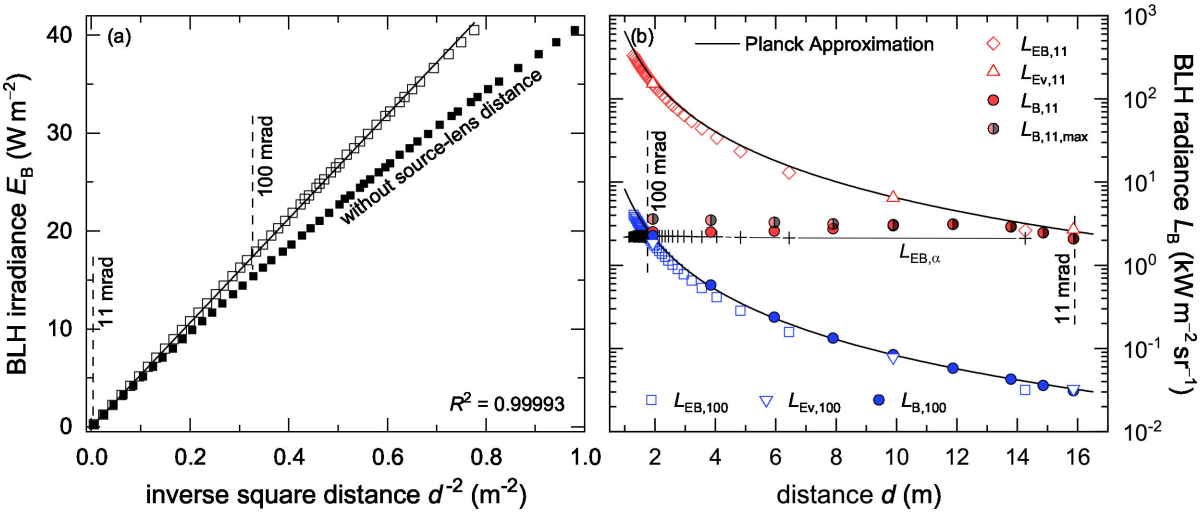

Fig. 5.6 (a) BLH weighted irradiances plotted versus d^{-2} with (open squares) and without (full squares) the additional source-lens distance of 12.5 cm. (b) Calculated radiances, $L_{EB,11}$ and $L_{EB,100}$ (open diamonds and squares), based on the data depicted in panel (a). $L_{B,11}$ and $L_{B,100}$ from radiance measurements are shown as full circles. Semi-filled circles reflect detected maximum BLH weighted radiances with $\gamma = 11$ mrad. Converted illuminances by means of the experimentally determined $K_{B,v} = (0.89 \pm 0.02)$ W klm^{-1} are included as triangles. The Planck Approximations are visualized by solid lines.

$L_{B,11}$ (partly hidden by $L_{B,11,max}$) should no longer depend on distance but match the physical radiance, $L_{EB,\alpha}$. Indeed, both mean values, $L_{B,11} = (2.7 \pm 0.3)$ kW m^{-2} sr^{-1} and $L_{EB,\alpha} = (2.22 \pm 0.03)$ kW m^{-2} sr^{-1}, are close to each other within their standard deviations. A separate measurement series aimed at finding the maximum BLH weighted radiances within 11 mrad, and the related mean $L_{B,11,max} = (3.2 \pm 0.2)$ kW m^{-2} sr^{-1} is in accordance with $L_{B,11}$.

Illuminances recorded at only three exemplary distances were converted by means of $K_{B,v} = (0.89 \pm 0.02)$ W klm^{-1}, determined from the spectral data in panel (a), and are presented as open triangles in Fig. 5.6 (b). With $E_v = 285$ lx measured at $d_0 = 15.86$ m and $K_{B,v}^{Planck} = 1.071$ W klm^{-1} taken from Tab. 2.3, the Planck Approximation according to Eq. 5.1 agrees with $L_{B,100}$ from radiance measurements, but lies above $L_{EB,100}$ and $L_{EB,11}$. The physical radiance follows as $L_{B,\alpha}^{Planck} = 2.7$ kW m^{-2} sr^{-1} in accordance with $L_{B,11} = (2.7 \pm 0.3)$ kW m^{-2} sr^{-1}.

5.2.3 Robe Spiider

The spotlight was operated at parameters similar to those described in Section 5.1.1, i. e. at 100 % intensity, 150 of 255 zoom, and 5600 K (channel 12 was set to 64). Spectral irradiances were recorded with a BTS2048-VL-TEC as a function of distance, and subsequently convoluted with $B(\lambda)$ to get E_B, plotted in Fig. 5.7 (a). Two different regimes are discernible whose linear least-squares fits intersect at $d^{-2} \approx 0.3$ m^{-2} equal to a distance of ~ 1.8 m. Based on the relatively large inner diameter of the Spiider's front side of $D = 25.8$ cm, this distance is equivalent to approximately 7 times D. However, there are important aspects to keep in mind. First, the intersection point

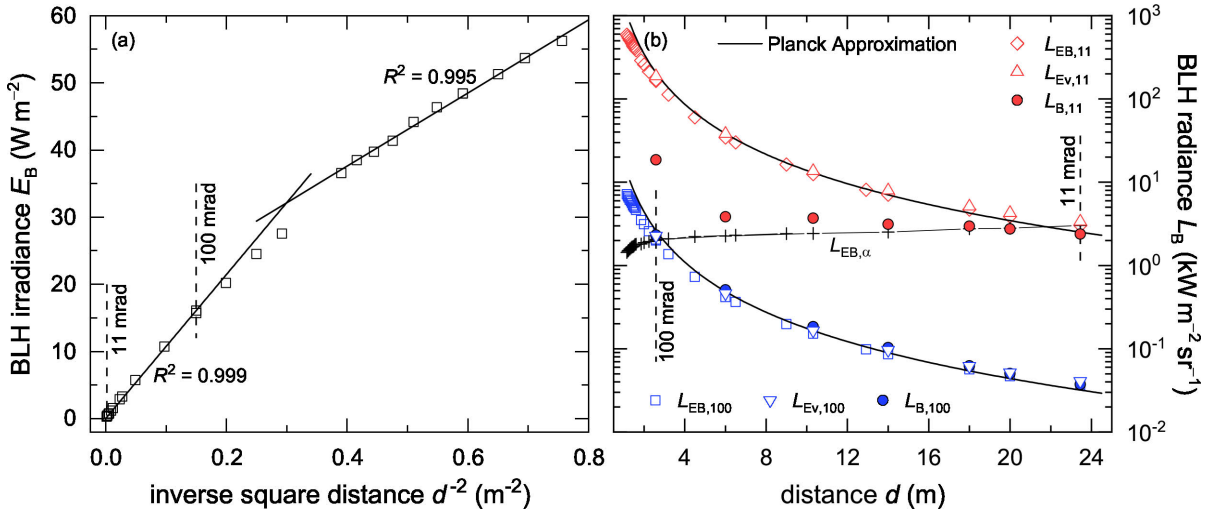

Fig. 5.7 (a) Verification of the inverse square law by means of distance dependent BLH weighted irradiances. Solid lines represent linear least-squares fits with given coefficients of determination, R^2. Converting these E_B to radiances yields $L_{EB,\alpha}$, $L_{EB,100}$, and $L_{EB,11}$ depicted in panel (b). Results from radiance measurements with an LDM-9811 are included as full circles, converted illuminances from a VL-3701 as triangles. Planck Approximations according to Eq. 5.1 are shown as solid lines.

strongly depends on the number of E_B taken for each linear fit into account. Assuming a $\pm 0.1\,\mathrm{m}^{-2}$ uncertainty, the intersection point would be found within 1.6 – 2.2 m or roughly 6 – 8 times D. Second, the front side diameter represents neither the emitting surface, because of spaces between the single lenses, nor the actual apparent source size that certainly will be much smaller. Third, E_B from two independent measurement series are depicted in Fig. 5.7 (a) that inherently contain errors from, for example, an imprecise detector alignment. Fourth, data points are missing, in particular around the intersection. As a conclusion, the inverse square law is only valid at distances longer than approximately 2.58 m equal to 10 times D or $\alpha = 100\,\mathrm{mrad}$. It should be complimented that an inverse distance dependence $\propto d^{-1}$ can exist for extended sources (Weber 2018); however, such a relation was not found for the Robe Spiider.

The E_B data from panel (a) were converted by means of Eq. (2.8) and (2.9) to $L_{EB,100}$, $L_{EB,11}$ and $L_{EB,\alpha}$, respectively. The mean physical radiance is given by $L_{EB,\alpha} = (2.4 \pm 0.3)\,\mathrm{kW\,m^{-2}\,sr^{-1}}$ only considering data for $\alpha \leq 100\,\mathrm{mrad}$. Direct L_B measurements, $L_{B,100}$, virtually agree with $L_{EB,100}$. At a greater distance, $L_{B,11}$ is close to the physical radiance whereas it strongly deviates near the spotlight. Upon approaching the Spiider, the 11 mrad FOV no longer averages of the whole front side but the centered 60 W LED more and more gains in importance compared to the surrounding 40 W LEDs.

With $K_{B,v}^{Planck} = 0.906\,\mathrm{W\,klm^{-1}}$ from Tab. 2.3 for $T_{cp} = 5600\,\mathrm{K}$ and an illuminance measurement at 10.32 m (chosen from the $\alpha \leq 100\,\mathrm{mrad}$ distance regime) carried out by a VL-3701, the Planck Approximations according to Eq. 5.1 more ore less agree with the other radiances, but start to deviate close to the lamp. The mean physical radiance $L_{B,\alpha}^{Planck} = 2.6\,\mathrm{kW\,m^{-2}\,sr^{-1}}$ is in accordance with the mean one derived from irradiance measurements.

Conclusion “Spotlight to Probe Distance”

Robe MegaPointe

→ as a consequence of the built-in point-like discharge lamp, the inverse square law is valid for all investigated distances
→ due to real ambient conditions, the BLH weighted physical radiances, $L_{\mathrm{EB},\alpha}$, are not independent of distance
→ all L_{B} values obtained from irradiance, illuminance, and radiance measurements more or less agree among each other
→ the Planck Approximation is accurate enough to describe distance dependent physical as well as spatially averaged BLH weighted radiances

ARRI L7-C

→ the source-lens displacement used in spot mode must be considered for a verification of the inverse square law
→ the extended source leads to virtually constant L_{B} for $\gamma = 11\,\mathrm{mrad}$, and related maximum BLH weighted radiances differ only slightly upon approaching the spotlight

Robe Spiider

→ the inverse square law can only be applied from $\sim 10D$ on because of the extended source character
→ the very inhomogeneous light emission resulting from the central 60 W and its surrounding 40 W LEDs leads to a large deviation of $L_{\mathrm{B},11}$ from the mean physical radiance close to the lamp
→ the Planck Approximation provides accurate descriptions of the spatially averaged and the physical radiances at sufficiently long lamp to probe distances

6 Risk Assessment

The current version of EN 62471 recommends a risk-group (RG) classification distance for GLS where 500 lx are reached and 200 mm for all other lamps. In contrast, exposures at workplaces must be assessed at variable distances to the radiation source where the employee is working. Hereinafter, the distance dependent data obtained in Section 5.2 will be further analyzed with regard to the BLH-ELVs, see Tab. 2.2, and the associated maximum permissible exposure durations (MPE), t_{max}. In a second step, a "test workplace" will be assessed that was also part of the project "High-Power Spotlights Risk Assessment" (HiPoSisAs) within the "Partnership for European Research in Occupational Safety and Health" (PEROSH). All MPEs will be used to evaluate a simplified BLH assessment method, the Planck Approximation.

6.1 MPEs as a Function of Distance

The BLH ELVs for exposure durations less than 10 000 s are either given as time-dependent effective

radiance, $L_{\mathrm{B}} = 10^6\,\mathrm{J\,m^{-2}\,sr^{-1}}\ t_{\mathrm{max}}^{-1}$, for $\alpha \geq 11$ mrad, or

irradiance, $E_{\mathrm{B}} = 100\,\mathrm{J\,m^{-2}}\ t_{\mathrm{max}}^{-1}$, for $\alpha < 11$ mrad,

see Tab. 2.2. According to ICNIRP 2013, three different averaging angles, γ_{ph}, should be used for measurements, see Eq. 2.10. Most exposures will endure less than 100 s, and ICNIRP recommends $\gamma_{\mathrm{ph}} = 11$ mrad which is conservative. For longer exposures, task-determined eye movements dominate and $\gamma_{\mathrm{ph}} = 110$ mrad. However, many radiance instruments are designed for a maximum FOV of 100 mrad. The third γ_{ph} is time-dependent and lies in between 11 and 110 mrad. Hereinafter, $\gamma_{\mathrm{ph}} = 11$ and 100 mrad will be applied.
Distance dependent radiance measurements of a MegaPointe with two fixed FOVs, $L_{\mathrm{B,100}}\,(d)$ and $L_{\mathrm{B,11}}\,(d)$ taken from Fig. 5.5 (b), were compared to the radiance ELV to determine $t_{\mathrm{max},\gamma}\,(d)$, full circles in Fig. 6.1 (a). At distances longer than $d_{11} \approx D\alpha^{-1} = 13.64$ m with $\alpha = 11$ mrad and $D = 0.15$ m, irradiances were recorded, and $t_{\mathrm{max,11}}\,(d)$ was calculated by means of the irradiance ELV (open circles).
MPEs can also be determined by a single E_{v} measurement at d_{11} (Planck Approximation). For this purpose, the CCT must be known which is given as 6300 K in the leaflet, so that $K_{\mathrm{B,v}}$ can be approximated from Tab. 2.3 with $K_{\mathrm{B,v}}^{\mathrm{Planck}} = 1.02\,\mathrm{W\,klm^{-1}}$. In combination with the inverse square law, see Section 2.2.1, $t_{\mathrm{max,11}}\,(d)$ can be determined via

$$t_{\mathrm{max,11}}\,(d) = \frac{100\,\mathrm{J\,m^{-2}}}{K_{\mathrm{B,v}}^{\mathrm{Planck}}\ E_{\mathrm{v}}} \left(\frac{d}{d_{11}}\right)^2, \tag{6.1}$$

solid line in Fig. 6.1 (a). The BLH weighted radiance at d_{11} is equal to the physical one and thus to $L_{\mathrm{B,100}}$ at $d_{100} = 1.5$ m, see Fig. 5.5 (b).

$$\begin{aligned} L_{\mathrm{B,100}}\,(d_{100}) &= L_{\mathrm{B,11}}\,(d_{11}) \\ &= \frac{K_{\mathrm{B,v}}^{\mathrm{Planck}}}{\Omega_{11}}\ E_{\mathrm{v}} \end{aligned}$$

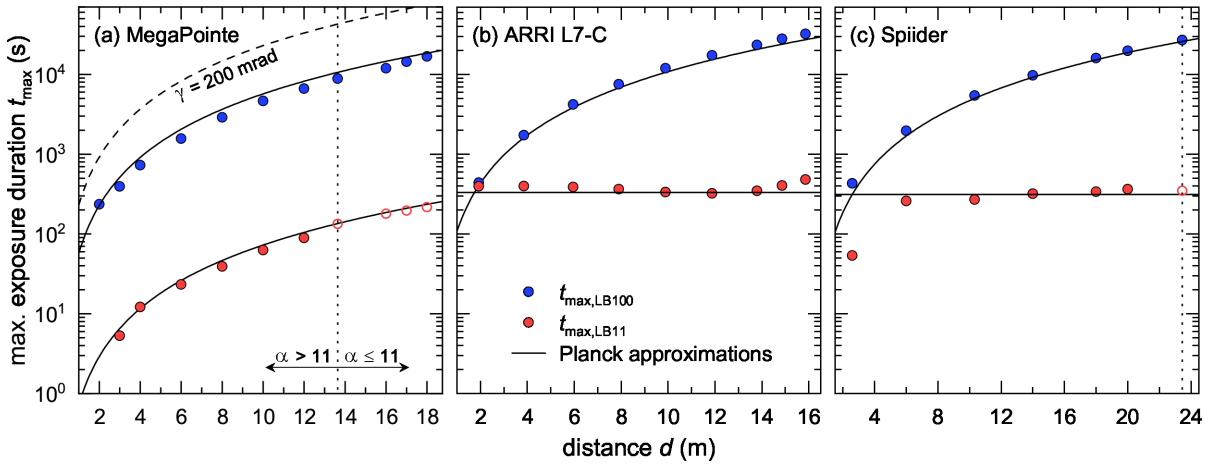

Fig. 6.1 Maximum permissible exposure durations, $t_{\mathrm{max}}\,(d)$, as a function of distance for (a) a Robe MegaPointe, (b) an ARRI L7-C, and (c) a Robe Spiider based on radiance measurements with $\gamma = 100$ mrad and 11 mrad FOV (full circles), irradiance measurements with open FOV (open circles), or determined by means of the Planck Approximation with a single E_{v} measurement (solid lines). For $\gamma = 200$ mrad, the Planck Approximation is shown as dashed line in panel (a). Vertical dotted lines separate the $\alpha > 11$ mrad from the $\alpha \leq 11$ mrad region.

Applying this conservation of radiance in conjunction with Eq. 6.1, distance dependent MPEs can be calculated for $\gamma_{\mathrm{ph}} = 100$ mrad,

$$t_{\mathrm{max,100}}\,(d) = \frac{10^6\,\mathrm{J\,m^{-2}\,sr^{-1}}}{L_{\mathrm{B,100}}\,(d)} = 10^4\,\mathrm{sr^{-1}}\;\Omega_{11}\left(\frac{d_{11}}{d_{100}}\right)^2 t_{\mathrm{max,11}}\,(d) \;\approx\; 80\;t_{\mathrm{max,11}}\,(d) \qquad \textbf{(6.2)}$$

and can be simplified by approximating $\Omega_{11} = 9.5 \times 10^{-5}$ sr with 10^{-4} sr, yielding MPEs that are 5 % longer (less restrictive). However, the squared ratio of d_{11} to d_{100}, being equal to the squared ratio of 100 mrad to 11 mrad, is given by 82.6; thus, the factor of 80 is slightly (3 %) more restrictive. Furthermore, the most important parameter influencing t_{max} is the accuracy of the E_{v} measurement itself. As can be seen for the ARRI L7-C and the Robe Spiider in Fig. 6.1 (b) and (c), respectively, the Planck Approximations for $t_{\mathrm{max,100}}$ (solid lines) result in shorter MPEs than compared to those derived from radiance measurements, thus, being more restrictive.

The Planck Approximation has an additional advantage. ICNIRP states that “If the visual task and the behavior can be characterized, a safety analysis can account for more realistic eye movements and a larger averaging angle can be used” (ICNIRP 2013). Assuming, for example, $\gamma_{\mathrm{ph}} = 200$ mrad, d_{100} needs only to be replaced by $d_{200} = 74.8$ cm in Eq. 6.2 yielding a factor of 4. The distance dependent MPEs are shown as dashed line in Fig. 6.1 (a).
Regarding the ARRI L7-C, all $L_{\mathrm{B,11}}$ measurements are more or less constant at distances shorter than $d_{11} = 15.86$ m. In such a case, d_{11} must be substituted by a variable d in Eq. 6.2 because $t_{\mathrm{max,11}}$ is no longer a function of distance. In general,

the same holds true for the Robe Spiider although the influence of the most powerful central LED on $L_{B,11}$ increases upon approaching the spotlight, and the MPEs decrease.

Finally, it is important to note that although the Planck Approximation is accurate enough to describe the distance dependence of MPEs calculated from BLH weighted radiance measurements, the semi-logarithmic presentation of Fig. 6.1 might be misleading with regard to the actual extent of deviation. For example, $t_{max,100}$ for the MegaPointe are up to 30 % and $t_{max,11}$ up to 20 % longer than those MPEs determined from radiance measurements. However, it is of crucial importance to consider all sources of error, see Section 7.3.

6.2 Workplace Exposure Scenario

In order to further verify the Planck Approximation, a test workplace was set up with the three spotlights assessed in the previous section and with two additional Ultralite PAR 56. All lamp parameters remained the same except for the MegaPointe with altered power resulting in a beam diameter of $D \approx 6$ cm. Vertical and horizontal spotlight positions, distances to the fixed detector location (height of 1.6 m), as well as apparent source sizes and CCTs are given in Tab. 6.1. The CCT of the Robe Spiider was set to 5600 K via the DMX protocol whereas it was adjusted to 6550 K by a knob on the ARRI L7-C. In the Ultralite PAR 56 manual, T_{cp} is given by 2750 K. $t \leq 10\,000$ s is assumed.

Tab. 6.1 Lengths and distances at the test workplace: D (diameter), p (horizontal position), h (height), and d_0 (distance to EOP). Apparent source sizes α and CCTs are also listed. For the MegaPointe, the beam diameter is approximately 6 cm.

	D (cm)	p (m)	h (m)	d_0 (m)	α (mrad)	T_{cp} (K)
Spiider	25.8	0	1.97	11.41	23	5600
PAR I	13.5	0.70	2.09	11.22	12	2750
L7-C	17.5	1.11	2.03	11.07	16	6550
MegaPointe	~ 6	1.80	1.91	11.12	5	6300
PAR II	13.5	2.63	2.07	11.46	12	2750

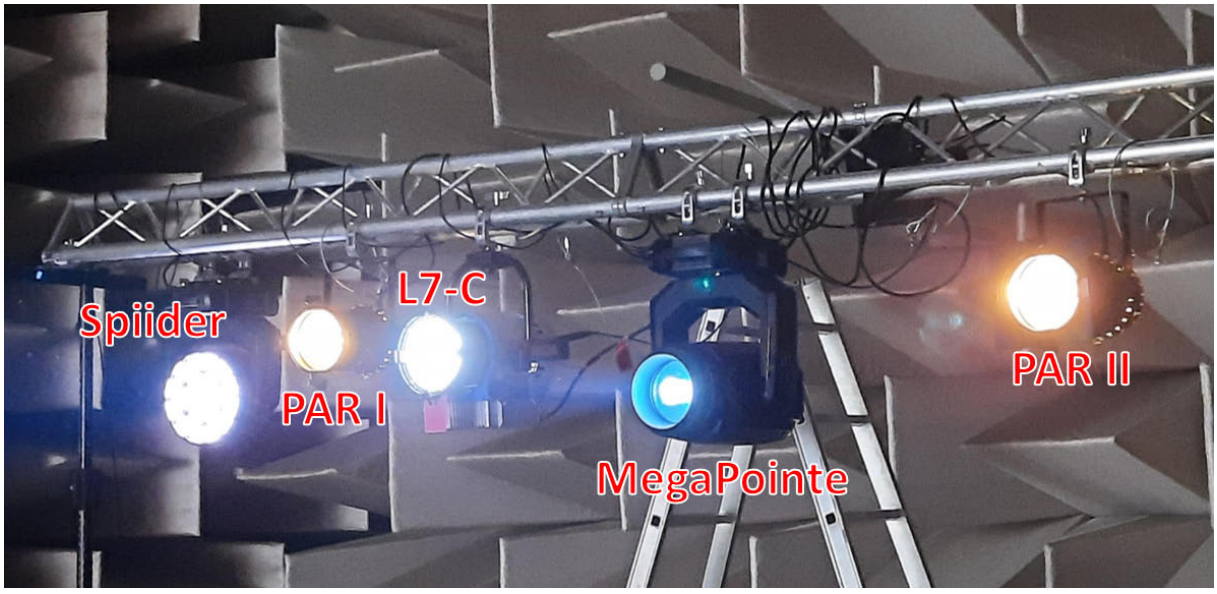

Tab. 6.2 Measured BLH weighted radiances with $\gamma_{ph} = 11\,\text{mrad}$, $L_{B,11}$ in $\text{kW}\,\text{m}^{-2}\,\text{sr}^{-1}$, and irradiance, E_B in $\text{W}\,\text{m}^{-2}$, as well as illuminances, E_v in klx. Calculated MPEs, t_{max}, are given in s with their percentage deviations, δ, in the last column.

	$L_{B,11}$	t_{max}	E_B	t_{max}	E_v	t_{max}	δ
Spiider	3.5	289	–	–	1.2	351	21
PAR I	0.48	2101	–	–	0.18	2084	−0.8
L7-C	2.2	460	–	–	0.36	495	8
MegaPointe	–	–	7.5	13	6.9	14	5
PAR II	0.33	3077	–	–	0.12	3047	−1

A glance at α in Tab. 6.1 reveals that radiances, $L_{B,11}$, must be measured except for the MegaPointe with $\alpha \leq 11\,\text{mrad}$ at 11.12 m for that its BLH weighted irradiance, E_B, can be recorded. The related measurement results are listed in Tab. 6.2. In case of radiances, MPEs were calculated with regard to $L_B = 10^6\,\text{J}\,\text{m}^{-2}\,\text{sr}^{-1}\,t_{max}^{-1}$ whereas for the MegaPointe, $E_B = 100\,\text{J}\,\text{m}^{-2}\,t_{max}^{-1}$ was used. Illuminances were multiplied with $K_{B,v}^{Planck}$ from Tab. 2.3, converted to L_B via $\Omega \approx 0.785\left(\frac{D}{d_0}\right)^2$, and then compared to the radiance ELV. The MPE for the MegaPointe directly follows from a comparison with the ELV given as irradiance.

$$t_{max} = \left(K_{B,v}^{Planck}\,E_v\right)^{-1}\begin{cases}100\,\text{J}\,\text{m}^{-2} & \alpha < \gamma = 11\,\text{mrad}\\ 7.85\,\text{kJ}\,\text{m}^{-2} & \alpha < \gamma = 100\,\text{mrad}\\ 785\,\text{kJ}\,\text{m}^{-2}\left(\frac{D}{d_0}\right)^2 & \alpha \geq \gamma\end{cases} \qquad \textbf{(6.3)}$$

MPEs determined by means of the Planck Approximation deviate less than 5 % from those based on radiance measurements for the halogen and discharge lamps whereas δ is much higher for both LED spotlights, especially for the Spiider with its inhomogeneously emitting surface and the large α. As already mentioned, the approximation of an LED emission spectrum with that of a blackbody radiator certainly is rather poor (ICNIRP 2020). In contrast, $K_{B,v}^{Planck}(T)$ lies above or close to the ARRI L7-C and the Robe Spiider $K_{B,v}$ values for several lamp parameters, see Fig. 5.4, actually yielding higher E_B thus shorter t_{max} (restrictive side). Probably, the E_v measurement has not been accurate enough. However, it should also be noted that δ assumes a correct radiance measurement and therefore has an inherent uncertainty.

An adjustment of the Planck Approximation towards more restrictive MPEs is the application of $\alpha = 11\,\text{mrad}$ for all spotlights, irregardless of their actual apparent source size at a certain distance. Then, the solid angle is constant with $\Omega_{11} \approx 10^{-4}\,\text{sr}$, and a comparison with the radiance ELV results in the upper part of Eq. 6.3 which is equal to the MPE based on the irradiance ELV. This adjustment works well if the real α is close to 11 mrad. For example, $t_{max} = 1919\,\text{s}$ and 2927 s compared to 2084 s and 3047 s for PAR I and II, but only 92 s for the Spiider in contrast to 351 s, see Tab. 6.2.

6.2.1 Planck Approximation Accuracy for Different Beam Angles

To evaluate the accuracy of MPEs determined via the Planck Approximation for different beam angles, exemplary BLH weighted radiances (11 mrad) and irradiances as well as illuminances were recorded for spot and flood mode of the Robe Spiider, the ARRI L7-C, and the Robe MegaPointe. Such a variation is not possible for both PAR spotlights.

t_{max} were calculated according to Eq. 6.3, and are listed in Tab. 6.3 together with their percentage deviations. δ_{spot} and δ_{flood} are, by and large, negative which means that the Planck Approximation yields more restrictive MPEs. An exception thereof is found for the MegaPointe operated in flood mode for that $\delta_{flood} = 15\,\%$. This difference could result from an off-center illuminance measurement accompanied by lower E_v values thus longer t_{max}.

It is important to emphasize that these measurements can only provide a rough hint of the Planck Approximation accuracy as a function of different beam angles. Further measurements must be performed with a higher angular resolution, also for additional spotlights.

6.2.2 Assessment of Retinal Thermal Hazards

The spectral characteristics of the MegaPointe with its weak but non-negligible IR-A radiation emission, see Fig. 3.5, at least suggest an estimation of retinal thermal hazards. The same is true for both PAR spotlights, however, with much less emission power. As the ELVs depend inversely on the apparent source size, see Tab. 2.2, the Robe Spiider with its large α will also be considered.
Assuming an exposure duration less than 10 s, the L_R ELV is time-dependent, and t_{max} can be determined. MPEs are far above realistic exposure scenarios with orders of magnitude of 10^7 s (for the MegaPointe with a measured $L_R > 103\,\mathrm{kW\,m^{-2}\,sr^{-1}}$) and beyond.

Note: L_R was measured with a PD-16RTH integral sensor, see Tab. 3.1, which is based on $R(\lambda) \leq 1$. This is in line with ICNIRP 2013 but a disagreement to 2006/25/EC. In addition, ICNIRP recommends an upper radiance limit of $28\,\mathrm{kW\,m^{-2}\,sr^{-1}}\alpha^{-1}$ for $t \geq 0.25$ s whereas the EU directive prescribes this value from 10 s on.

Tab. 6.3 MPEs in s for spot and flood mode determined from BLH weighted radiance or in case of the MegaPointe from irradiance measurements. Illuminances were recorded, and related t_{max} were calculated via the Planck Approximation, see Eq. 6.3. Percentage deviations, δ in %, are also listed.

	spot			flood		
	$L_{B,11}$ / E_B	E_v	δ_{spot}	$L_{B,11}$ / E_B	E_v	δ_{flood}
Spiider	55	47	−14	1538	1405	−9
L7-C	435	374	−14	1887	1464	−22
MegaPointe	2.5	2.2	−14	31	35	15

Conclusion “Risk Assessment”

MPEs as a Function of Distance

→ a single E_{v} measurement at d_{11} is sufficiently accurate to describe distance dependent MPEs not only for 11 mrad but also for 100 mrad averaging angle
→ an approximate relation is given by $t_{\mathrm{max,100}}\,(d) \approx 80\; t_{\mathrm{max,11}}\,(d)$
→ the Planck Approximation allows a simple calculation of distance dependent MPEs for any γ_{ph}

Workplace Exposure Scenario

→ MPEs can be calculated easily with the Planck Approximation by means of an E_{v} measurement together with known CCT, diameter, and distance, see Eq. 6.3
→ percentage deviations with respect to MPEs derived from radiance measurements are worst for LED spotlights ($< 20\,\%$)
→ an over-restrictive simplification of the Planck Approximation that can be regarded as an orientation measurement is the use of $\alpha = 11$ mrad for all spotlights
→ upon varying beam angles, MPEs deviate roughly by $\pm 20\,\%$
→ MPEs for RTHs are much longer than realistic exposure scenarios, and several discrepancies exist between 2006/25/EC and ICNIRP 2013 regarding RTHs

7 Summary and Outlook

7.1 Instrument Comparison

The instrument's measurement error is an essential quantity that must be checked regularly to guarantee accurate results as well as to be able to take countermeasures, for example, in the form of a re-calibration. In addition, different instruments usually provide different results. An evaluation of a simplified BLH measurement method should consider such inaccuracies. Consequently, for this project, a three-step process was carried out to obtain information about measurement uncertainty for spotlights.

Step 1 was an instrument comparison with respect to a calibrated radiance standard irrespective of the measurands, i. e. $E(\lambda)$, $L(\lambda)$, E_v, or L_B. Irradiances and illuminances were converted to radiances and luminances, respectively, by means of known ground glass window diameter, measurement distance, and CCT. Results from radiance measuring devices agreed with the reference values within the expanded uncertainties ($k = 2$), whereas L_B and L_v determined from conversions showed maximum standard deviations of $\pm$7 %, especially at longer distances, probably due to the effect of stray light on low level illuminances.

The next step with higher measurement demands was carried out by means of an LED Fresnel stage light, an ARRI L7-C. Its lens no longer has a homogeneous emission distribution, but the deviations are still comparably small, see Fig. 3.6. In general, BLH weighted radiances determined from irradiances or illuminances were found again with higher values at longer distances. It was unexpected that the standard deviations were below $\pm$8 % as for the SRS8, despite the increased measurement demands.

The same is true for the third step of the instrument comparison. A Robe Spiider was used, equipped with 18×40 W and one centered 60 W LED; thus, having a highly inhomogeneously emitting surface. The mean L_v and L_B determined for 2.58 m, 10.32 m, and 23.45 m were accompanied by standard deviations of roughly $\pm$10 % (excluding the SRT200) being comparable to the previous results irrespective of the more challenging measurement conditions.

Finally, a test of the Planck Approximation accuracy was performed with the E_v data obtained in the previous sections. The related mean BLH weighted radiances deviated less than 20 % from their analogs based on E_B and L_B. With higher radiances and thus shorter MPEs, the Planck Approximation is more restrictive. From an occupational safety and health point of view, it can be regarded as a promising simplified BLH assessment method.

7.2 Influencing Factors

The analysis of lamp parameters affecting BLH started with a closer look on white-light generation of the ARRI L7-C and the Robe Spiider as a function of CCT. Both spotlights showed complex spectral changes. The correlation of these CCT-dependent E_B and E_v data was analyzed subsequently. It was found that E_B does not need to be maximum for the highest T_cp and that it can increase for constant or even smaller E_v.

The dimmer intensity was varied in the second measurement series. For the ARRI L7-C as well as for the Robe Spiider, ideal linearities were found for $E_\mathrm{B}\,(E_\mathrm{v})$ with an 80 % E_B reduction for half of the maximum output power. Varying the dimmer intensity can be accompanied by a CCT change.

The data of both measurement series were plotted in a $K_\mathrm{B,v}(T_\mathrm{cp})$ diagram and compared to pre-calculated $K_\mathrm{B,v}^\mathrm{Planck}$. Most of the experimentally determined $K_\mathrm{B,v}$ values were smaller than those for the blackbody radiator, except for the Robe Spiider operated at CCTs roughly below 4000 K for that the BLH efficacies of luminous radiation lay above $K_\mathrm{B,v}^\mathrm{Planck}(T_\mathrm{cp})$. Additional results from distance dependent measurements agreed very well with data from CCT and dimmer intensity variation and were accompanied by changes in T_cp, probably due to ambient stray light. The fact that $K_\mathrm{B,v}^\mathrm{Planck}$ can be regarded as an upper limit in many cases, yielding shorter thus more restrictive MPEs, is in favor of the Planck Approximation.

Distance dependent spectral irradiances for Robe's discharge lamp MegaPointe, measured up to 18 m, perfectly fulfilled the inverse square law. The converted E_B matched the L_B from direct radiance measurements as well as those derived from illuminances. The physical BLH weighted radiances, $L_{\mathrm{EB},\alpha}$, were not constant, probably due to ambient light, but increased upon moving away from the lamp. $L_{\mathrm{B},\gamma}^\mathrm{Planck}\,(d)$, calculated by means of the Planck Approximation, could parametrize the experimentally determined BLH weighted radiances very well. Overall, with knowledge of the spotlight's diameter D, one illuminance measurement E_v at the distance d_0, and with a pre-calculated $K_\mathrm{B,v}^\mathrm{Planck}$ from a look-up-table, see Tab. 2.3, simple equations can be deduced (equal to Eq. 5.1).

$$L_{\mathrm{B},\gamma}^\mathrm{Planck} \approx K_\mathrm{B,v}^\mathrm{Planck}\; E_\mathrm{v}\; d_0^2 \begin{cases} 10^4\; d^{-2} & \alpha < \gamma = 11\,\mathrm{mrad} \\ 127\; d^{-2} & \alpha < \gamma = 100\,\mathrm{mrad} \\ 1.27\; D^{-2} & \alpha \geq \gamma \end{cases}$$

In general, similar results were obtained for the ARRI L7-C and the Robe Spiider but with some specialties. Due to the technical design of the ARRI L7-C, its Fresnel lens is shifted with respect to the LED light engine if the stage light is operated in spot mode. This displacement has to be taken into account when evaluating the inverse square law. In addition, the extend source character leads to more or less constant L_B for an 11 mrad FOV that virtually agree with the physical ones. The same is true for the Robe Spiider; however, due to the centered 60 W LED surrounded by several 40 W LEDs, the measured $L_{\mathrm{B},11}$ strongly increase in relation to $L_{\mathrm{EB},\alpha}$ upon approaching the lamp.

7.3 Simplified BLH Risk Assessment Approach

In many cases, radiance measurements are prescribed for the BLH risk assessment at workplaces. Appropriate instruments can be expensive, and their operation is challenging. Irradiances can be recorded if the apparent source size α is smaller than 11 mrad what is often fulfilled only at long distances. The idea to use a cost-effective luxmeter for illuminance measurements finally led to the Planck Approximation.

The ratio of BLH weighted irradiance to illuminance is called BLH efficacy of luminous radiation, $K_{\mathrm{B,v}}$, and can be calculated for any blackbody radiator with known absolute temperature. The resulting $K_{\mathrm{B,v}}^{\mathrm{Planck}}(T_{\mathrm{cp}})$ curve is close to experimentally determined ones for many light sources although LED emission spectra are apparently not well-described by a thermal radiator. By means of a simple E_{v} measurement and given CCT (usually written in the manual or tunable via DMX protocol), pre-calculated $K_{\mathrm{B,v}}^{\mathrm{Planck}}$ values for blackbody radiators can be used to determine E_{B} and via the diameter of the emitting surface L_{B}.

It could be demonstrated in this work that one single E_{v} measurement is accurate enough to describe the distance dependence of MPEs derived from radiance measurements not only with 11 mrad but also with 100 mrad FOV. Even more, the Planck Approximation can account for any γ_{ph} if the exposure scenario is characterized accordingly. At most workplaces, usually only one distance has to be evaluated. For this case, simple equations can be deduced on the basis of the Planck Approximation (equal to Eq. 6.3)

$$t_{\mathrm{max}} = \left(K_{\mathrm{B,v}}^{\mathrm{Planck}}\ E_{\mathrm{v}}\right)^{-1} \begin{cases} 100\,\mathrm{J\,m^{-2}} & \alpha < \gamma = 11\,\mathrm{mrad} \\ 7.85\,\mathrm{kJ\,m^{-2}} & \alpha < \gamma = 100\,\mathrm{mrad} \\ 785\,\mathrm{kJ\,m^{-2}} \left(\frac{D}{d_0}\right)^2 & \alpha \geq \gamma \end{cases}$$

It is obvious that an approximation has a lower accuracy than the original measurement. In case of the Planck Approximation, percentage deviations with respect to MPEs determined from distance dependent radiance measurements are around or below 30 %. A BLH risk assessment at an exemplary test workplace showed percentage deviations lower than 10 % except for an LED spotlight (Robe Spiider) with a very irregular light emission distribution and a large apparent source size. Orienting investigations of the Planck Approximation accuracy depending on different beam angles yielded mostly negative percentage deviations (restrictive side) with roughly $\pm$20 %. By and large, an overall accuracy of $\pm$30 % can be concluded from the project results.

Contextualizing this finding, one should remember the mean percentage deviations of L_{B} and L_{v} measurements from different instruments for selected spotlights, Sections 4.2 and 4.3, approximately ranging from 5 – 12 %. Certain devices can have much larger percentage deviations.
Apart from measurement accuracies, the true viewing behavior of the exposed worker is the most important factor influencing MPEs, but it is also the most imprecise one. Based on the assumed exposure duration queried during risk assessment, ICNIRP recommends two fixed averaging angles and a time-dependent one, see Eq. 2.10, that are themselves just approximations to the actual retinal exposures. The inaccuracies that accompany exposure durations and averaging angles can be hardly estimated but certainly will be high.

7.4 Future Work

Overall, considering the sum of error sources mentioned above, the Planck Approximation holds the potential to be a promising procedure for a simplified BLH risk assessment at workplaces. The limited number of tested spotlights for this project makes it difficult to

draw general conclusions, and although a “test workplace” has been built up, an actual exposure situation of employees will certainly differ. A current PEROSH project entitled “High-Power Spotlights Risk Assessment (HiPoSisAs)” also focuses on the search for a simplified workplace risk assessment method, and the Planck Approximation can be evaluated therein, at least at a few locations.

Moreover, some influencing parameters could only be investigated exemplarily. For example, the viewing angle or the line of sight of the exposed person towards the light source will certainly have a strong effect on BLH, additionally depending on the beam angle. It is unclear how accurate the Planck Approximation will be if a look in the lamp strongly deviates from the perpendicular axis. In the same context, the source size α might play an important role.

Further questions that have not been addressed at all arise for workplaces with many spotlights: What about exposure situations where two or more lamps are within an, for example, 100 mrad FOV? How can it be assessed correctly? And if the Planck Approximation is applicable, in what manner?

Apart from these unsolved problems, the fact that experimentally determined $K_{\mathrm{B,v}}$ are close to those for a blackbody radiator for many spotlight parameter settings provides interesting opportunities. For example, one could think about $K_{\mathrm{B,v}}$ tables pre-calculated by the manufacturer for common parameter combinations. As a result, just one illuminance measurement could be sufficient for a BLH risk assessment. Expense, costs, and required metrological expertise could be reduced, but the outcome would still provide sufficient protection for workers.

References

BAUER S. 2021. Blue-Light Hazard of Light-Emitting Diodes Assessed with Gaussian Functions. *Int. J. Environ. Res. Public Health* **18**(2), 680. doi: 10.3390/ijerph18020680.

BAUER S., OTT G., JANßEN M., SCHMITZ M., MÜCKENHEIM U. 2017. Optical Radiation Exposure During Welding – Recording and Assessment. baua: Report. 1st Edition. Dortmund/Berlin/Dresden: Federal Institute for Occupational Safety and Health. doi: 10.21934/baua:bericht20170523.

BERLIEN H.-P., BROSE M., FRANEK J., GRAF M.-J., HALBRITTER W., JANßEN W., OTT G., REIDENBACH H.-D., ROMANUS E., SCHMITZ B., SIEKMANN H., UDOVIČIĆ L., WEISKOPF D. Statement on ICNIRP Guidelines on Limits of Exposure to Incoherent Optical Radiation. baua: Focus, 1–15. doi: 10.21934/baua:focus20160509.

CHAOPU Y., WENQING F., JIANCHENG T., FAN Y., YANFENG L., CHUN L. 2018. Change of Blue Light Hazard and Circadian Effect of LED Backlight Displayer with Color Temperature and Age. *Opt. Express* **26**(21), 27021–27032. doi: 10.1364/oe.26.027021.

DELTA OHM. HD2402 Photo-Radiometer / Dosimeter for Non-Coherent Artificial Optical Radiations (A.O.R.) Measurement; Manual. Rev. 1.1, 2010.

EUROPEAN COMMITTEE FOR ELECTROTECHNICAL STANDARDIZATION. EN 62471:2008 Photobiological Safety of Lamps and Lamp Systems.

EUROPEAN COMMITTEE FOR STANDARDIZATION. EN 12198-1:2000+A1:2008 Safety of Machinery – Assessment and Reduction of Risks Arising from Radiation Emitted by Machinery – Part 1: General Principles.

EUROPEAN COMMITTEE FOR STANDARDIZATION. EN 14255-2:2005 Measurement and Assessment of Personal Exposures to Incoherent Optical Radiation – Part 2: Visible and Infrared Radiation Emitted by Artificial Sources in the Workplace.

EUROPEAN COMMITTEE FOR STANDARDIZATION. prEN 12464-1:2019 Light and Lighting – Lighting of Work Places – Part 1: Indoor Work Places.

FEDERAL MINISTRY OF LABOUR AND SOCIAL AFFAIRS (BMAS). 2013. Technical Rules Optical Radiation (TROS) – Incoherent Optical Radiation. *GMBl.* **64**(65–67), 1302–1366.

FIORENTIN P., SCROCCARO A. 2014. A Simplified Approach to the Assessment of Photobiological Safety of LED Sources. *IEEE International Instrumentation and Measurement Technology Conference*. Montevideo, Uruguay, 792–795.

FITZPATRICK T. B. 1988. The Validity and Practicability of Sun-Reactive Skin Types I Through VI. *Arch. Dermatol.* **124**(6), 869–871.

HAFERKEMPER N., PEPLER W. 2019. Photobiological Safety of LED-based Lighting Systems – Theory and Practical Hazard Assessment. *Adv. Opt. Techn.* **8**(1), 67–76. doi: 10.1515/aot-2018-0053.

HERNÁNDEZ-ANDRÉS J., LEE R. L., ROMERO J. 1999. Calculating Correlated Color Temperatures Across the Entire Gamut of Daylight and Skylight Chromaticities. *Appl. Opt.* **38**(27), 5703–5709. doi: 10.1364/ao.38.005703.

HUNT R. W. G., POINTER M. R. 2011. *Measuring Colour*. 4th ed. United Kingdom, West Sussex: Wiley.

INTERNATIONAL COMMISSION ON ILLUMINATION. CIE Position Statement on the Blue Light Hazard. 2019.

INTERNATIONAL COMMISSION ON NON-IONIZING RADIATION PROTECTION. 1997. Guidelines on Limits of Exposure to Broad-Band Incoherent Optical Radiation (0.38 to 3 µm). *Health Phys.* **73**(3), 539–554.

INTERNATIONAL COMMISSION ON NON-IONIZING RADIATION PROTECTION. 2004. Guidelines on Limits of Exposure to Ultraviolet Radiation of Wavelengths Between 180 nm and 400 nm (Incoherent Optical Radiation). *Health Phys.* **87**(2), 171–186. doi: 10.1097/00004032-200408000-00006.

INTERNATIONAL COMMISSION ON NON-IONIZING RADIATION PROTECTION. 2013. ICNIRP Guidelines on Limits of Exposure to Incoherent Visible and Infrared Radiation. *Health Phys.* **105**(1), 74–96. doi: 10.1097/hp.0b013e318289a611.

INTERNATIONAL COMMISSION ON NON-IONIZING RADIATION PROTECTION. 2020. Light-Emitting Diodes (LEDS): Implications for Safety. *Health Phys.* **118**(5), 549–561. doi: 10.1097/hp.0000000000001259.

INTERNATIONAL ELECTROTECHNICAL COMMISSION. IEC 62471-7 Photobiological Safety of Lamps and Lamp Systems – Part 7: Light Sources and Luminaires Primarily Emitting Visible Radiation. CDV, 25 March 2022.

INTERNATIONAL ELECTROTECHNICAL COMMISSION. IEC TR 62471-2:2009 Photobiological Safety of Lamps and Lamp Systems – Part 2: Guidance on Manufacturing Requirements Relating to Non-Laser Optical Radiation Safety. Withdrawn 2021.

INTERNATIONAL ELECTROTECHNICAL COMMISSION. IEC TR 62778:2014 Application of IEC 62471 for the Assessment of Blue Light Hazard to Light Sources and Luminaires.

INTERNATIONAL ORGANIZATION FOR STANDARDIZATION/INTERNATIONAL COMMISSION ON ILLUMINATION. ISO/CIE 11664-1:2019 Colorimetry – Part 1: CIE Standard Colorimetric Observers.

INTERNATIONAL ORGANIZATION FOR STANDARDIZATION/INTERNATIONAL COMMISSION ON ILLUMINATION. ISO/CIE 11664-3:2019 Colorimetry – Part 3: CIE Tristiumuls Values.

JOINT COMMITTEE FOR GUIDES IN METROLOGY (JCGM). JCGM 200:2012 International Vocabulary of Metrology – Basic and General Concepts and Associated Terms. 3rd Edition, 2012.

JUDD D. B. 1951. Report of U.S. Secretariat Committee on Colorimetry and Artificial Daylight. *Proceedings of the Twelfth Session of the CIE*. Paris, France.

LI C., CUI G., MELGOSA M., RUAN X., ZHANG Y., MA L., XIAO K., LUO M. R. 2016. Accurate Method for Computing Correlated Color Temperature. *Opt. Express* **24**(13), 14066–14078. doi: 10.1364/oe.24.014066.

LIU J., ZHUANG X. B., YAO H., ZHANG S. D. 2014. Methodology for Measurement of the Blue Light Hazard of Light-Emitting Diodes with Imaging Luminance Meter. *Mechanical*

Materials and Manufacturing Engineering III. Vol. 455. Appl. Mech. Mater, 460–465. doi: 10.4028/www.scientific.net/amm.455.460.

MCCAMY C. S. 1992. Correlated Color Temperature as an Explicit Function of Chromaticity Coordinates. *Color Res. Appl.* **17**(2), 142–144. doi: 10.1002/col.5080170211.

MODENESE A., GOBBA F. 2019. Macular Degeneration and Occupational Risk Factors: a Systematic Review. *Int. Arch. Occ. Environ. Health* **92**, 1–11. doi: 10.1007/s00420-018-1355-y.

O'HAGAN J., PRICE L. L. A., KHAZOVA M. 2016. Low-energy Light Bulbs, Computers, Tablets and the Blue Light Hazard. *Eye* **30**, 230–233. doi: 10.1038/eye.2015.261.

REIDENBACH H.-D., DOLLINGER K., BECKMANN D., AL GHOUZ I., OTT G., BROSE M. 2014. Blendung durch künstliche optische Strahlung unter Dämmerungsbedingungen. Dortmund/Berlin/Dresden: Bundesanstalt für Arbeitsschutz und Arbeitsmedizin.

REIDENBACH H.-D., DOLLINGER K., OTT G., JANßEN M., BROSE M. 2008. Blendung durch optische Strahlungsquellen. Dortmund/Berlin/Dresden: Bundesanstalt für Arbeitsschutz und Arbeitsmedizin.

SCHULMEISTER K., BUBERL A., WEBER M., KITZ E. 2013. Simplified Method to Assess the UV and Blue Light Hazard of Lamps. *Proceedings of the International Laser Safety Conference*. Orlando, USA, 357–365.

SCHULMEISTER K., BUBERL A., WEBER M., VEES G., BRUSL H., KITZ E. 2011. Gefährdungsermittlung bei Beleuchtung: LUX-Grenzwerte für UV- und sichtbare Strahlung. *Tagungsbericht NIR 2011*. Ed. by H.-D. REIDENBACH, K. DOLLINGER, G. OTT. Dortmund, Germany, 551–572.

SCHULMEISTER K., O'HAGAN J., SLINEY D. H. 2019. Lamp and LED Safety – Classification vs. Realistic Exposure Analysis. *Proceedings of the International Laser Safety Conference*. Orlando, USA, 174–183.

SCIENTIFIC COMMITTEE ON HEALTH, ENVIRONMENTAL AND EMERGING RIKS (SCHEER). Opinion on Potential Risks to Human Health of Light Emitting Diodes (LEDs). 2018.

SHARPE L. T., STOCKMAN A., JAGLA W., JÄGLE H. 2005. A Luminous Efficiency Function, $V^*(\lambda)$, for Daylight Adaptation. *J. Vision* **5**(11), 948–968. doi: 10.1167/5.11.3.

SHIBUYA T., AKIBA T., IWANAGA T. 2021. Assessment of the Blue Light Hazard for Light Sources with Non-Uniform Luminance. *LEUKOS* **17**(2), 205–209. doi: 10.1080/15502724.2020.1774775.

SLINEY D. H., BERGMANN R., O'HAGAN J. 2016. Photobiological Risk Classification of Lamps and Lamp Systems – History and Rationale. *LEUKOS* **12**(4), 213–234. doi: 10.1080/15502724.2016.1145551.

SŁOMIŃSKI S. 2016. Selected Problems in Modern Methods of Luminance Measurement of Multisource LED Luminaires. *Light and Engineering* **24**(1), 45–50.

THE EUROPEAN PARLIAMENT AND THE COUNCIL OF THE EUROPEAN UNION. Directive 2006/25/EC of the European Parliament and of the Council of 5 April 2006 on the Minimum Health and Safety Requirements Regarding the Exposure of Workers to

Risks Arising from Physical Agents (Artificial Optical Radiation) (19th Individual Directive Within the Meaning of Article 16(1) of Directive 89/391/EEC).

VOS J. J. 1978. Colorimetric and Photometric Properties of a 2° Fundamental Observer. *Color Res. Appl.* **3**(3), 125–128. doi: 10.1002/col.5080030309.

WEBB A. R., ENGELSEN O. 2006. Calculated Ultraviolet Exposure Levels for a Healthy Vitamin D Status. *Photochem. Photobiol.* **82**(6), 1697–1703. doi: 10.1562/2006-09-01-ra-670.

WEBER M., SCHULMEISTER K., KITZ E. 2016. Optische Strahlung: UV- und Blaulicht-gefährdung von Theater- und Bühnenbeleuchtung. AUVA Report R53. Seibersdorf/Wien: Seibersdorf Laboratories.

WEBER M., SCHULMEISTER K., KITZ E. 2018. Assessment of the Blue Light Hazard of Theatre- and Stage-Lighting. *NIR 2018: Wellen – Strahlung - Felder*. Ed. by H.-D. REIDENBACH, M. BROSE, S. JOOSTEN. Dresden, Germany, 249–267.

WEBER M., SCHULMEISTER K., KITZ E., BRUSL H. 2011. Vereinfachte Beurteilung einer möglichen Überschreitung der Grenzwerte für optische Breitbandstrahlung auf Basis des Blendungseindruckes und der Oberflächentemperatur. *Tagungsbericht NIR 2011*. Ed. by H.-D. REIDENBACH, K. DOLLINGER, G. OTT. Dortmund, Germany, 444–460.

Abbreviations

BLH	blue-light hazard
CCD	charge-coupled device
CCT	correlated color temperature
CEN	European Committee for Standardization
CENELEC	European Committee for Electrotechnical Standardization
CIE	International Commission on Illumination
ELV	exposure limit value
FOV	field of view
GLS	general lighting service
ICNIRP	International Commission on Non-Ionizing Radiation Protection
IEC	International Electrotechnical Commission
IR	infrared
LED	light-emitting diode
MPE	maximum permissible exposure duration
pc-LED	phosphor-conversion white-light emitting diode
PEROSH	Partnership for European Research in Occupational Safety and Health
RG	risk group according to EN 62471
RGBW	red, green, blue, white
RTH	retinal thermal hazard
TH	thermal hazards
UVR	ultraviolet radiation

Acknowledgment

I would like to thank Joelle Nicolay for patiently measuring most of the data collected for this project. Marco Janßen gave advice regarding the spotlight parameter settings, helped with the realization of the different experimental setups, and supported the lamp purchase.
Erik Romanus gratefully accompanied the whole project beginning from the initial idea until this report. Lars Adolph enabled F 2483 in the first place by his support in various in-house committees.
Last but not least, a heartfelt thank-you goes out to Hannah Rolf who helped with all about LaTeX.

Appendix

BLH of LEDs Assessed with Gaussian Functions

The following publication excerpt (abstract and conclusion) are part of the open-access publication "*Blue-Light Hazard of Light-Emitting Diodes Assessed with Gaussian Functions*" (Bauer 2021) that was written during the work on project F 2483. The paper applies Gaussian functions in order to approximate LED emission spectra with the aim to estimate their BLH; thus, supporting workplace risk assessment.

Abstract. The high blue proportion of phosphor-conversion white-light emitting diodes (pc-LEDs), especially of those with higher correlated color temperatures (CCT), raises concern about photochemically induced retinal damages. Although almost all general lighting service LEDs are safe, other applications exist, like spotlights for theaters or at construction sites, that can pose a severe blue-light hazard (BLH) risk, and their photobiological safety must be assessed. Because of required but challenging radiance measurements, a calculative approach can be supportive for risk assessment. It is the aim of this work to exploit Gaussian functions to study LED parameter variations affecting BLH exposure. Gaussian curve approximations for color LEDs, the BLH action spectrum, and the spectral luminous efficiency for photopic vision enabled analytically solving the BLH efficiency, η_{B}, and the BLH efficacy of luminous radiation, $K_{\mathrm{B,v}}$. It was found that sigmoidal functions describe the CCT dependence of η_{B} and $K_{\mathrm{B,v}}$ for different color LEDs with equal spectral bandwidth. Regarding pc-LEDs, variations of peak wavelengths, intensities, and bandwidths led to linear or parabolic shaped chromaticity coordinate correlations. η_{B} and $K_{\mathrm{B,v}}$ showed pronounced CCT dependent extrema that might be exploited to reduce BLH. Finally, an experimental test of the presented Gaussian approach yielded its successful applicability for color and pc-LEDs but a minor accuracy for blue and green LEDs.

Conclusion. The adaptation of Gaussian functions to color LED emission spectra, to the BLH action spectrum, and to the spectral luminous efficiency for photopic vision allowed to derive analytical solutions for both weighted LED signals, S_{B} and S_{v}, for the BLH efficiency, η_{B}, and the BLH efficacy of luminous radiation, $K_{\mathrm{B,v}}$; however, the latter having no simple mathematical expression. Analyzing the peak wavelength dependence showed that photochemically induced retinal damage is highest for a blue LED with $\lambda_0 = 444.8\,\mathrm{nm}$, and that a green LED with $\lambda_0 = 559.1\,\mathrm{nm}$ is perceived as the brightest one. With increasing bandwidths, $\Delta\lambda_0$, all color LEDs converge towards $\eta_{\mathrm{B}} = 0.17$ and $K_{\mathrm{B,v}} = 9.5 \times 10^{-4}\,\mathrm{W\,lm^{-1}}$ at a CCT of 5462 K. For any constant $\Delta\lambda_0$, η_{B} and $K_{\mathrm{B,v}}$, depending on peak wavelength and CCT, can be described by sigmoidal functions. Regarding pc-LEDs, a variation of both peak intensities, S_0 (blue LED) and S_{ph} (phosphor), resulted in a linear x-y-correlation, increasing bandwidths, $\Delta\lambda_0$ and $\Delta\lambda_{\mathrm{ph}}$, led to parabolic shaped x-y-curves accompanied by smaller x values, and changing λ_0 showed narrow parabola-like x-y-data, whereas λ_{ph} variations yielded broad x-y-patterns. η_{B} and $K_{\mathrm{B,v}}$ both increased and shifted to higher CCT with growing blue LED signal intensity, S_0, or decreasing phosphor emission, S_{ph}, coinciding with most of the results for a $\Delta\lambda_0$ change. Exploiting the minima and avoiding the maxima of the curved CCT dependent η_{B} and $K_{\mathrm{B,v}}$, that appeared upon varying phosphor excitation bandwidth and both peak intensities, might be used to minimize pc-LEDs' BLH risk concurrently preserving the desired CCT.

A comparison of the analytical η_{B} and $K_{\mathrm{B,v}}$ solutions with experimental values revealed that red, orange, and yellow LEDs are within 5 % deviation. Presumably due to the spectroradiometer's noise, $K_{\mathrm{B,v}}$ for blue and green LEDs as well as η_{B} for green LEDs are less accurate. For most of the pc-LEDs, the percentage deviations are within 0 to 7 %.

Finally, the use of analytical BLH equations for color LEDs, the possibility to exploit the CCT dependence extrema of η_{B} and $K_{\mathrm{B,v}}$ for future pc-LEDs with less BLH, and the accuracy of the calculated data demonstrated the suitability of Gaussian functions to simulate LED emission spectra; thus, supporting risk assessment. However, this calculative approach has not been tested for tri- or tetra-chromatic LEDs, for arrays superimposing warm and cold pc-LEDs, or for organic LEDs. In addition to the most frequently used YAG phosphors, several others exist, and for many of them it is thought that their emitted light can be approximated by Gaussian functions, too, because of the fundamental physics of excitation and emission. However, no such phosphors have been examined for the present work. Furthermore, parameter variations influencing maximum permissible exposure durations have also not been addressed, yet, and the introduced Gaussian approach has not been compared to additional metrological and mere calculative BLH evaluation methods. Overall, this lack of knowledge provides work for future research.